multi-Risk sciEnce for resilienT commUnities undeR a changiNgclimate

Codice progetto MUR: **PE00000005** – **I33C22006910006**

Deliverable title: An integrated model for scenario generation combining process-based and data-driven approaches.

Deliverable ID: 8.3.2

Due date: 31 March 2026

Submission date: xxxxx

AUTHORS

Alberto Montanari (UNIBO), Marco Borga (UNIPD), Marco Marani (UNIPD), Salvatore Grimaldi (Università della Tuscia), Elena Volpi (Università RomaTre)

1. Technical references

Project Acronym	RETURN
Project Title	multi-Risk sciEnce for resilienT commUnities undeR a changiNg climate
Project Coordinator	Andrea Prota UNIVERSITA DEGLI STUDI DI NAPOLI FEDERICO II domcalca@unina.it
Project Duration	December 2022 – November 2025 (36 months)

Deliverable No.	DV8.3.2
Dissemination level*	CO
Work Package	WP3 - Generation of specific hazard indicators based on state-of-the-art and high-resolution climatic scenarios to support hazard assessment at multiple scales
Task	T 8.3.2 - Seamless integration of numerical, statistical, and deep learning models for scenario generation.
Lead beneficiary	UNIBO
Contributing beneficiary/ies	UNIPD

* PU = Public

PP = Restricted to other programme participants (including the Commission Services)

RE = Restricted to a group specified by the consortium (including the Commission Services)

CO = Confidential, only for members of the consortium (including the Commission Services)

Document history

Version	Date	Lead contributor	Description
0.1	10.03.2026	Alberto Montanari (UNIBO)	First draft
0.2	18.03.2026	Alberto Montanari (UNIBO), Salvatore Grimaldi (Università della Tuscia), Elena Volpi (Università RomaTre), Marco Marani (UNIPD), Marco Borga (UNIPD)	Critical review and proofreading

2. Abstract

Based on the activities carried out in Task 8.3.2, this deliverable introduces a methodology for the generation of climate and weather scenario at the local level. The distinguishing feature of the proposed approach is the integration of physically based climate models with an advanced stochastic weather generator, allowing to preserve the statistical features of the historical climate and incorporate the climate change projections delivered by climate models.

The present deliverables includes two papers submitted for publication, describing the procedure and its application to the Arno River Basin.

The methodology is an innovative product of the RETURN project, allowing a seamless and synergetic integration of models for producing an innovative information to support technical design of risk mitigation policies and projects at the local level.

Table of contents

3. Introduction

The RETURN methodology for generating local climate scenarios relies on the integration of the CoSMoS model (version CoSMoS-2S) and the projections for statistics of future climate delivered by any selected climate model.

The deliverable describes the application of the CoSMoS model, which leadsto estimation of its parameters to match the statistical behaviours of the historical climate. The integration of the projections of climate models can be attained by accordingly varying the CoSMoS parameters.

The CoSMoS model was introduced by Papalexiou (2018). It is capable of simulating intermittent hydroclimatic processes such as precipitation. The marginal probability distribution of the data can be continuous, mixed-type, discrete or binary. These behaviours need to reproduced as well as joint probability distributions and autocorrelation function. By preserving these features we ensure the generation of synthetic time series with high degree of realism and accuracy, therefore giving the opportunity to identify extreme events beyond what has been observed. Furthermore, by modifying the parameters of the model according to predicted climate change, one can simulate the behaviours of expected future climate therefore mitigating surprise.

The basic assumption underlying CoSMoS is that any process -stationary or cyclostationary- can be generated by transforming a specific "parent" Gaussian process. In the case of a multivariate process, each process within the group has a corresponding parent Gaussian process and analytical transformations of both auto and cross-correlation functions are employed. By exploiting the relationship with the parent Gaussian processes CoSMoS is able simulate a wide range of hydroclimatic phenomena, spanning from intermittent processes like precipitation, heavy-tailed processes such as river discharge, processes with bounded marginals like relative humidity as well as discrete (rain days/month) and binary cases (wet/dry conditions).

The most recent extension of CoSMoS by Papalexiou (2022), preserves the main statistical characteristics of the hydrological processes such as intermittency, marginal distributions and correlation functions. Within this approach, it is suggested that any observed intermittent time series with a specific marginal distribution, is transformed in a time series with a mixed-uniform marginal distribution. In particular, this approach enables that a given time series with a specific probability of zeros and a specified marginal distribution is transformed in a time series with a one-parameter mixed-uniform distribution.

The next section of the deliverable presents a copy of a paper submitted to a scientific journal describing CoSMoS-2S and its application to the Arno River. The final section presents a second paper (in Italian) providing more details on the rainfall simulation for the Arno River Basin.

4. Bridging Flexibility and Usability: Configuring CoSMoS-2s for Operational Rainfall Simulation in the Arno River

Bridging Flexibility and Usability: Configuring CoSMoS-2s for Operational Rainfall Simulation in the Arno River Basin

Francesco Cappelli[1*], Simon Michael Papalexiou[2], Yannis Markonis[3], Elena Volpi[4], Salvatore Grimaldi[1]

(1) Dipartimento per la Innovazione nei sistemi Biologici, Agroali-mentari e Forestali, Università degli Studi della Tuscia, Italy
(2) Department of Civil Engineering, University of Calgary, Calgary, Canada
(3) Faculty of Environmental Sciences, Czech University of Life Sciences Prague, Prague, Czech Republic
(4) Dipartimento di Ingegneria Civile, Informatica e delle Tecnologie Aeronautiche, Università degli Studi di Roma Tre, Italy

Abstract

Rainfall simulation models are essential for hydrological studies, supporting applications in flood control, urban planning, agriculture, and climate change adaptation. A key challenge is developing models that effectively capture rainfall intermittency while remaining computationally efficient and practical for operational use. One recently introduced approach, the two-state intermittent model CoSMoS-2s, simulates rainfall time series while preserving arbitrary marginal distributions and autocorrelation structures. However, its practical implementation requires robust and consistent parameterization to ensure reliability. Here, we present a systematic configuration of CoSMoS-2s that minimizes parameter requirements while maintaining strong performance, improving its ease of calibration and operational applicability. To validate its real-world utility, we test the model using a large database of daily rainfall time series from seventy rain gauges with contemporaneous observations spanning 20 years—a scenario where data limitations pose a significant challenge. The results demonstrate that CoSMoS-2s effectively reproduces key rainfall characteristics, including wet and dry spell durations, dry-day probabilities, statistical properties of nonzero rainfall amounts, and extreme rainfall behavior. Compared to previous implementations, this minimal parameterization enhances usability without compromising accuracy. These findings indicate that CoSMoS-2s is a robust and versatile tool for hydrological modeling, particularly in data-scarce regions where reliable rainfall simulations are critical.

Keywords: Stochastic simulation model, Rainfall Simulation, Daily rainfall time series, Complete Stochastic Modelling Solution (CoSMoS)

1. Introduction

Rainfall simulation models are essential in climatology, hydrology, meteorology, and environmental sciences, supporting risk assessment, infrastructure planning, water resource management, and climate change impact studies (e.g., Beck et al., 2020; Clark et al., 2004; Iizumi et al., 2017; Kim et al., 2021; Li et al., 2021; Papalexiou, 2018, 2022). Stochastic models can help design resilient infrastructure, optimize water allocation, and assess flood and drought risks by generating realistic rainfall scenarios. These models are used in hydrological simulations, providing precipitation inputs for rainfall-runoff analysis, reservoir operations, stormwater management, etc. For example, a key application is stress-testing infrastructure under different precipitation scenarios to ensure long-term functionality. Stochastic models can also be linked with covariates, such as temperature, and be used in climate change studies to assess shifts in intensity, frequency, and duration in future rainfall patterns; this in turn, can inform adaptation strategies in water and food security, flood mitigation, etc. (e.g., Chandler et al., 2007; Singer et al., 2018; Rios Gaona et al., 2024, Fisher et al. 2025). Their ability to generate multiple synthetic rainfall sequences allows also ensemble forecasting which is pivotal in robust uncertainty analysis in hydrology.

In general, rainfall models aim to capture the inherent variability of precipitation and different frameworks have been used (Volpi et al., 2024). Cluster-based models, such as the Neyman-Scott (Neyman & Scott, 1958) and Bartlett-Lewis (Rodriguez-Iturbe et al., 1987) rectangular pulse models, represent storms as clusters of pulses with random intensities and durations. These models use Poisson-distributed storm arrivals, with individual cells following specific distributions. Various extensions have improved their flexibility by refining storm durations, cell intensities, and temporal structures (Cowpertwait, 1991; Wheater et al., 2005). Another widely used approach is Markov Chain modeling (Gabriel & Neumann, 1957, 1962), which simulates rainfall occurrence based on wet/dry state transitions. Higher-order and multi-state variations (e.g., Stern & Coe, 1984)

enhance the representation of wet/dry sequences, while hybrid models integrate continuous distributions to improve rainfall intensity simulations (e.g., Wilks & Wilby, 1999).

Multifractal approaches also exist targeting to capture scale-invariant properties of precipitation. Multiplicative cascade models (Schertzear & Lovejoy, 1987) have been applied to generate fine-resolution rainfall fields while preserving variability across scales. These methods have been used for stochastic disaggregation of daily rainfall (Gaume et al., 2007; Molnar & Burlando, 2005, Cappelli et al. 2024b) and for space-time modeling of precipitation extremes (Veneziano et al., 2006). Disaggregation techniques further refine rainfall simulations by ensuring consistency between different temporal scales. Recent schemes, such as DiPMaC (Papalexiou et al., 2018), explicitly preserve probability distributions and correlations while accommodating non-stationary characteristics, enhancing the accuracy of fine-scale precipitation modeling. Beyond these approaches, Gaussian-based models have been extensively applied in rainfall simulation. Autoregressive moving average processes (Box & Jenkins, 1970; Matalas, 1967) have been used to generate synthetic time series, while threshold-based transformations enable their use for intermittent rainfall (Bárdossy & Plate, 1992; Glasbey & Nevison, 1997). Copula-based methods further enhance dependence structures across sites (Bárdossy & Pegram, 2009; Serinaldi, 2009), and correlation transformation techniques allow for improved representation of rainfall intermittency and marginal distributions (Papalexiou, 2022).

Here we focus on the CoSMoS (Complete Stochastic Modelling Solution), introduced by Papalexiou (2018), which provides a unified framework for the stochastic modeling of hydroclimatic processes, with several extensions developed in recent years (Papalexiou, 2022; Papalexiou, et al., 2023; Cappelli et al., 2024a). Specifically, we use the two-state intermittent model (CoSMoS-2s) (Papalexiou, 2022), which integrates a binary process for rainfall occurrence with a continuous process for rainfall amounts. This approach enables the reproduction of both linear and nonlinear autocorrelation structures (ACS), as well as the intermittency and marginal distribution of nonzero values, capturing rainfall characteristics across multiple scales. CoSMoS-2s seamlessly integrates occurrence or intensity, ensuring that wet/dry sequences and nonzero rainfall amounts are realistically represented while allowing for total flexibility in the choice of arbitrary marginal distributions and correlation structures. This dual control over intermittency and intensity enhances adaptability across different climatic and hydrological settings but also requires careful parameterization.

The strength of CoSMoS-2s lies in its ability to balance flexibility with practical implementation, yet this also introduces challenges. While its adaptability makes it suitable for diverse climatic and hydrological settings, it also shifts the burden of selecting appropriate modeling choices to practitioners. A highly flexible model allows for extensive customization, but without proper guidance, this flexibility can become a limitation rather than an advantage. Theoretical advancements provide a broad range of modeling choices yet applying them effectively requires rigorous evaluation and careful parameterization to ensure consistency with real-world rainfall characteristics. This study addresses that gap by demonstrating how CoSMoS-2s can be applied in a parsimonious yet robust manner, making it both practical and reliable. To assess its real-world applicability, we conduct a large-scale case study using 70 raingauges within the Arno River Basin, where the relatively short 20-year time series present a challenging test for model validation. By evaluating its ability to reproduce key rainfall properties, we aim to bridge the gap between theoretical innovation and practical hydrological modeling, highlighting CoSMoS-2s as a powerful yet accessible tool for rainfall simulation.

The paper is organized as follows: Section 2 presents the theoretical background of the rainfall simulation model and details the implementation strategies. Section 3 provides a brief overview of the case study area. Section 4 thoroughly evaluates the model's performance, and Section 5 summarizes the key findings and presents the conclusions.

2. Summary of the CoSMoS-2s Model

In this section, we briefly summarize the specifics of the CoSMoS-2S model, focusing on the modelling choices and its calibration and implementation. Section 2.1 outlines the theoretical foundations of the framework, while Section 2.2 provides a step-by-step guide to its practical application. Finally, Section 2.3 discusses implementation strategies and calibration techniques to ensure accurate representation of real-world hydroclimatic processes.

2.1. Conceptual Note on the Modelling Framework

In general, the CoSMoS-2s model provides a framework for simulating intermittent hydroclimatic processes, such as rainfall at any temporal scale. The model reproduces intermittent rainfall through a combination of two distinct stochastic components:

1. Rainfall occurrence is modeled as a binary process, generating a sequence of ones and zeros to distinguish between dry (0, no rainfall) and wet (1, nonzero rainfall) conditions. This process has its own dependence

structure (meaning past wet/dry states influence future states), designed to capture the persistence and clustering of dry and wet spells over time while accurately reproducing their frequencies.

2. The magnitude of rainfall is modeled as a separate stochastic process with a flexible continuous probability distribution and an associated dependence structure, ensuring realistic temporal variability and statistical consistency with observed precipitation patterns.

The CoSMoS-2s model is an integral component of the broader CoSMoS framework, designed to simulate hydroclimatic processes across various scales and dimensions, including univariate, multivariate, and multisite settings, as well as spatiotemporal random fields. These fields can range from purely static to highly dynamic systems exhibiting complex anisotropies and advection components. As previously mentioned, CoSMoS-2s is specifically tailored for intermittent processes such as precipitation, offering multiple modeling configurations that result in a diverse set of variants. Both the binary and continuous components can be driven by different parent processes, including Gaussian, t-copula, or other copula-based structures. This flexibility allows, for example, the generation of intermittent time series where nonzero values preserve the dependence structure of any chosen copula.

Notably, CoSMoS-2s enables the analytical approximation of binary sequences with arbitrary correlation structures and offers a rank-based formulation that preserves Spearman's rank correlations. This rank-based approach can be applied analytically, eliminating the need for numerically solving integral transformations or fitting correlation functions. In this study, we explore and apply this variant to demonstrate its operational effectiveness.

2.2. Step-by-Step Implementation of the Rank-Based CoSMoS-2s

The first state of the CoSMoS-2s model involves creating a binary time series that represents wet (rain) and dry (no rain) periods while preserving the temporal dependencies observed in real rainfall data. The process consists of the following steps:

1. Extract the binary sequence from observed data: Convert the observed precipitation time series into a binary sequence by replacing all nonzero values with 1 and all zero values with 0.
2. Assess key characteristics of the binary process: Determine the probability of zero p_0 of the binary time series and estimate the empirical ACS $\hat{\rho}_B(\tau)$ which characterizes how dry and wet states persist over time. Note that for a binary time series the Pearson autocorrelation and Spearman's rank correlation are the same.
3. Optionally, use the $\hat{\rho}_B(\tau)$ to fit a parametric ACS to describe parsimoniously the temporal dependence of wet/dry states.
4. Compute parameters for the parent Gaussian process: For the estimated p_0 find c_{p_0} using

$$c_{p_0} = a\left(\sqrt{p_0(1-p_0)} + \left(p_0(1-p_0)\right)^b\right) \quad (1)$$

with $a = 0.81$ and $b = 0.10$. Then compute the ACS of the parent Gaussian process from

$$\rho_Z(\tau) = 1 - \left(1 - \rho_B(\tau)^{c_{p_0}}\right)^2 \quad (2)$$

where $\rho_B(\tau)$ are the estimated autocorrelations (for any lag) of the binary time series.

5. Generate a parent Gaussian time series: Simulate a standard Gaussian time series $z(t)$ using an autoregressive (AR) model of sufficiently large order to reproduce $\rho_Z(\tau)$.
6. Transform to a binary time series: Convert the Gaussian generated values $z(t)$ to a binary sequence $b(t)$ by applying the threshold transformation: $b(t) = 0$ if $z(t) \leq z_{p_0}$, and $b(t) = 1$ if $z(t) > z_{p_0}$ where $z_{p_0} = -\sqrt{2}\mathrm{erfc}^{-1}(2p_0)$.

This process generates a binary time series that matches the observed probability of zero ensuring the same frequency of wet and dry periods. Additionally, it preserves the temporal dependence structure, closely replicating the clustering of wet and dry states over time.

The second step in the rank-based CoSMoS-2s model involves generating a continuous time series representing rainfall amounts on wet days. This process ensures that the generated values follow the observed rainfall distribution while reproducing the Spearman's rank autocorrelation $\rho_S(\tau)$. The steps are as follows:

1. Estimate the autocorrelations of the continuous process: Compute the empirical Spearman's autocorrelation $\hat{\rho}_S(\tau)$ using positive rainfall values from observed data.

2. Optionally, use the $\hat{\rho}_S(\tau)$ to fit a parametric ACS $\rho(\tau)$ to describe the temporal dependence of rainfall magnitudes instead of using the empirical values.
3. The parent Gaussian ACS $\rho_Z(\tau)$ is obtained using

$$\rho_Z(\tau) = 2\sin\left(\frac{\pi}{6}\rho_S(\tau)\right) \quad (3)$$

where $\rho_S(\tau)$ are the estimated autocorrelations (for any lag) of the binary time series.
4. Fit a probability distribution to nonzero rainfall values: Estimate a parametric cumulative distribution function (CDF) $F_X(x)$ from the observed nonzero rainfall values.
5. Generate a Gaussian time series with the desired ACS: Simulate a Gaussian time series $z(t)$ using an AR model of sufficiently large order to reproduce $\rho_Z(\tau)$.
6. Transform the Gaussian time series into a positive rainfall time series: Convert the Gaussian series to a rainfall series by applying $x(t) = Q_X\left(\Phi_Z(z(t))\right)$ where Q_X is the quantile function of the fitted rainfall distribution and Φ_Z is the standard Gaussian CDF.

This approach ensures that the generated rainfall magnitudes maintain the observed probability distribution while preserving the Spearman's autocorrelation structure which acts as a proxy in reproducing the dependence structure among the wet days.

Each process is designed to accurately reproduce key rainfall characteristics: the binary process ensures the correct frequency and clustering of wet and dry periods, while the continuous process captures the temporal dependence of rainfall magnitudes and preserves the observed distribution. The final rainfall time series is generated by multiplying the binary and continuous series, ensuring that rainfall occurs only on wet days and follows the observed statistical properties. For further details on the CoSMoS-2s model beyond the rank-based configuration, please refer to Papalexiou (2022).

2.3. Tuning CoSMoS-2s in Italy's Arno River Basin

In the previous section, we outlined the step-by-step procedure for applying the rank-based CoSMoS-2s model. However, several key configurations still require careful consideration. Specifically, these include defining seasonality, selecting the marginal distribution, choosing between parametric or empirical autocorrelations, and determining the order of the autoregressive model. The following choices were primarily guided by the need to establish a minimal configuration that minimizes numerical estimations and parameter complexity. Additionally, some decisions were informed by the preliminary analysis of rainfall data in the Arno River Basin.

Regarding seasonality, rainfall patterns typically vary across the year, and it is common to assume that statistical properties remain consistent within each season, allowing model parameters to be calibrated accordingly. However, determining the optimal number of seasons is not trivial and often involves a degree of subjectivity. As noted in Papalexiou (2022), a conventional approach is to treat each month as a separate season and calibrate the model monthly. Given the moderate length of the rainfall records in the Arno River Basin, we opted for a simpler and more practical approach by using the four meteorological seasons: Winter (December–February), Spring (March–May), Summer (June–August), and Autumn (September–November). This strategy reduces model complexity while maintaining accuracy, as aggregating months into broader seasons provides more stable parameter estimates when the data supports this generalization.

Selecting an appropriate marginal distribution is crucial, as it directly affects both the accuracy and parsimony of the model. Several valid options exist, including the Gamma, Weibull, and Generalized Gamma distributions, with more complex choices being particularly suitable for finer time scales. While three-parameter distributions offer greater flexibility in describing the data, they also increase computational complexity. A preliminary analysis of rainfall in the Arno River Basin indicated that the well-known two-parameter Gamma distribution provides a good balance between simplicity and accuracy, making it a suitable choice. The Gamma distribution, with probability density function

$$f_{\mathcal{G}}(x;\beta,\gamma) = \frac{1}{\beta\,\Gamma(\gamma)}\left(\frac{x}{\beta}\right)^{\gamma-1}\exp\left(-\frac{x}{\beta}\right) \quad (4)$$

and β and γ being positive scale and shape parameters respectively, effectively captures the distribution of nonzero rainfall values based on visual and quantitative inspection. Given the chosen seasonal framework, we fitted the Gamma distribution separately for each of the four seasons to ensure seasonally consistent parameterization. The distribution was fitted numerically by optimizing its parameters to minimize the difference between the empirical and theoretical cumulative distribution functions, ensuring an accurate and

parsimonious representation of nonzero rainfall values. Other methods, such as method of moments, L-moments, or maximum likelihood estimation, could also be used (see Nerantzaki and Papalexiou, 2022, for a detailed review of fitting methods).

The last two key modeling choices involve selecting either a parametric or empirical ACS and determining the order of the AR model. These choices are interrelated, as the strength and structure of the ACS guide the appropriate AR order. To avoid the complexity of fitting a parametric ACS model, which would require numerical estimation of additional parameters, we opted for the empirical ACS, offering greater flexibility and direct alignment with the observed data. Analysis of daily rainfall in the Arno River Basin—consistent with typical daily rainfall behavior—revealed weak autocorrelation beyond short lags. Both the binary and continuous processes showed that a two-lag autocorrelation structure sufficiently captures rainfall persistence. Consequently, we set the AR model order to $p = 2$, ensuring it effectively represents short-term dependencies without overfitting.

3. Operational Application in the Arno River Basin

This section presents the performance evaluation of CoSMoS-2s. Section 3.1 introduces the study area, dataset, and data selection process. Section 3.2 examines the model's performance at a single rain gauge, while Section 3.3 extends the analysis to the entire dataset.

3.1. Study Area and Data Selection

To evaluate the performance of the CoSMoS-2s rainfall simulation model, we applied it to real-case studies using data from the Arno River Basin's rain gauge network. The basin, covering approximately 8,230 km², lies primarily within the Tuscany region in Central Italy and spans the Northern Apennine chain. Its topography transitions from mountains to rolling hills and flatlands, eventually reaching the Tyrrhenian Sea. The region receives an average annual precipitation of about 900 mm, exhibiting significant sub-annual variability. The basin is densely populated, with major urban centers including Florence and Pisa.

The Arno River Basin rain gauge network consists of 123 stations, with a recently compiled dataset serving as a benchmark for various rainfall modeling studies beyond this work. To ensure the availability of sub-hourly data—critical for evaluating high-resolution rainfall models—we focused on a 20-year period (2001–2020) and initially selected 81 stations with 15-minute resolution and less than 10% missing data per year. Although this study focuses on daily rainfall simulations, CoSMoS-2s outputs will be used in a separate study to drive a disaggregation model for finer-scale rainfall generation. Therefore, selecting stations with 15-minute resolution ensures the dataset remains suitable for future assessments.

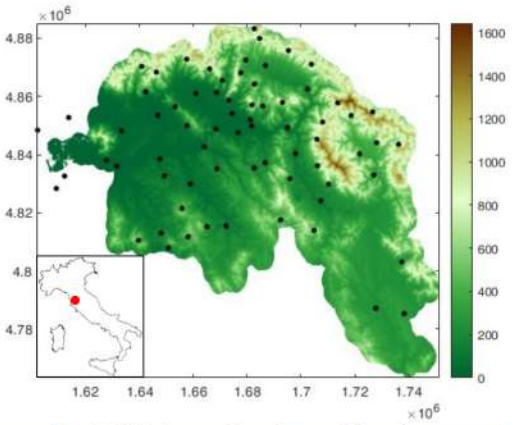

Figure 1: Case study data set - 70 rainfall time series observed in rain gauges (black dots) located the Arno River Basin, Italy.

Additionally, a preliminary analysis was conducted to assess data quality and characterize rainfall patterns at each location. This included: (1) dry spell frequencies at daily and 15-minute timescales, (2) maximum recorded rainfall values at the same timescales, and (3) autocorrelation structures at a daily resolution for lags of 1, 2, and 3 days. These checks identified two stations with unrealistic correlation structures and extreme values, leading to their exclusion. Additional filtering was necessary to ensure suitability for disaggregation

model applications, as certain stations had anomalous parameter values due to limited sample sizes (see Cappelli et al., 2025; under review). After applying these criteria, 70 rainfall time series were retained for analysis (Figure 1 shows their spatial distribution).

The case study analysis begins with a detailed evaluation of a single rain gauge (Section 3.2), comparing observed and simulated time series. It then extends to all selected stations (Section 3.3) to provide a broader assessment of model performance.

3.2. Simulating Rainfall at a Single Location

The selected daily time series (Figure 2a) exhibits short-term dependence, as evident from the rapid decline in ACS coefficients after lag 1, indicating that precipitation on previous days has little influence on subsequent values (Figure 2b). The empirical cumulative distribution function (ecdf) further characterizes the data distribution, revealing that approximately 60% of the values are zero, highlighting the probability of zero in the observed time series (Figure 2c). Beyond the zero values, most observations are concentrated within a relatively narrow range, with cumulative probability increasing gradually from low to high values; for instance, 75% of the values fall below 0.8.

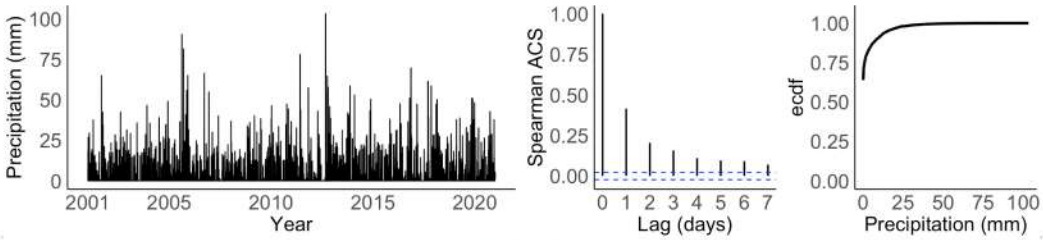

Figure 2: Plots of the daily time series for station TOS01001284: (a) observed daily time series, (b) empirical Spearman's ACS, and (c) empirical cumulative distribution function (ecdf).

Table 1 provides a detailed summary of the data, categorized by quarterly seasonality. For each season, summary statistics are reported for nonzero values.

Table 1: Summary statistics of the observed daily time series, including sample size, mean, standard deviation, minimum, percentiles (25th, 50th, 75th, 90th, 95th, 99th), maximum, the third and fourth L-moments.

Season	*n*	*mean*	*sd*	*min*	*25%*	*50%*	*75%*	*90%*	*95%*	*99%*	*max*	*L-mom3*	*L-mom4*
Winter	821	6.26	8.73	0.2	0.4	2.4	8.8	17.40	23.60	38.56	54.8	0.47	0.20
Spring	716	6.50	7.65	0.2	0.8	3.8	9.4	17.00	21.95	35.16	47.6	0.39	0.15
Summer	387	6.64	10.01	0.2	0.6	2.8	9.7	17.56	22.14	42.62	90.4	0.48	0.23
Autumn	711	8.82	13.22	0.2	0.4	3.0	11.7	25.60	36.90	58.60	103.2	0.50	0.23

The large sample size (n) in Winter and Spring seasons enhances the reliability of their statistics compared to Summer, which has a smaller sample size. Autumn has the highest mean value (8.82) and the greatest dispersion (sd = 13.22), followed by summer (mean = 6.64, sd = 10.01), while winter has the lowest mean (6.26). The maximum values indicate that extreme events are more frequent in Autumn (max = 103.2) and Summer (90.4), compared with Winter (54.8) and Spring (47.6). Quantile analysis confirms that Autumn and Summer seasons have heavier tails and a higher probability of extreme events, as evidenced by higher L-mom3 and L-mom4. Winter and Spring, on the other hand, exhibit less skewed distributions, with less variability.

The Gamma distribution parameters (Table 2, left side) are estimated by numerically minimizing the distance between the empirical and theoretical distribution functions. Winter and Autumn seasons are characterized by a more skewed distribution, indicative of rare but intense events, and b) Spring and Summer seasons have more symmetrical distributions, suggesting less intense and more frequent precipitation. Finally, Autumn is the season with the greatest variability in precipitation, suggesting that it is more prone to extreme and unpredictable events.

Table 2: Gamma parameter estimates after calibration and the Spearman's ACS coefficients ($\rho_S(1)$, $\rho_S(2)$ and $\rho_S(3)$) of the Binary and Continuous time series.

Season	*Gamma Parameters*		*Binary TS*			*Continuous TS*		
	Shape	*Scale*	$\rho_S(1)$	$\rho_S(2)$	$\rho_S(3)$	$\rho_S(1)$	$\rho_S(2)$	$\rho_S(3)$
Winter	0.47	13.68	0.42	0.18	0.10	0.15	0.06	0.05
Spring	0.64	10.93	0.38	0.19	0.15	0.06	-0.02	0.01
Summer	0.53	12.48	0.26	0.09	0.08	-0.06	-0.08	-0.02
Autumn	0.42	21.56	0.36	0.173	0.09	0.10	-0.01	-0.01

Spearman's ACS values of the Binary and Continuous (Table 2, right side) across seasons reveal distinct tem poral dependence patterns. For the binary time series, correlation is highest at lag 1 ($\rho_S(1)$) and decreases wit h increasing lag. Winter season shows the strongest dependence ($\rho_S(1)$ = 042), followed by Spring (0.38), A utumn (0.36), and Summer (0.26), indicating greater persistence of wet states in colder seasons. For the conti nuous time series, correlation is generally lower, suggesting weaker dependence in rainfall intensity compare d to wet/dry states. Winter and Autumn seasons show moderate positive correlations ($\rho_S(1)$ = 0.15, 0.10), wh ile Spring and Summer exhibit weaker or even negative values ($\rho_S(1)$ = −0.06 in Summer).

To evaluate the adequacy of the selected Gamma distribution in describing the data, we provide a visual comparison of the exceedance probabilities obtained from the fitted parametric distribution for nonzero rainfall values with those derived from the empirical distribution providing the 95% confidence interval (gray region) of the Gamma distribution (Figure 3). For the four seasons, the results show a good agreement, confirming the Gamma distribution's effectiveness in accurately representing non-zero values. The Gamma distribution provides a good approximation of the distribution of nonzero values, although some discrepancies emerge, particularly for higher values of precipitation. The Winter (Figure 3a) and Spring (Figure 3b) seasons show similar behavior, with good agreement between the empirical and theoretical distributions. Summer (Figure 3c) and Autumn (Figure 3d), on the other hand, show greater dispersion in the highest values of precipitation. In particular, Summer has the widest confidence interval, suggesting that the Gamma distribution may not adequately capture the tail of the distribution.

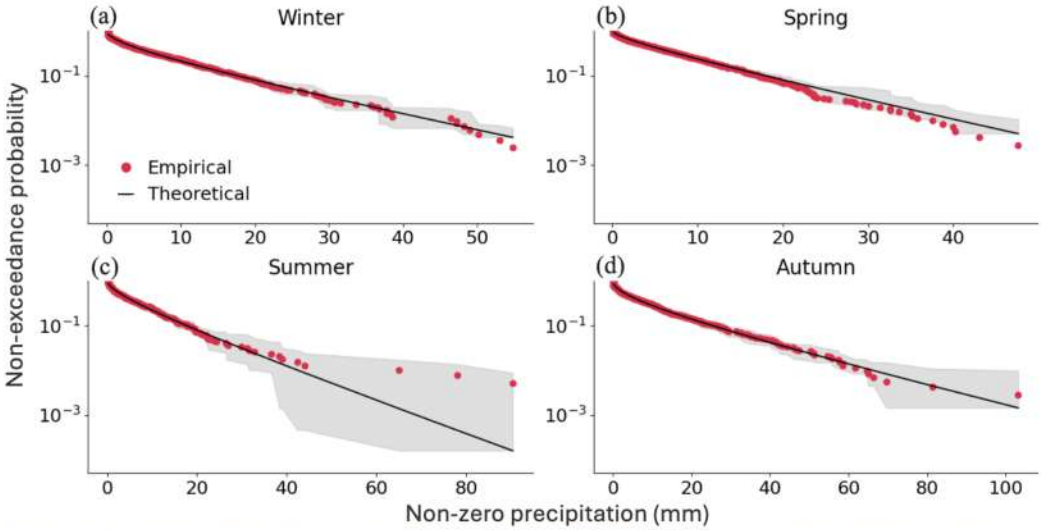

Figure 3: Probability plots showing the Gamma fitted distribution to nonzero rainfall, its 95% confidence interval (gray region), and the empirical distribution for the four seasons: (a) Winter, (b) Spring, (c) Summer, and (d) Autumn.

Following calibration, we then evaluate the model's performance by comparing several statistical and hydrological properties estimated from the entire observed time series with those of 100 simulated daily time series, without accounting for the quarterly seasonality. We start analyzing the comparison of the probability of zero (p_0) and summary statistics (mean, standard deviation, 97.5th, 99th, and 99.9th percentiles) of the 100 simulated daily time series, represented by boxplots, alongside the observed daily time series, which is marked with red crosses (Figure 4). Note that the red crosses lie within the boxplots indicating that the simulated time series closely replicate the characteristics of the observed time series. Moreover, the simulated values align well with the central tendency and dispersion of the observed data, as reflected by the proximity of the red crosses to the median and interquartile ranges of the boxplots. In addition, the red crosses fall within the range of the simulated extreme percentiles (Figure 4e and 4f), suggesting that the simulations successfully capture not only the average behavior but also the variability and rare events present in the observed data.

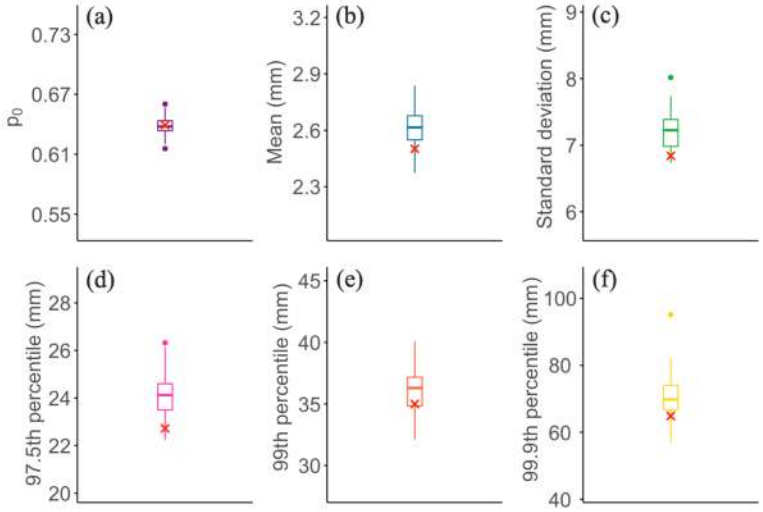

Figure 4: Plots of the comparison between the summary statistics of the nonzero values of the observed daily time (red cross) with those of the 100 simulated (boxplots) daily time series: (a) probability of zero p_0, (b) Mean, (c) Standard deviation, (d) 97.5th percentile, (e) 99th percentile and (f) 99.9th percentile.

We evaluate the performance of the minimalistic CoSMoS-2s setting applied here by assessing its ability to accurately reproduce the monthly seasonal components (Figure 5) of the observed daily time series within the 100 simulated daily time series. The objective is to compare the monthly mean values derived from the observed time series (depicted as red diamonds) with the distribution of monthly mean precipitation values resulting from the simulated time series (represented by violin plots). Within each violin plot, the white boxplot highlights the quartiles and median. Fall months (September-November) exhibit greater variability in the simulations compared to the summer months (June-August). In some months (e.g., April, May, October), the observed values align closely with the median of the simulated data. However, in other months (e.g., January, September, November), discrepancies arise, with the model tending to either overestimate or underestimate the mean monthly precipitation. This discrepancy could be attributed to the choice of using a quarterly seasonality approach or to the limited ability of the marginal distribution to fully capture the characteristics of the data. We also clarify that the distribution was fitted using the least squares method, which does not explicitly preserve the mean and standard deviation of the data. Therefore, any slight deviations in these statistics are not limitations of the model itself, but rather a consequence of the fitting approach. If the method of moments had been used instead, the fitted gamma distribution would have explicitly matched the observed mean and standard deviation. However, we opted for the least squares method because it offers a better overall fit across the entire distribution, particularly in capturing the shape and tail behavior more accurately.

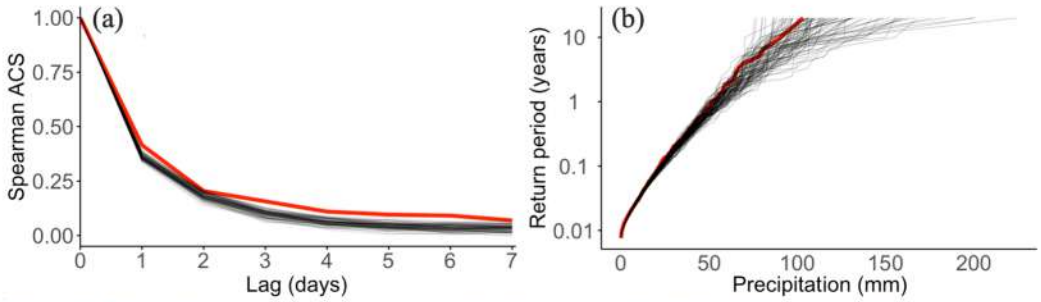

Figure 7: Plots of the comparison between (a) the Spearman ACS of the 100 simulated (black lines) and observed (red line) daily time series, (b) the daily rainfall accumulation as a function of the return period based on the 100 simulated (black lines) and observed (red line) time series.

Finally, the model's performance is evaluated by analyzing the rainfall events. For this analysis, events are selected based on a rule that requires a minimum 24-hour dry period between two consecutive and independent events. This allows us to focus on key characteristics of the rainfall events, such as event duration (D_e), total precipitation amount (H), and peak intensity (h_{max}). After identifying events in both the observed and simulated time series, we compare the empirical cumulative distribution functions of duration (Figure 8a), total precipitation (Figure 8b), and peak intensity (Figure 8c). Overall, the simulated and observed values for durations, total amounts, and peaks show good agreement. However, some differences emerge in the tails of the distributions, indicating discrepancies between the simulated and observed values for extreme events. To provide a comprehensive overview of the proposed analysis, we also compare the 90th, 95th, 99th, and 99.9th percentiles of event duration (Figure 8d), total event precipitation (Figure 8e), and peak event (Figure 8f). The results suggest that the CoSMoS-2s model effectively reproduces the event-scale characteristics of the observed daily time series. Although there is increased variability at the higher percentiles (Figure 8d, 8e, 8f), the agreement between the observed values and the simulated ones remains strong, indicating that the model can capture the behavior of extreme events with reasonable accuracy.

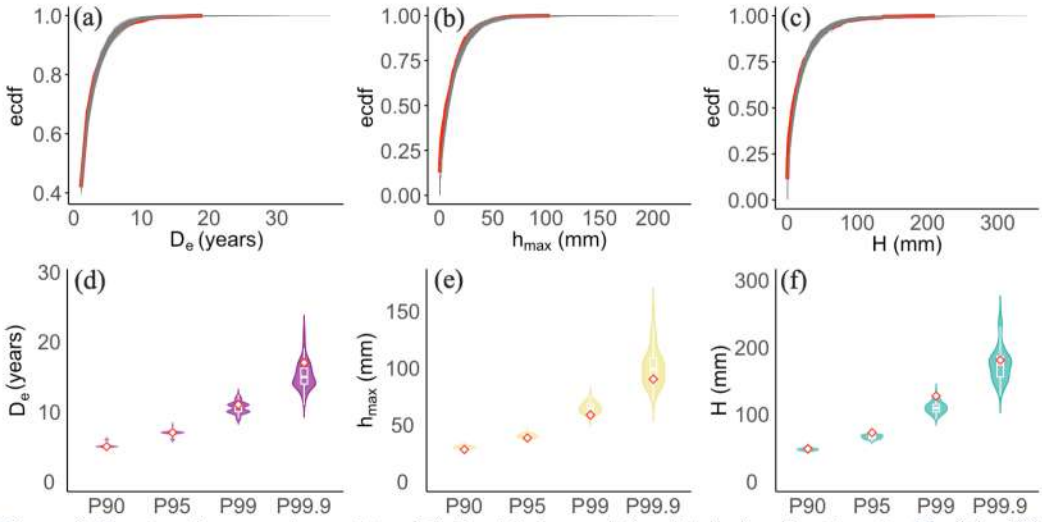

Figure 8: Event-scale comparisons plots of 1) Empirical cumulative distribution functions (ecdf) of the 100 simulated daily time series (black lines) and that of the observed (red line) daily time series for: (a) the duration D_e, (b) total precipitation H and (c) peaks h_{max}; 2) 90th, 95th, 99th and 99.9th (P90, P95, P99, P99.9) percentiles of the 100 simulated (violin plots) and those of observed (red diamonds) daily time series for: (d) the duration D_e, (e) total precipitation H and (f) peaks h_{max}.

Figure 5: Comparison between monthly seasonal components of observed (red diamond ◇) and those of the 100 simulated (violin plots) daily time series

In Figure 6, the comparison of the highest (1st), median (10th), and lowest (20th) ranked annual maximum rainfall depths across various durations (1 to 6 days), computed from 100 simulated daily time series (violin plots) and the observed record (red diamonds), reveals that the observed annual maximum rainfall values fall within the range of variability of the simulated extremes for all considered durations. However, for the highest ranked annual maximum rainfall depths (Figure 6a), greater variability is observed across different durations. Overall, the simulated daily time series can be considered to adequately replicate the ranked annual maximum rainfall depths for different daily durations when compared to the observed series.

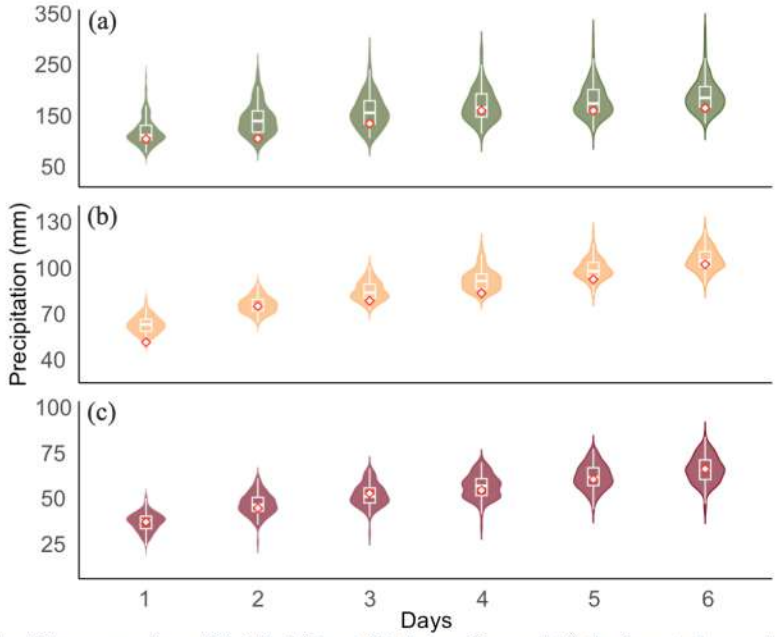

Figure 6: Plots of the comparison of: (a) the highest, (b) the median, and (c) the lowest observed ranked annual maxima at different durations (red diamonds) and the annual maxima extracted from the 100 simulated daily time series (violin plots).

Generally, it is essential for a rainfall simulation model to accurately replicate both the autocorrelation structure of the observed time series and the rainfall to ensure reliable predictions. The autocorrelation structures of the 100 simulated daily time series (Figure 7a) closely resemble that estimated from the observed data, indicating the ability of CoSMoS-2s model to accurately reproduce the Spearman's ACS. Furthermore, the comparison of the daily rainfall accumulation as a function of the return period based on the 100 simulated and observed time (Figure 7b), shows that the results are tightly clustered for lower return periods, demonstrating good agreement with the observed relationship. However, as the return period increases, so does the variability of the simulated rainfall amounts, which is a common feature in extreme value analysis. This increased dispersion at higher return periods reflects the inherent uncertainty of rarer events, indicating that while the model can capture the overall trend, its accuracy diminishes for extreme and infrequent events.

Based on the comprehensive comparisons between the simulated and observed daily time series, we can conclude that the model effectively captures the key statistical properties of daily precipitation data with a high degree of accuracy for the considered raingauge. Furthermore, despite the limited sample size of the observed data, the model successfully reproduces the statistical properties of the rainfall time series.

3.3. Model Performance Across the Entire Dataset

In this section, the previous analyses are extended to the entire Arno River dataset to evaluate the model's capability in reproducing key statistical properties of the observed daily time series. To provide a clear view of the model's performance, we select 24 indicators because they comprehensively capture different aspects of the statistical properties of the simulated time series. These indicators help evaluate the model's ability to replicate real-world precipitation patterns at various temporal scales, which is crucial for accurate simulations. The three groups of indicators are defined as follows:

1. Annual Maxima indicators: 18 indicators related to the 1st (highest), the 10th (median), and the 20th (lowest) ranked annual maxima rainfall intensities at the different time scale extracted from the corresponding 100 simulated time series, named as HRAM-Dn (Highest Ranked Annual Maxima with duration n); MRAM-Dn (Median Ranked Annual Maxima with duration n); and LRAM-Dn (Lowest Ranked Annual Maxima with duration n) where n ranges from 1 to 6 days.
2. Percentile indicators: three indicators related to the three percentiles (97.5th, 99th, and 99.9th), named P97.5, P99, and P99.9.
3. Spearman's ACS indicators: three indicators related to the Spearman's ACS coefficients for lags equal to 1, 2, and 3, denoted as $\rho_S(1), \rho_S(2)$ and $\rho_S(3)$.

Each indicator is defined as the ratio between the median of the 100 values resulting from the simulated time series and the value calculated from the observed time series. Choosing the median helps ensure that the analysis is not influenced by outliers, leading to more robust and reliable results. The ratio indicates whether the model tends to overestimate or underestimate a specific statistical property under consideration. Specifically,

1. A ratio close to 1 indicates that the median is near the observed value, indicating good reproduction of a specific property
2. A ratio greater than 1 suggests a tendency of the model to overestimate.
3. A ratio less than 1 indicates a tendency of the model to underestimate.

The performance of the CoSMoS-2s model is evaluated by analyzing the behavior of the proposed indicators calculated for the entire Arno River Basin dataset. The indicator distributions (Figure 9) resulting from the analysis provide a clear understanding of the model performance. The distribution of HRAM-Dn indicators (Figure 9a) exhibits greater variability compared to the distributions of MRAM-Dn and LRAM-Dn indicators (Figure 9b and 9c), as expected. The latter two are characterized by lower variability and their distributions are centered around 1, indicating the model's ability to reproduce these properties accurately. The HRAM-Dn indicators suggest that the model slightly overestimates the highest ranked annual maxima rainfall intensities at different durations. The percentile indicators (represented by gold distributions in Figure 9d) show that CoSMoS-2s is generally perform well in reproducing the extreme values observed in the daily time series. However, for the 99.9th percentile, there is a tendency for the model to overestimate the extreme tail of the distribution. Finally, the Spearman's ACS coefficient indicators (orange distributions in Figure 9d) show that the model underestimates the Spearman's ACS coefficients, with the underestimation becoming more pronounced as the time lag increases. This matches the findings in Figure 7a, which pertain to a single raingauge. The results highlight the model's ability to closely mimic intermittent processes, despite some minor over- or underestimations in some statistical properties. These discrepancies could potentially be mitigated by using longer time series, which would provide more information and allow for greater accuracy.

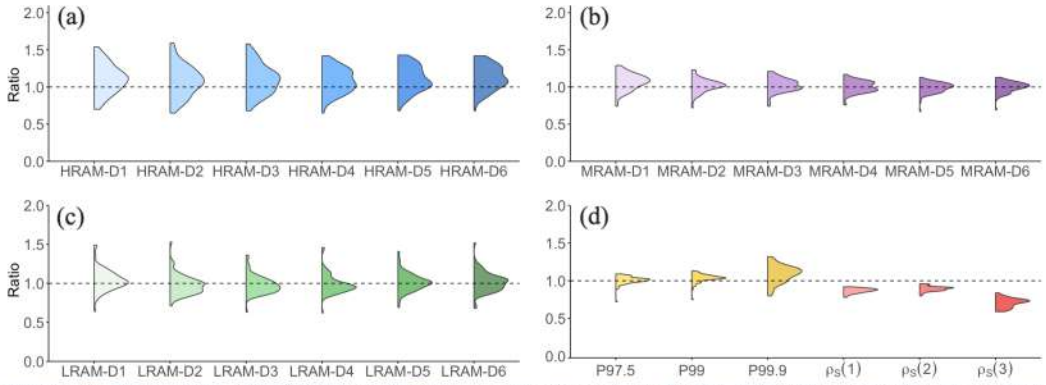

Figure 9: Plots of the CoSMoS-2s performance evaluation across the 70 daily time series based on three criteria: (a) the 1st (highest), (b) 10th (median), and (c) 20th (lowest) ranked annual maxima at six durations extracted from 100 simulated time series, denoted as HRAM-Dn (Highest Ranked Annual Maxima for duration n), MRAM-Dn (Median Ranked Annual Maxima for duration n), and LRAM-Dn (Lowest Ranked Annual Maxima for duration n), where n ranges from 1 to 6 days; (d) the 97.5th, 99th, and 99.9th percentiles of the rainfall distribution (P97.5, P99, and P99.9) and the Spearman's ACS coefficients at lag 1, 2 and 3 ($\rho_S(1), \rho_S(2)$ and $\rho_S(3)$).

5. Conclusion

In this study, we conduct a comprehensive evaluation of the two-state intermittent model (CoSMoS-2s) applied for single-site time series generation, as introduced by Papalexiou (2022), using real-world case studies. Our aim is to bridge the model's inherent flexibility with its practical usability by assessing its performance in real-world scenarios, ensuring that it remains both theoretically robust and operationally applicable, even under data-limited conditions. We used a single daily time series from a raingauge in the Arno River Basin and the entire Arno River dataset, comprising 70 daily time series. In addition to the inherent challenges of working with real data, a significant difficulty arises from the limited data availability, as each time series covers only a 20-year period. To address this, we implemented a data grouping based on quarterly seasonality, rather than the monthly scale approach suggested in Papalexiou (2022).

To assess the model's performance, we generated 100 daily time series using the observed daily time series and compared various statistical properties, including summary statistics, Spearman autocorrelation structure, monthly seasonal components, as well as the highest, median, and lowest ranked annual maxima rainfall intensities at different durations. At the event scale, properties such as event duration, total event amount, and event peak were also analyzed. Crucially, our study aimed to configure CoSMoS-2s in a parsimonious manner, ensuring easy calibration while preserving strong performance—an essential factor for operational applications. Across the case studies, the model demonstrated a remarkable ability to reproduce an intermittent process while preserving statistical characteristics. Furthermore, the implementation was computationally efficient due to the choice of quarterly seasonality and the use of empirical Spearman's ACS over a parametric one. By employing a Gamma distribution (2 parameters) and considering four seasons, the model was streamlined to only eight parameters. This minimalistic setup not only reduces computational burden but also enhances the model's applicability in practical hydrological studies, particularly in data-scarce regions.

Overall, these results highlight that CoSMoS-2s is not only a theoretically flexible model but also a practical and robust tool for rainfall simulation under real-world constraints. By validating its performance in an operationally relevant setting, this study reinforces its potential for use in hydrological applications where data availability and calibration effort are limiting factors.

Acknowledgments

This study was carried out within the RETURN Extended Partnership and was performed as part of the IAHS HELPING Working Group on "Hydrologic Design: Solutions and Communication".

Authors' contributions Conceptualization: all authors; Methodology: SM.P.; Software and Validation: F.C.; Formal analysis and Investigation: all authors; Data Curation: F.C.; Writing (original draft): F.C., SM.P.; Writing (review & editing): all authors; Visualization and Supervision: all authors; Funding Acquisition: E.V., S.G.

Funding Elena Volpi e Salvatore Grimaldi acknowledge support from the European Union Next-GenerationEU (National Recovery and Resilience Plan – NRRP, Mission 4, Component 2, Investment 1.3 – D.D. 1243 2/8/2022, PE0000005).

Data availability Datasets were generated or analysed during the current study will be made available on request.

Code availability Not applicable.

Declarations

Ethics approval This work complied with all the necessary ethical approval processes.

Competing interest The authors declare no competing interests.

Consent to participate Not applicable.

Consent for publication The author agrees to publish.

References

Baum, R. (1957). The correlation function of smoothly limited Gaussian noise. IRE Transactions on Information Theory, 3(3), 193–197. https://doi.org/10.1109/TIT.1957.1057415.

Bardossy, A., & Plate, E. J. (1992). Space-time model for daily rainfall using atmospheric circulation patterns. Water Resources Research, 28(5), 1247–1259. https://doi.org/10.1029/91WR02589

Bardossy, A., & Pegram, G. G. S. (2009). Copula based multisite model for daily precipitation simulation. Hydrology and Earth System Sciences, 13(12), 2299.

Beck, H. E., Wood, E. F., McVicar, T. R., Zambrano-Bigiarini, M., Alvarez-Garreton, C., Baez-Villanueva, O. M., et al. (2020). Bias correction of global high-resolution precipitation climatologies using streamflow observations from 9372 catchments. Journal of Climate, 33(4), 1299–1315. https://doi.org/10.1175/JCLI-D-19-0332.1

Box, G. E. P., & Jenkins, G. M. (1970). Time series analysis: Forecasting and control. Holden Day.

Cappelli F., S.M. Papalexiou, Y. Markonis, and S. Grimaldi (2024a). PyCoSMoS: An advanced toolbox for simulating real-world hydroclimatic data, *Environmental Modelling & Software*, 178,106076.

Cappelli, F.; Volpi, E.; Langousis, A.; Deidda, R.; Perdios, T.; Furcolo, P.; Grimaldi, S. (2024b). Sub-daily rainfall simulation using multifractal canonical disaggregation: A parsimonious calibration strategy based on Intensity-Duration-Frequency curves. *Stoch Environ Res Risk Assess* (2024). https://doi.org/10.1007/s00477-024-02827-8

Cappelli, F.; Volpi, E.; Langousis, A.; Deidda, R.; Perdios, T.; Grimaldi, S. (2025). Rainfall simulation based on the parsimonious calibration of a multifractal canonical disaggregation scheme in the Arno River Basin, Italy (under review).

Clark, M., Gangopadhyay, S., Hay, L., Rajagopalan, B., & Wilby, R. (2004). The Schaake shuffle: A method for reconstructing space–time variability in forecasted precipitation and temperature fields. Journal of Hydrometeorology, 5(1), 243–262. https://doi.org/10.1175/1525-754

Chandler, R. E., Isham, V. S., Wheater, H. S., Onof, C. J., Leith, N., Frost, A. J., & Segond, M. L. (2007). Spatial-temporal rainfall modelling with climate change scenarios. *Dept. for Environment, Food and Rural Affairs, UK*.

Cowpertwait, P. S. P. (1991). Further developments of the Neyman-Scott clustered point process for modeling rainfall. Water Resources Research, 27(7), 1431–1438. https://doi.org/10.1029/91WR00479

Cox, D. R., and Isham, V. (1980). Point processes. CRC Press.

Deidda, R. (2000). Rainfall downscaling in a space-time multifractal framework. Water Resources Research, 36(7), 1779–1794. https://doi.org/10.1029/2000WR900038.

Fischer, S., Dallan, E., Fiori, A., Grimaldi, S., Kochanek, K., Prieto, C., Reis, D.S., Jr. & Volpi, E. (2025) Hydrological design in the HELPING decade–inspiring the community to innovate the hydrological design concept, Hydrological Sciences Journal, 70 (3), pp. 375 - 389, 10.1080/02626667.2024.2436634

Gabriel, K. R., & Neumann, J. (1957). On a distribution of weather cycles by length. Quarterly Journal of the Royal Meteorological Society, 83(357), 375–380. https://doi.org/10.1002/qj.49708335714

Gabriel, K. R., & Neumann, J. (1962). A Markov chain model for daily rainfall occurrence at Tel Aviv. Quarterly Journal of the Royal Meteorological Society, 88(375), 90–95. https://doi.org/10.1002/qj.49708837511

Gaume, E., Mouhous, N., & Andrieu, H. (2007). Rainfall stochastic disaggregation models: Calibration and validation of a multiplicative cascade model. Advances in Water Resources, 30(5), 1301–1319. https://doi.org/10.1016/j.advwatres.2006.11.007

Glasbey, C. A., & Nevison, I. M. (1997). Rainfall modeling using a latent Gaussian variable. In T. G. Gregoire, D. R. Brillinger, P. J. Diggle, E. Russek-Cohen, W. G. Warren, & R. D. Wolfinger (Eds.), Modeling longitudinal and spatially correlated data (pp. 233–242). Springer. https://doi.org/10.1007/978-1-4612-0699-6_20

Grassberger, P. (1983). Generalized dimensions of strange attractors. Physics Letters A, 97(6), 227–230. https://doi.org/10.1016/0375-9601(83)90753-3

Iizumi, T., Takikawa, H., Hirabayashi, Y., Hanasaki, N., & Nishimori, M. (2017). Contributions of different bias-correction methods and reference meteorological forcing data sets to uncertainty in projected temperature and precipitation extremes. Journal of Geophysical Research: Atmospheres, 122(15), 7800–7819. https://doi.org/10.1002/2017JD026613

Kim, S., Joo, K., Kim, H., Shin, J.-Y., and Heo, J.-H. (2021). Regional quantile delta mapping method using regional frequency analysis for regional climate model precipitation. Journal of Hydrology, 596, 125685. https://doi.org/10.1016/j.jhydrol.2020.125685

Langousis, A., and D. Veneziano (2007). Intensity-duration-frequency curves from scaling representations of rainfall, *Water Resources Research*, 43 (2), doi: 10.1029/2006WR005245.

Langousis, A., and Veneziano, D. (2007). Intensity-duration-frequency curves from scaling representations of rainfall. Water Resources Research, 43(2), W02422. https://doi.org/10.1029/2006WR005245.

Langousis, A., D. Veneziano, P. Furcolo, C. Lepore (2009). Multifractal rainfall extremes: Theoretical analysis and practical estimation, *Chaos, Solitons and Fractals*, 39 (3), pp. 1182-1194, https://doi:10.1016/j.chaos.2007.06.004.

Li, C., Zwiers, F., Zhang, X., Li, G., Sun, Y., and Wehner, M. (2021). Changes in annual extremes of daily temperature and precipitation in CMIP6 models. Journal of Climate, 34(9), 3441–3460. https://doi.org/10.1175/JCLI-D-19-1013.1

Matalas, N. C. (1967). Mathematical assessment of synthetic hydrology. Water Resources Research, 3(4), 937–945. https://doi.org/10.1029/WR003i004p00937

Mandelbrot, B. B. (1982). The fractal geometry of nature (2nd prt. ed.). Times Books.

Markov, A. A. (1906). Rasprostranenie zakona bol'shih chisel na velichiny, zavisyaschie drug ot druga. Izvestiya Fiziko-Matematicheskogo Obschestva Pri Kazanskom Universitete, 2-ya seriya, 5(94), 135–156.

Molnar, P., & Burlando, P. (2005). Preservation of rainfall properties in stochastic disaggregation by a simple random cascade model. Atmospheric Research, 77(1), 137–151. https://doi.org/10.1016/j.atmosres.2004.10.024

Nerantzaki, S. D., & Papalexiou, S. M. (2022). Assessing extremes in hydroclimatology: A review on probabilistic methods. Journal of Hydrology, 605, 127302. https://doi.org/10.1016/j.jhydrol.2021.127302

Neyman, J., & Scott, E. L. (1958). Statistical approach to problems of cosmology. Journal of the Royal Statistical Society: Series B, 20(1), 1–43. https://doi.org/10.1111/j.2517-6161.1958.tb00272.x

Papalexiou S.M. (2018). Unified theory for stochastic modelling of hydroclimatic processes: Preserving marginal distributions, correlation structures, and intermittency, *Advances in Water Resources*, 115, pp. 234 – 252.

Papalexiou, S. M. (2022). Rainfall generation revisited: Introducing CoSMoS-2s and advancing copula based intermittent time series modeling. Water Resources Research, 58, e2021WR031641. https://doi.org/10.1029/2021WR031641

Papalexiou, S. M., Serinaldi, F., & Clark, M. P. (2023). Large-domain multisite precipitation generation: Operational blueprint and demonstration for 1,000 sites. *Water Resources Research*, *59*(3), e2022WR034094.

Rios Gaona, M. F., Michaelides, K., & Singer, M. B. (2024). STORM v. 2: A simple, stochastic rainfall model for exploring the impacts of climate and climate change at and near the land surface in gauged watersheds. *Geoscientific Model Development*, *17*(13), 5387-5412.

Rodriguez-Iturbe, I., Cox, D. R., & Isham, V. (1987). Some models for rainfall based on stochastic point processes. Proceedings of the Royal Society of London—Series A: Mathematical and Physical Sciences, 410(1839), 269–288.

Schertzear, D., & Lovejoy, S. (1987). Physical modeling and analysis of rain and clouds by anisotropic scaling multiplicative processes. In 1987, rainfall fields: Estimation, analysis, and prediction (pp. 9693–9714). American Geophysical Union (AGU). https://doi.org/10.1002/9781118782071.ch16

Serinaldi, F. (2009). Copula-based mixed models for bivariate rainfall data: An empirical study in regression perspective. Stochastic Environmental Research and Risk Assessment, 23(5), 677–693. https://doi.org/10.1007/s00477-008-0249-z

Singer, M. B., Michaelides, K., & Hobley, D. E. (2018). STORM 1.0: a simple, flexible, and parsimonious stochastic rainfall generator for simulating climate and climate change. *Geoscientific Model Development*, *11*(9), 3713-3726.

Spearman, C. (1904). The proof and measurement of association between two things. American Journal of Psychology, 15(1), 72–101. https://doi.org/10.2307/1412159

Stern, R. D., & Coe, R. (1984). A model fitting analysis of daily rainfall data. Journal of the Royal Statistical Society: Series A, 147(1), 1–34. https://doi.org/10.2307/2981736

Veneziano, D., Langousis, A., & Furcolo, P. (2006). Multifractality and rainfall extremes: A review. Water Resources Research, 42(6), W06D15. https://doi.org/10.1029/2005WR004716

Volpi E., Grimaldi, S., Aghakouchak, A., Castellarin, A., Chebana, F., Papalexiou, S.M., Aksoy, H., Bárdossy, A., Cancelliere, A., Chen, Y., Deidda, R., Haberlandt, U., Eris, E., Fischer, S., Francés, F., Kavetski, D., Rodding Kjeldsen, T., Kochanek, K., Langousis, A., Mediero Orduña, L., Montanari, A., Nerantzaki, S.D., Ouarda, T.B.M.J., Prosdocimi, I., Ragno, E., Rajulapati, C.R., Requena, A.I., Ridolfi, E., Sadegh, M., Schumann, A., & Sharma, A. (2024) The legacy of STAHY: milestones, achievements, challenges, and open problems in statistical hydrology, Hydrological Sciences Journal, 69 (14), pp. 1913 - 1949, 10.1080/02626667.2024.2385686

Wheater, H. S., Chandler, R. E., Onof, C. J., Isham, V. S., Bellone, E., Yang, C., et al. (2005). Spatial-temporal rainfall modeling for flood risk estimation. Stochastic Environmental Research and Risk Assessment, 19(6), 403–416. https://doi.org/10.1007/s00477-005-0011-8

Wilks, D. S., & Wilby, R. L. (1999). The weather generation game: A review of stochastic weather models. Progress in Physical Geography: Earth and Environment, 23(3), 329–357. https://doi.org/10.1177/030913339902300302

5. Multisite Rainfall Simulation in the Arno River Basin in Italy

Multisite Rainfall Simulation in the Arno River Basin in Italy

Summary

This document presents a comprehensive multisite precipitation simulation framework based on the two-state CoSMoS-2s model, designed to realistically reproduce the spatiotemporal characteristics of rainfall across a large domain. Building on the limitations of earlier stochastic rainfall models, CoSMoS-2s explicitly separates the simulation into a binary process for wet/dry states and a continuous process for rainfall intensities, each modeled using Gaussian vector autoregressive (VAR) processes. A semiparametric strategy was employed to combine empirical and parametric components, balancing accuracy and computational feasibility across 70 stations. The binary and nonzero components were calibrated using seasonally adaptive statistics, transformed via correlation transformation functions, and simulated independently before being recombined to produce final time series. The model was evaluated through detailed station-level diagnostics and additional assessments at the multi-station and catchment scale, including comparisons of autocorrelations, distributional moments, wet/dry spell statistics, and scaling properties. Results showed excellent agreement between observed and simulated rainfall characteristics at all spatial scales. Notably, cross-correlations, L-moments, and spell durations were well preserved, with only a minor underestimation of the standard deviation in aggregated catchment precipitation—likely due to spatial averaging. Overall, the CoSMoS-2s framework demonstrated robust performance, capturing key features of rainfall variability, intermittency, and dependence structure over both time and space.

1. Methodology and Model Overview

Rainfall is characterized by intermittent and highly variable behavior across different temporal and spatial scales, which makes its simulation inherently challenging. Numerous stochastic models have been proposed over recent decades, including cluster-based point processes (e.g., Neyman-Scott and Bartlett-Lewis), Markov chains for wet/dry transitions, multifractal approaches leveraging scale-invariance, and autoregressive or copula-based frameworks to model temporal and spatial dependence. Despite their utility, none of these methods individually reproduces all essential features of rainfall processes comprehensively.

To overcome these limitations, the Complete Stochastic Modelling Solution (CoSMoS) framework was developed, which combines flexible marginal distributions with transformed Gaussian processes to simultaneously reproduce rainfall intermittency, marginal behavior, and correlation structures. Within this framework, two main variants exist: the single-state CoSMoS-1s (Papalexiou, 2018) and the two-state CoSMoS-2s model (Papalexiou, 2022). The CoSMoS-1s treats rainfall as a single intermittent process using mixed-type marginals and autocorrelation structures, whereas the CoSMoS-2s separates rainfall simulation into two distinct processes—a binary wet/dry process and a continuous rainfall intensity process—allowing explicit preservation of each component's autocorrelation structure and marginal distributions.

Recent analyses (Papalexiou, 2022) have demonstrated that CoSMoS-2s outperforms CoSMoS-1s in realistically reproducing key rainfall characteristics, such as wet and dry spell distributions, moment scaling, and extremes across multiple temporal scales. Its superior performance is attributed to the two-state modeling approach, explicitly capturing rainfall intermittency and intensity dynamics separately.

Multisite precipitation simulation introduces additional complexity, particularly when applied over large spatial domains. Despite advances in remote sensing technologies and availability of high-resolution datasets, such data typically have limited temporal coverage, necessitating stochastic modeling for generating realistic long-term scenarios. Traditional modeling approaches (point processes, resampling, and disaggregation) often face scalability and accuracy issues when extended spatially, especially regarding extreme events and wet/dry spells. Although parametric time series approaches provide scalability, they remain computationally challenging and are rarely applied to extensive station networks.

In a previous study (Papalexiou et al., 2023), the CoSMoS-1s framework was adapted for large-domain multisite simulation by employing a transformation strategy. To address the computational burden associated with estimating correlation transformation functions (CTFs) for each pair of stations, the approach transformed all time series to mixed-type Uniform distributions. This allowed the use of a single, site-independent CTF, significantly improving computational efficiency. However, since this method inherits the limitations of the CoSMoS-1s approach, the present study instead utilizes a multisite extension of the CoSMoS-2s framework, thereby leveraging its demonstrated advantages in accurately simulating rainfall intermittency and dependence structures across large spatial scales.

2. Challenges and Strategies for Multisite Simulation

Multisite rainfall simulation involves capturing complex dependencies both spatially and temporally, dealing with heterogeneity in marginal distributions across locations, and managing computational burdens for large-scale scenarios. As highlighted by Papalexiou et al. (2023), three general modeling strategies, that is, nonparametric, parametric, and semiparametric, can address these challenges, each with distinct strengths and limitations.

- Nonparametric strategies aim to directly reproduce observed spatial cross-correlations and site-specific autocorrelations using empirical estimates derived from transformed time series. This method offers maximum flexibility and accuracy in replicating observed dependencies but becomes computationally intensive and often impractical at large scales due to the complexity involved in estimating and inverting dense correlation matrices.
- Parametric strategies provide a scalable alternative by fitting analytical spatiotemporal correlation structures (STCS). These structures describe correlations as mathematical functions of spatial distance and temporal lag, significantly reducing computational complexity. For example, Papalexiou and Serinaldi (2020) introduced the Clayton-Weibull STCS, a compact model suitable for large-domain simulation. However, parametric models, while efficient, might fail to capture detailed local dependencies accurately due to their parsimonious nature.
- Semiparametric strategies blend empirical and parametric components, using observed correlations at specific temporal lags or spatial scales and parametric structures elsewhere. This hybrid approach combines computational tractability with local realism and accuracy, effectively addressing spatial heterogeneity and nonstationarities. Nevertheless, preserving exact lag-0 correlations is impossible when station-specific autocorrelation structures vary significantly. Papalexiou et al. (2023) demonstrated that this limitation is generally minor if station autocorrelations are reasonably similar.

This study applies the semiparametric approach within the CoSMoS-2s framework, balancing accuracy and computational feasibility to effectively simulate rainfall across multiple sites.

3. Application and Implementation Details

In the multisite CoSMoS-2s implementation, rainfall simulation involves two coupled but distinct processes: (1) a binary process for wet/dry occurrences and (2) a continuous process for rainfall intensity on wet days. Each component is modeled separately using Gaussian parent vector autoregressive (VAR) processes.

3.1 Simulation of the Binary (Wet/Dry) Process

The binary simulation involves the following steps:

1. Transformation to binary series: Original rainfall records at each of the 70 stations are converted into binary sequences (wet days assigned as 1, dry days as 0).
2. Cross-correlations: Empirical lag-0 cross-correlation matrices are estimated monthly across all stations.
3. Autocorrelation structures (ACS): Station-specific empirical autocorrelations are computed separately for each month.
4. ACS parameterization: A parametric Weibull autocorrelation structure is fitted to these empirical ACS values for each station.
5. Correlation transformation: Both empirical lag-0 correlation matrices and the parametric ACS estimates are transformed via a binary correlation transformation function (CTF) to their Gaussian equivalents.
6. Gaussian VAR model: A VAR(10) model with diagonal parameter matrices is utilized, reproducing spatial lag-0 cross-correlations and temporal autocorrelation structures at each station explicitly up to ten days.
7. Probability of zero: Daily probabilities of zero rainfall at each station are estimated using a two-month moving window based on observed data.
8. Binary outcome generation: Gaussian simulations are converted into wet/dry states by applying the daily zero-probability thresholds derived previously in the Gaussian time series.

3.2 Simulation of the Nonzero (Rainfall Intensity) Process

The nonzero rainfall intensities are simulated with a similar but specialized approach:

1. Estimation of parameters: Daily mean and standard deviation of nonzero rainfall at each station are computed using a two-month moving window.
2. Marginal distributions: Gamma distributions parameterized by the seasonal patterns of the mean and standard deviation are fitted individually for each station and each day.
3. Conditional cross-correlations: Monthly empirical lag-0 cross-correlation matrices are estimated conditionally on days with nonzero rainfall across all stations.
4. Conditional ACS: Empirical conditional autocorrelation structures for nonzero values are estimated for each station and month.
5. Parametric ACS fitting: Parametric Weibull ACS models are fitted to the empirical conditional ACSs for each station.
6. Gaussian correlation transformation: Empirical conditional cross-correlation matrices and parametric ACS estimates are transformed into Gaussian correlation structures via a correlation transformation function (CTF), incorporating the previously fitted Gamma distributions.

7. Gaussian VAR simulation: A VAR(1) Gaussian model with diagonal parameter matrices reproduces the spatial cross-correlations and temporal autocorrelations for each station's nonzero rainfall series.
8. Intensity generation: The simulated Gaussian series are transformed back into rainfall intensities using the inverse of the fitted Gamma distributions on a daily basis.

Finally, the multisite precipitation series are generated by multiplying the binary wet/dry simulations by the nonzero rainfall intensity simulations, producing realistic synthetic rainfall records that preserve key statistical properties at all stations. Further methodological and technical details are discussed comprehensively in Papalexiou (2018, 2022) and Papalexiou et al. (2023).

4. Results

4.1 Simulation Assessment per Station

In this study, synthetic precipitation time series spanning 2000 years were generated for each station, provided as four segments of 500 years each. Each station's simulated series was assessed thoroughly by comparing simulated results against the 20-year observed precipitation characteristics. Specifically, a detailed multi-panel graphical summary was created per station, comprising multiple diagnostic plots to evaluate the performance and realism of the simulation comprehensively. Below, we provide the first multi-panel graph for the first station (Pluviometro 00) and next we describe each graph's purpose, construction, and usefulness.

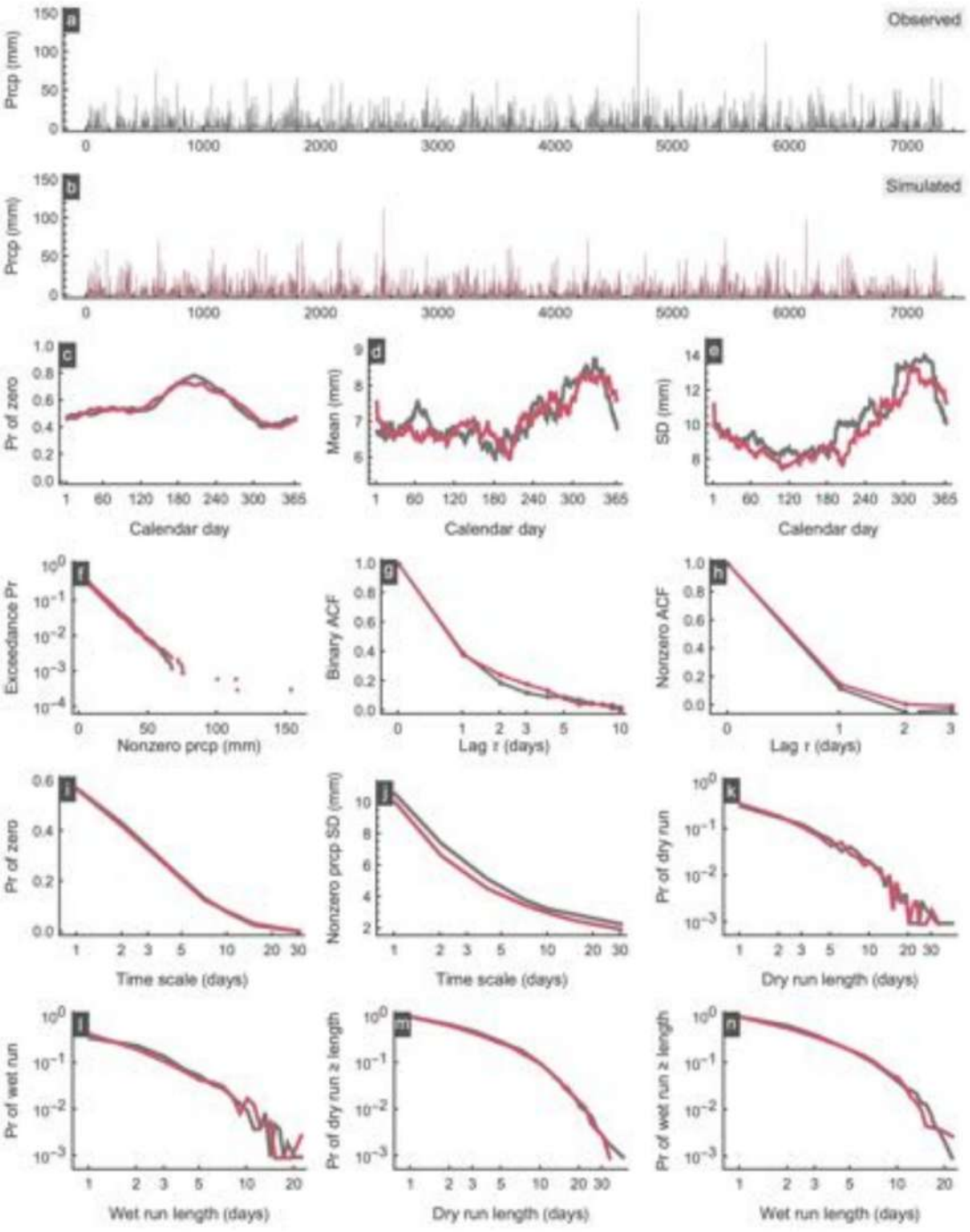

Figure 1. Simulation assessment for the first station (Pluviometro 00). (a) and (b) observed and simulated time series; (c) probability of zero rainfall; (d) mean rainfall intensity; (e) standard deviation of rainfall intensity; (f) exceedance probability of nonzero rainfall; (g) binary autocorrelation structure; (h) nonzero rainfall autocorrelation structure; (i) scaling of probability of zero; (j) scaling of standard deviation; (k) probability mass function of dry spell length; (l) probability mass function of wet spell length; (m) complementary cumulative distribution of dry spell length; (n) complementary cumulative distribution of wet spell length.

- **Panels (a) and (b): Observed and Simulated Rainfall Time Series**. These panels visually depict rainfall daily amount over time, comparing observed precipitation (panel a) and simulated precipitation (panel b). This direct comparison quickly illustrates whether the simulation realistically captures the variability, intensity, and intermittency observed in the actual rainfall record.
- **Panel (c): Seasonal Probability of Zero Rainfall**. This graph shows the daily probability of zero rainfall (dry days) throughout the year. It compares the seasonal pattern of observed and simulated probabilities, assessing the model's ability to reproduce the annual cycle of intermittency.
- **Panel (d): Seasonal Mean Rainfall Intensity.** This plot illustrates the average rainfall intensity on wet days for each calendar day, highlighting the seasonal cycle. Comparing observed and simulated values ensures the model accurately represents seasonal patterns of rainfall intensity.
- **Panel (e): Seasonal Standard Deviation of Rainfall Intensity.** Here, the variability of rainfall on wet days throughout the year is shown. This comparison verifies that the simulation correctly reproduces daily variability and seasonal fluctuations observed historically.
- **Panel (f): Exceedance Probability of Nonzero Rainfall.** This probabilistic plot provides empirical exceedance probabilities for nonzero daily rainfall amounts, comparing observed and simulated distributions. It ensures the simulated intensities are realistic across the full range, particularly for higher rainfall amounts that are critical for extremes analysis.
- **Panel (g): Autocorrelation Structure (ACS) of the Binary (Wet/Dry) Process.** This plot shows the autocorrelation of wet/dry sequences, comparing observed and simulated values for different temporal lags (1 to 10 days). It evaluates how well the simulation captures persistence in rainfall occurrence.
- **Panel (h): Autocorrelation Structure (ACS) of Nonzero Rainfall Intensities.** Similar to the binary ACS, this graph presents the autocorrelation of nonzero rainfall intensities. It helps verify that the simulation realistically preserves the temporal dependence of rainfall amounts.
- **Panel (i): Scaling of Probability of Zero Rainfall with Time Scale.** This plot examines how the probability of zero rainfall days scales as daily data are aggregated into larger time scales (up to 30 days). It checks whether the simulation maintains realistic intermittency characteristics across multiple temporal resolutions.
- **Panel (j): Scaling of Standard Deviation for Nonzero Rainfall with Time Scale.** Depicting the standard deviation of nonzero rainfall aggregated over varying time scales, this plot assesses if the simulation maintains realistic variability when transitioning from daily to longer time scales.
- **Panel (k) and (m): Probability of Dry Spell Length.** These graphs evaluate how well the simulation captures the characteristics of dry spells. Panel (k) shows the probability mass function (PMF)—the probability of observing a dry spell of exactly a specified length, while panel (m) displays the complementary cumulative distribution function (CCDF)—the probability of observing a dry spell of at least the specified length. Together, these plots verify the accurate simulation of dry-spell durations, which are essential for drought risk assessment.

- **Panel (l) and (n): Probability of Wet Spell Length.** Analogously, these panels assess the durations of wet spells. Panel (l) depicts the probability mass function (PMF), representing the probability of a wet spell lasting exactly a given number of days, whereas panel (n) shows the complementary cumulative distribution function (CCDF), indicating the probability of a wet spell lasting at least that duration. These plots help confirm the model's effectiveness in reproducing prolonged rainfall events, which are critical for flood management and water resource planning.

All these detailed graphical evaluations for each individual station are provided in the Annex (see Figures A1 to A69). Overall, these results demonstrate that the simulated rainfall series closely match the observed statistical properties, confirming the excellent performance of the adopted modeling approach.

4.2 Simulation Assessment of Multiple Stations and at the Catchment Scale

Beyond the previous detailed analysis conducted for each individual station, additional assessments are provided here to evaluate the performance of the simulation collectively across all stations and at the catchment scale. Specifically, we present side-by-side comparisons of several key statistics across all stations between observed and simulated data, evaluate the lag-0 correlation matrices for both wet/dry (binary) and nonzero rainfall processes, and examine aggregated precipitation at the catchment scale.

These additional analyses are presented through three separate figures, each focusing on a distinct aspect of the simulation assessment. Specifically:

Observed and simulated lag-0 correlation plot (Figure 2). The first row (panels a–c) shows the lag-0 correlation matrices for the binary (wet/dry) rainfall process, with the observed correlation matrix (a), the simulated correlation matrix (b), and the histogram of differences between the simulated and observed correlations (c). The second row (panels d–f) provides the same information for the nonzero rainfall process, including observed correlations (d), simulated correlations (e), and the histogram of their differences (f).

These plots demonstrate the effectiveness of the simulation in capturing spatial dependencies across stations for both rainfall occurrence and intensity. Notably, the color patterns in the correlation matrices are nearly identical between observed and simulated data for both the wet/dry and nonzero processes, indicating strong spatial agreement. This is further confirmed by the histograms of correlation differences, which are tightly centered around zero and show very low deviations, highlighting the high fidelity of the simulated spatial dependence structure. It is also evident that the binary (wet/dry) process exhibits stronger cross-correlations across stations compared to the nonzero rainfall process—reflecting the higher spatial coherence of rainfall occurrence relative to intensity.

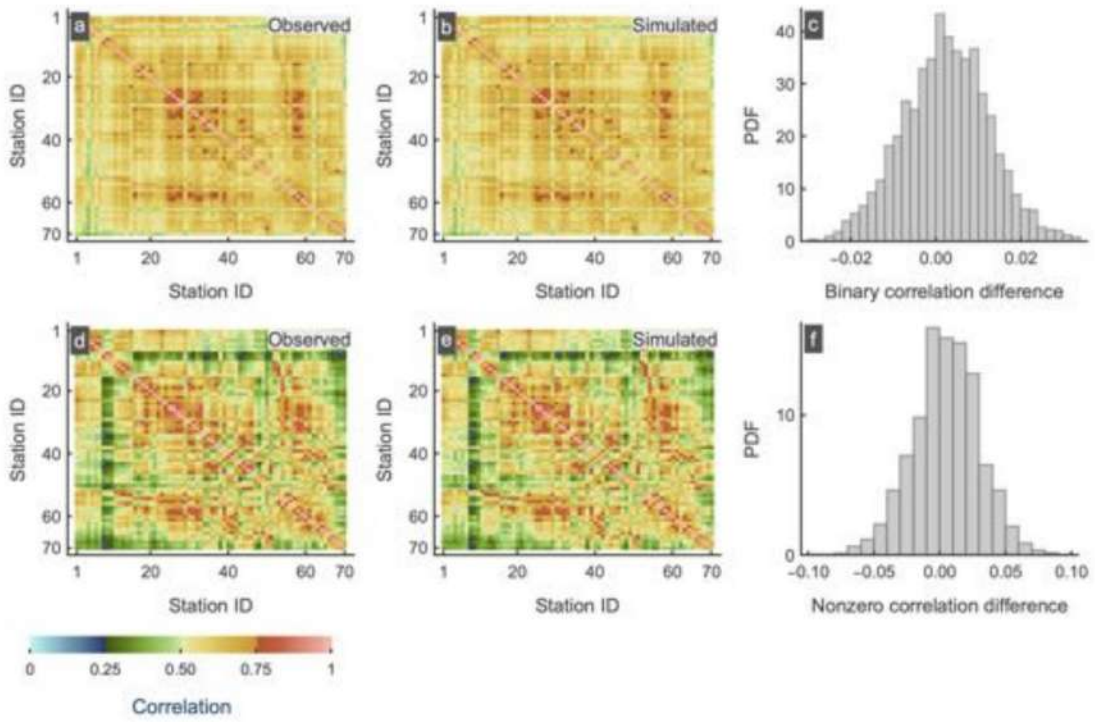

Figure 2. Cross-correlations among stations. (a–c) Observed and simulated lag-0 correlation matrices for the binary (wet/dry) process and their differences; (d–f) same for the nonzero rainfall process. See text for details.

Station-level statistics comparison (Figure 3). This analysis presents observed and simulated statistics computed from the full time series at each of the 70 stations, without seasonal or monthly stratification. The six metrics evaluated are: (a) probability of zero rainfall, (b) mean rainfall intensity, (c) L-variation, (d) L-skewness, (e) mean wet spell length, and (f) mean dry spell length.

The L-variation and L-skewness provide robust, distribution-free measures of variability and asymmetry, respectively, offering a more stable characterization of rainfall properties than traditional moments. Wet and dry spell statistics reflect persistence patterns essential for hydrological applications, including drought and flood modeling. The results indicate that inter-station variability is relatively low, suggesting a hydrologically homogeneous basin. Most importantly, the agreement between observed and simulated statistics is consistently strong across all stations, confirming that the model effectively captures key rainfall characteristics over space and time.

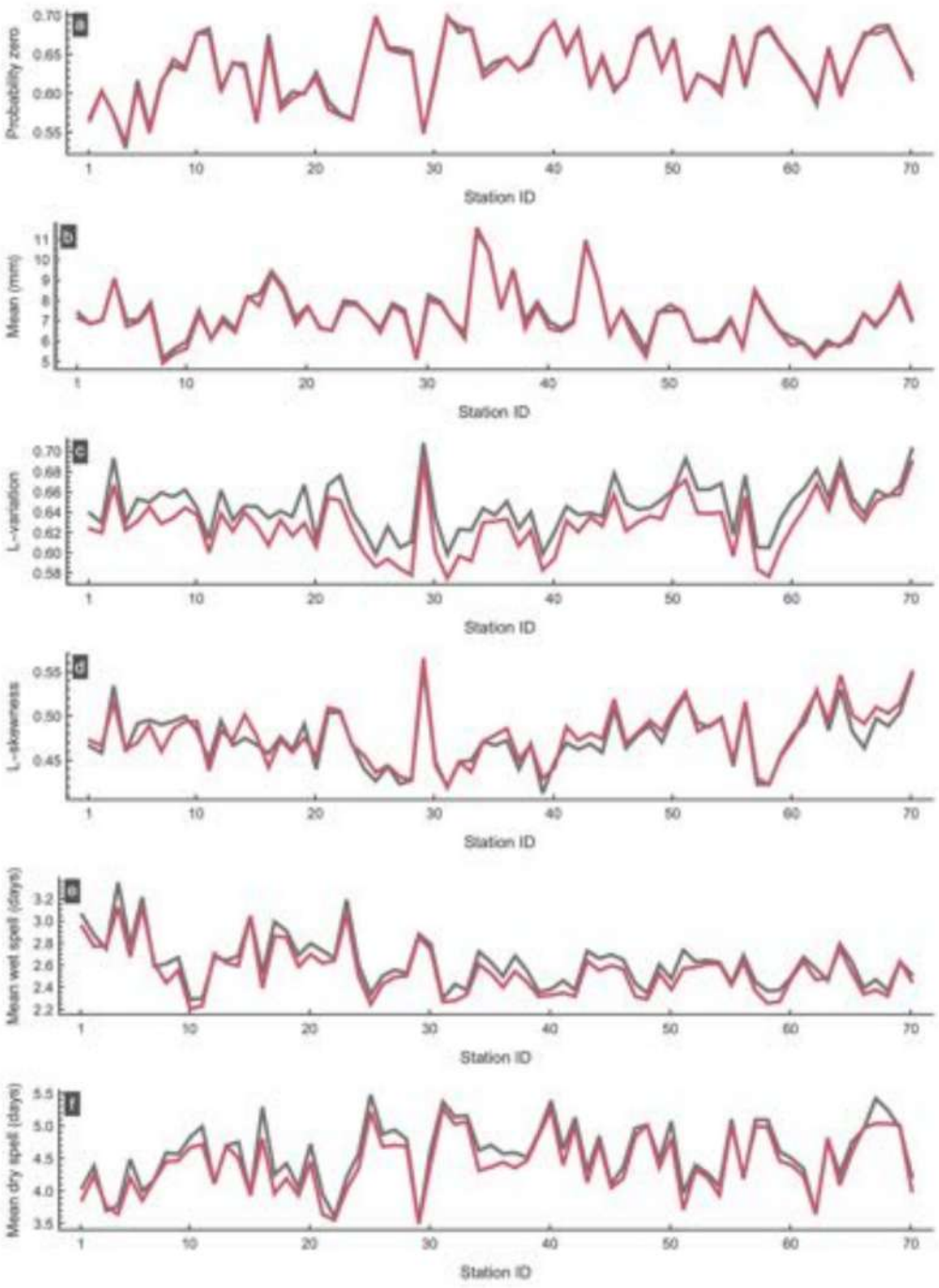

Figure 3. Comparison of observed and simulated station-level statistics: (a) probability of zero rainfall, (b) mean rainfall intensity, (c) L-variation, (d) L-skewness, (e) mean wet spell length, and (f) mean dry spell length.

Catchment-scale simulation assessment (Figure 4). This figure presents a detailed evaluation of the simulated and observed mean daily precipitation aggregated across all 70 stations, representing the catchment-scale behavior. The analysis follows the structure of the previous station-level multipanel plots and includes: (a–b) observed and simulated aggregated daily time series; (c) seasonal probability of zero precipitation; (d) seasonal mean rainfall intensity; (e) seasonal standard deviation of rainfall intensity; (f) exceedance probability of nonzero rainfall; (g) binary

autocorrelation structure; (h) nonzero rainfall autocorrelation structure; (i) scaling of the probability of zero rainfall with time scale; (j) scaling of standard deviation; (k) probability mass function of dry spell lengths; (l) probability mass function of wet spell lengths; (m) complementary cumulative distribution of dry spell lengths; and (n) complementary cumulative distribution of wet spell lengths.

This assessment demonstrates that the simulation effectively reproduces key statistical properties of rainfall at the catchment scale, including variability, persistence, and extremes. The agreement between observed and simulated series is excellent across all evaluated metrics. The only noticeable deviation is a slight underestimation of the standard deviation of the aggregated catchment rainfall (panel e), which may reflect the smoothing effect introduced during spatial aggregation. Nonetheless, the overall alignment confirms the robustness and reliability of the simulation framework at both the station and catchment levels.

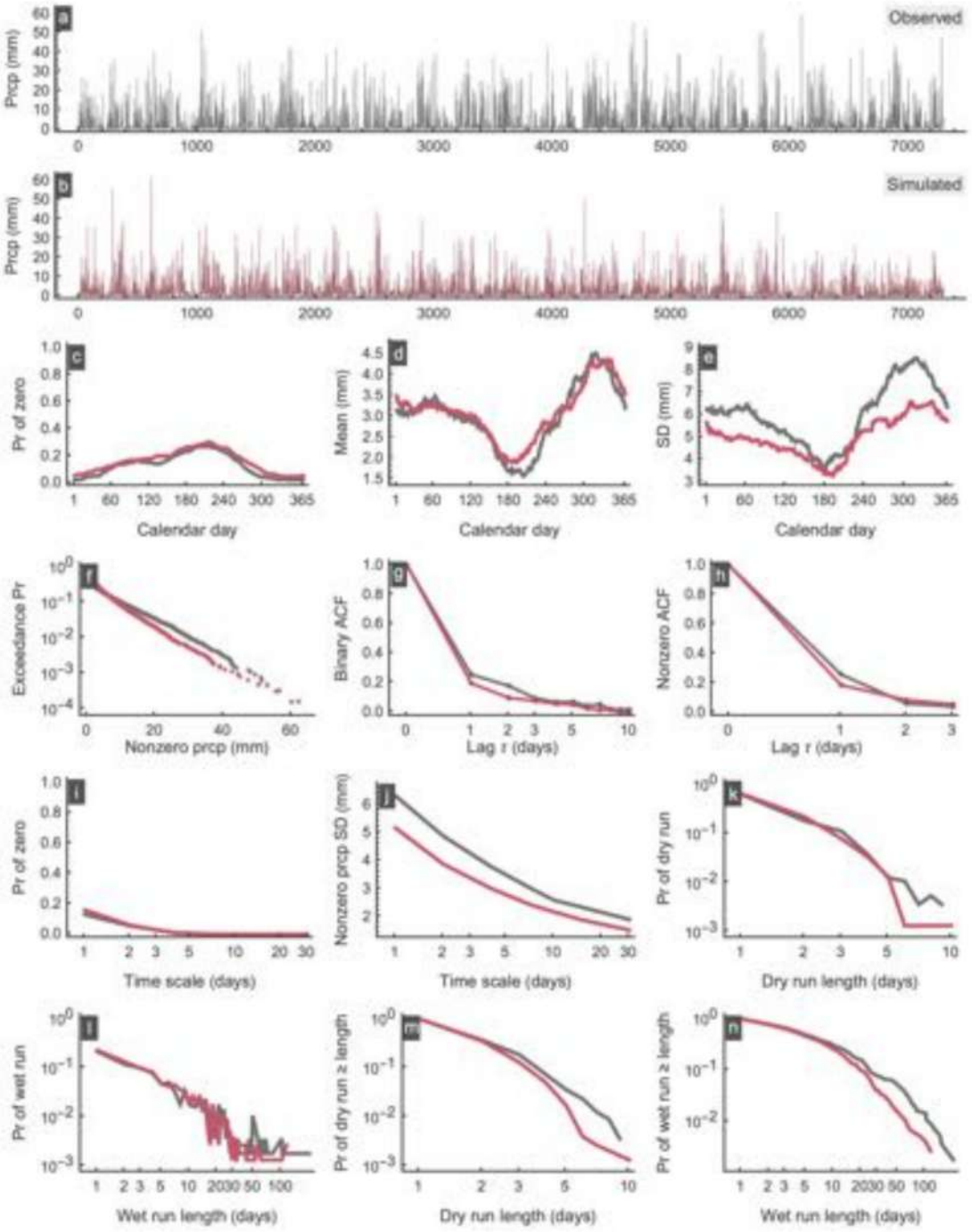

Figure 4. Assessment of observed and simulated catchment-scale mean daily precipitation aggregated from all 70 stations. Panels include (a–b) daily time series, (c) seasonal probability of zero, (d) seasonal mean, (e) seasonal standard deviation, (f) exceedance probability, (g–h) autocorrelation structures, (i–j) scaling metrics, and (k–n) dry/wet spell statistics. See text for details.

Appendix A: Additional Figures

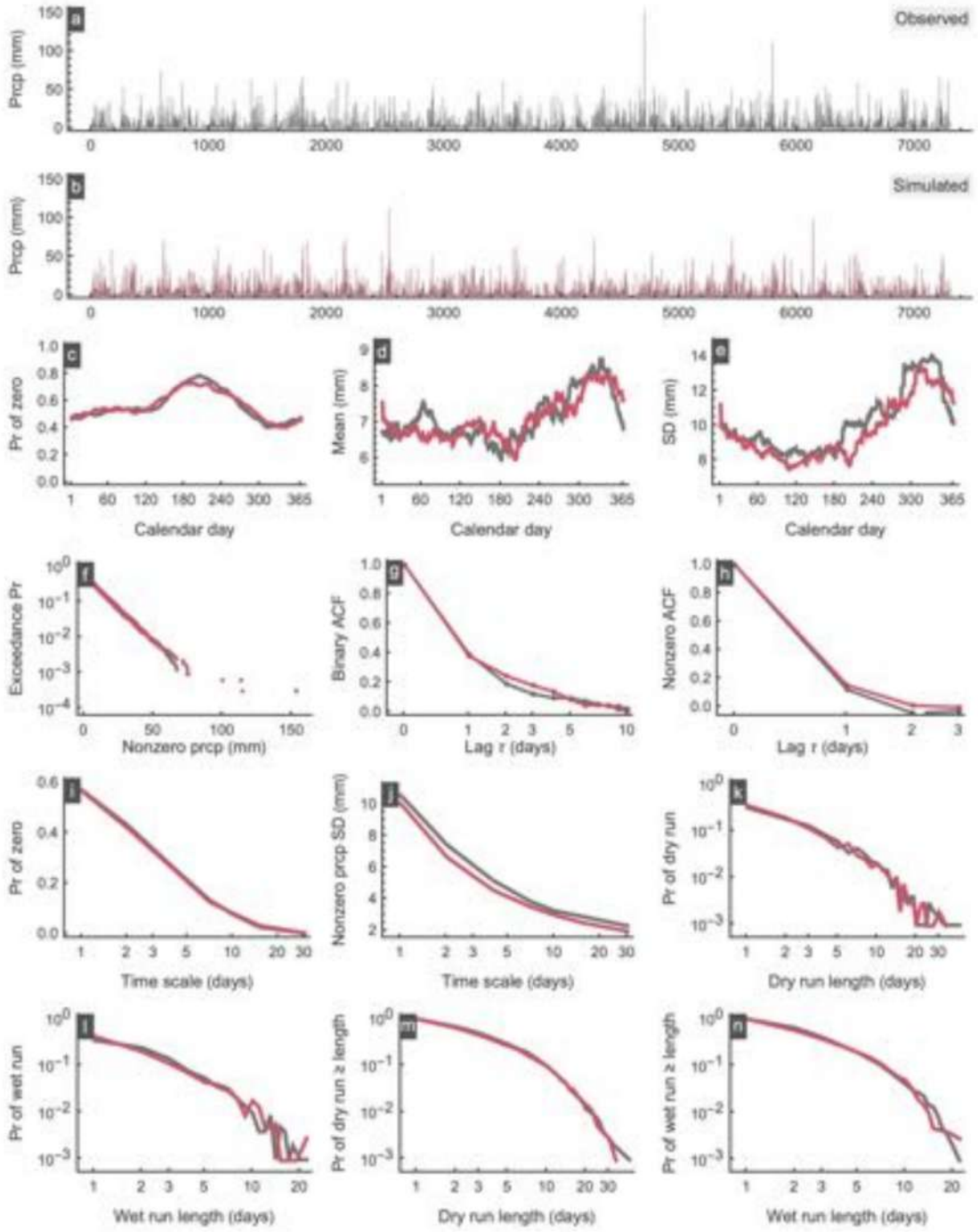

Figure A1. Simulation results for station PluvioMetro 00.

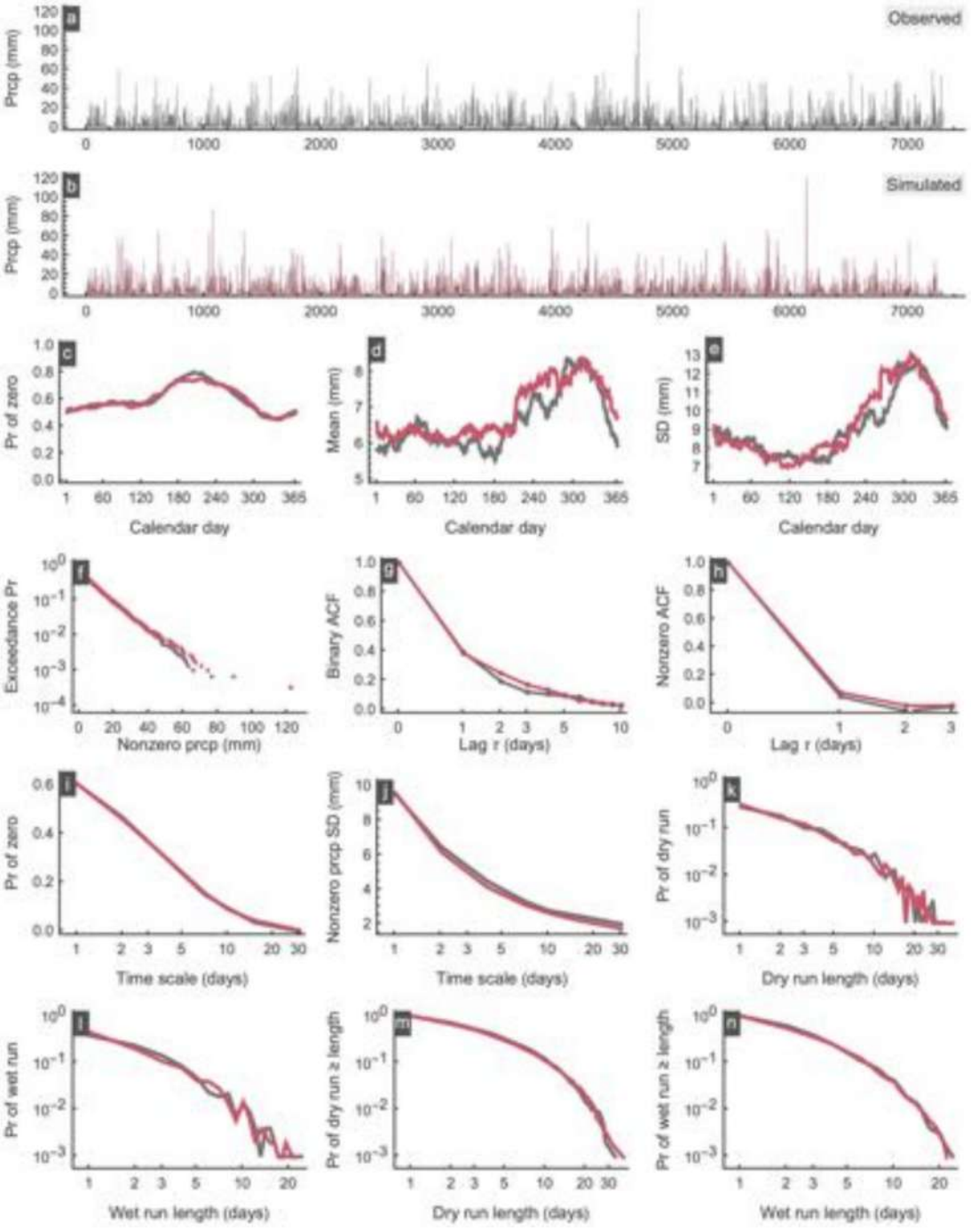

Figure A2. Simulation results for station PluvioMetro 01.

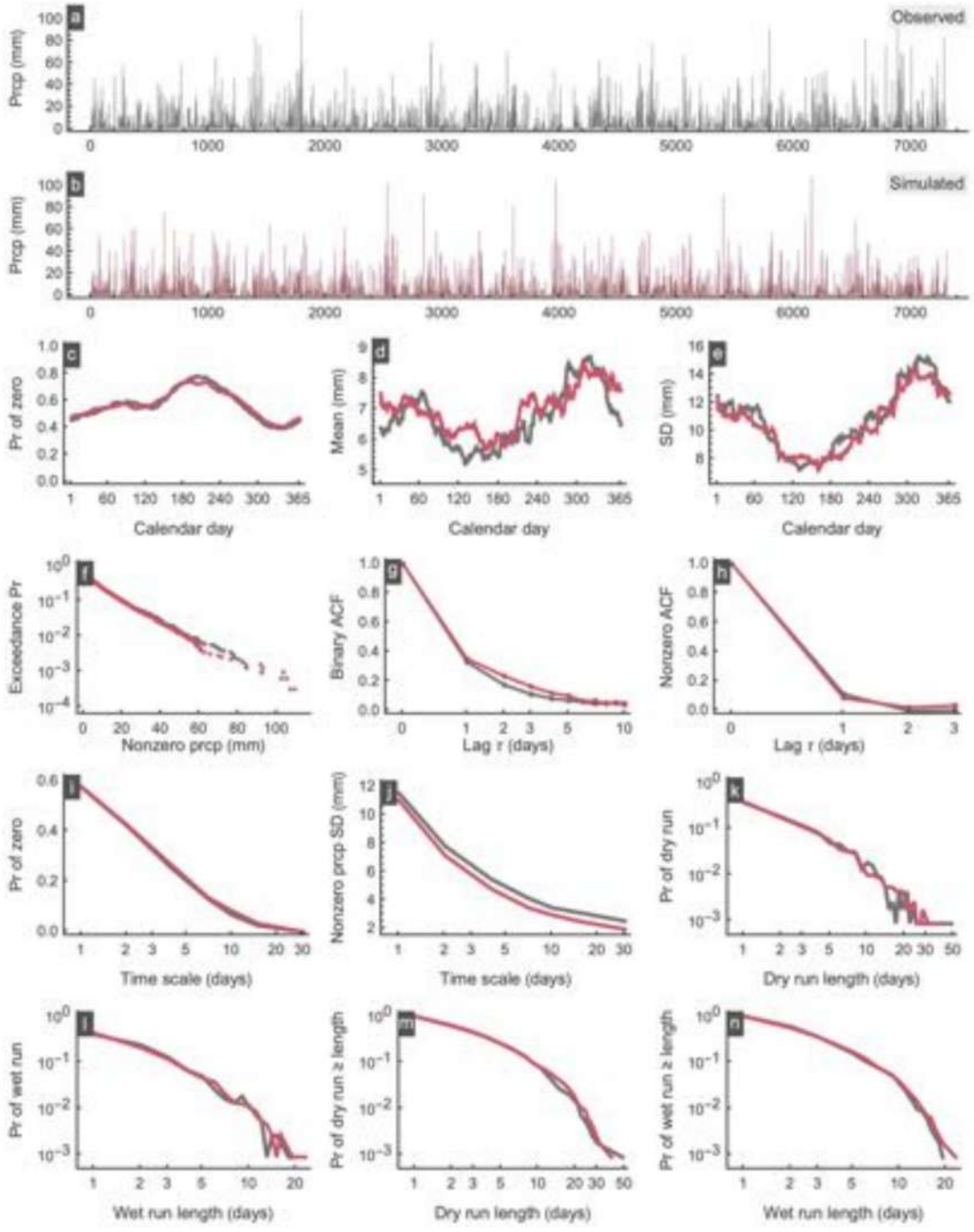

Figure A3. Simulation results for station PluvioMetro 02.

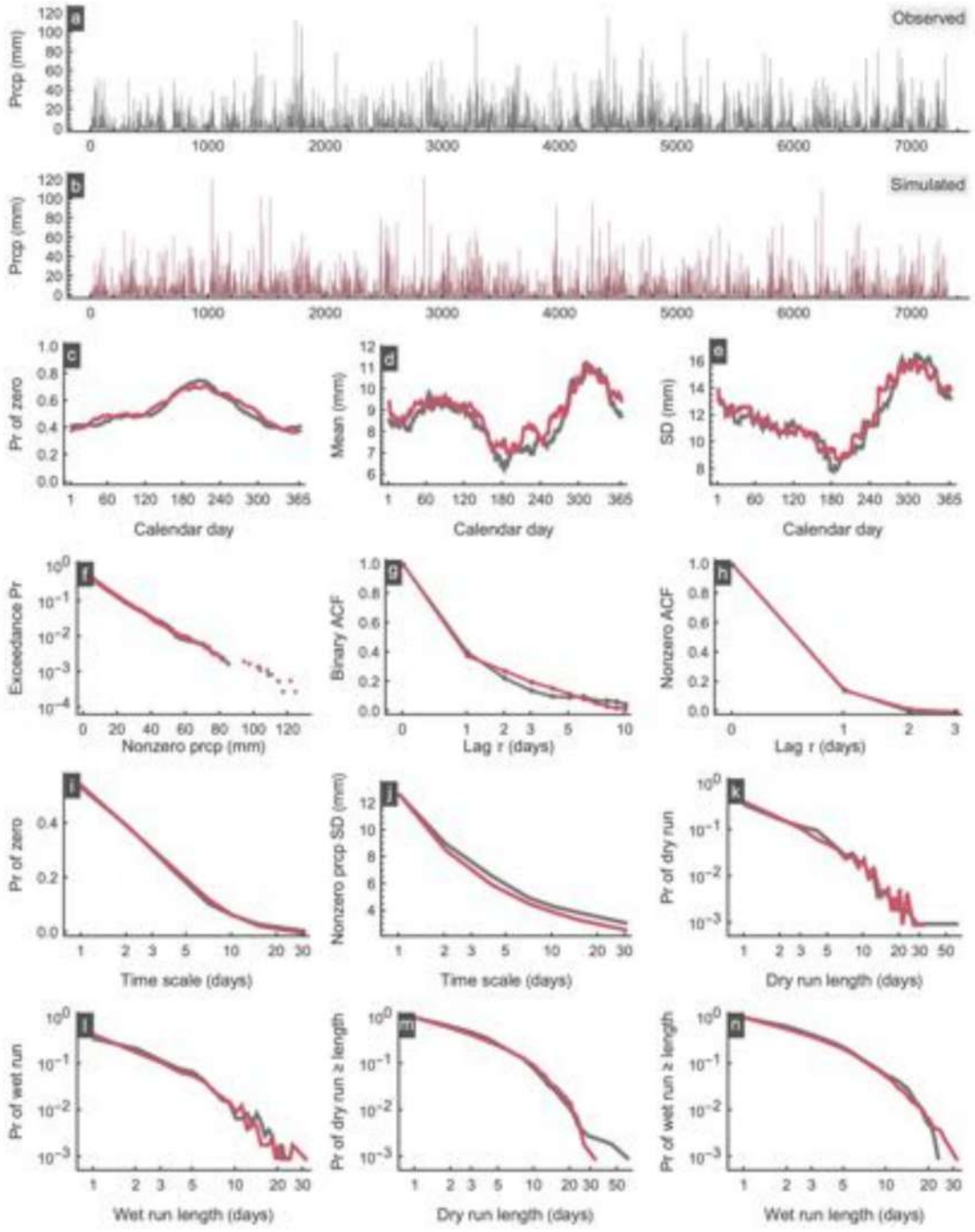

Figure A4. Simulation results for station PluvioMetro 03.

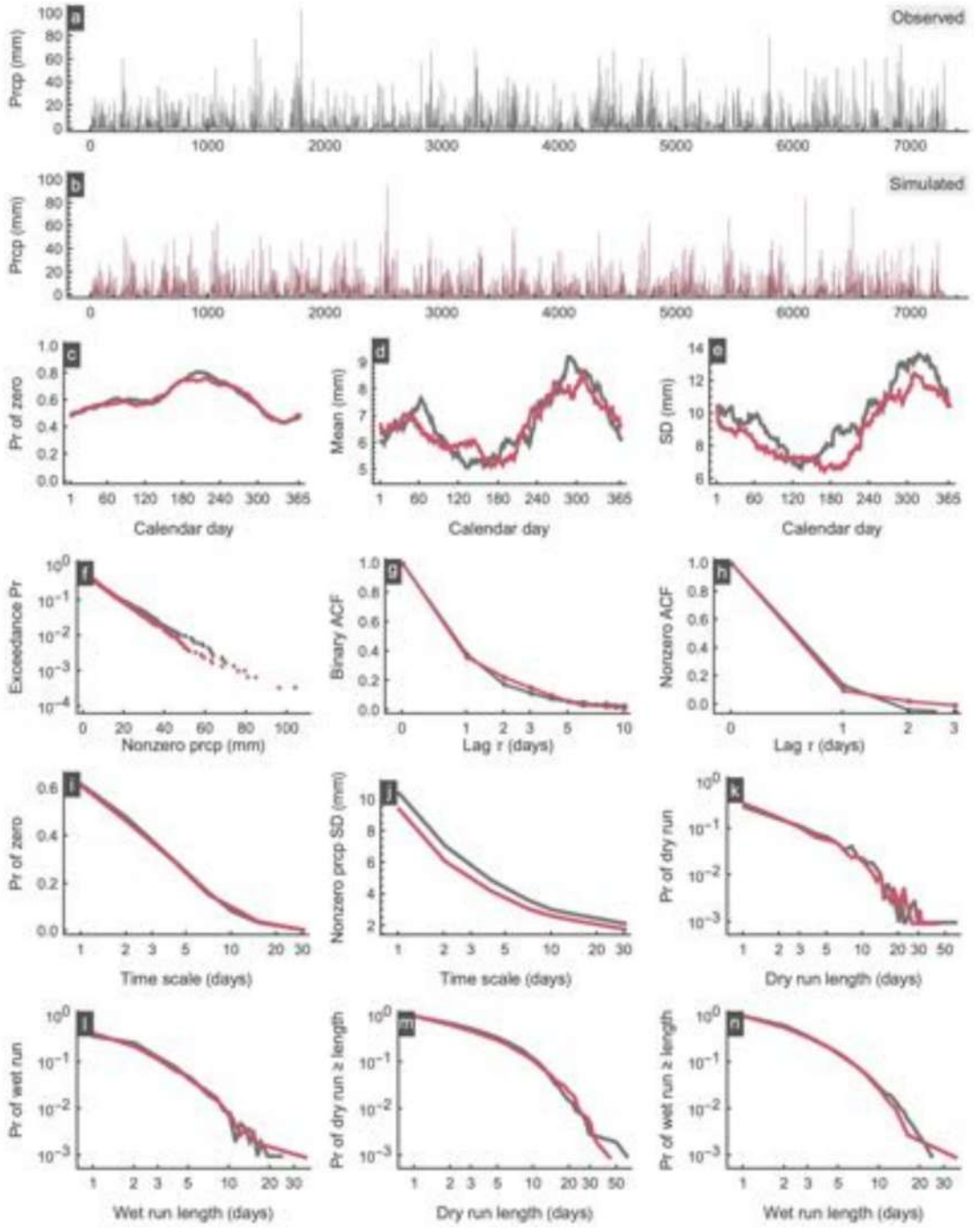

Figure A5. Simulation results for station PluvioMetro 04.

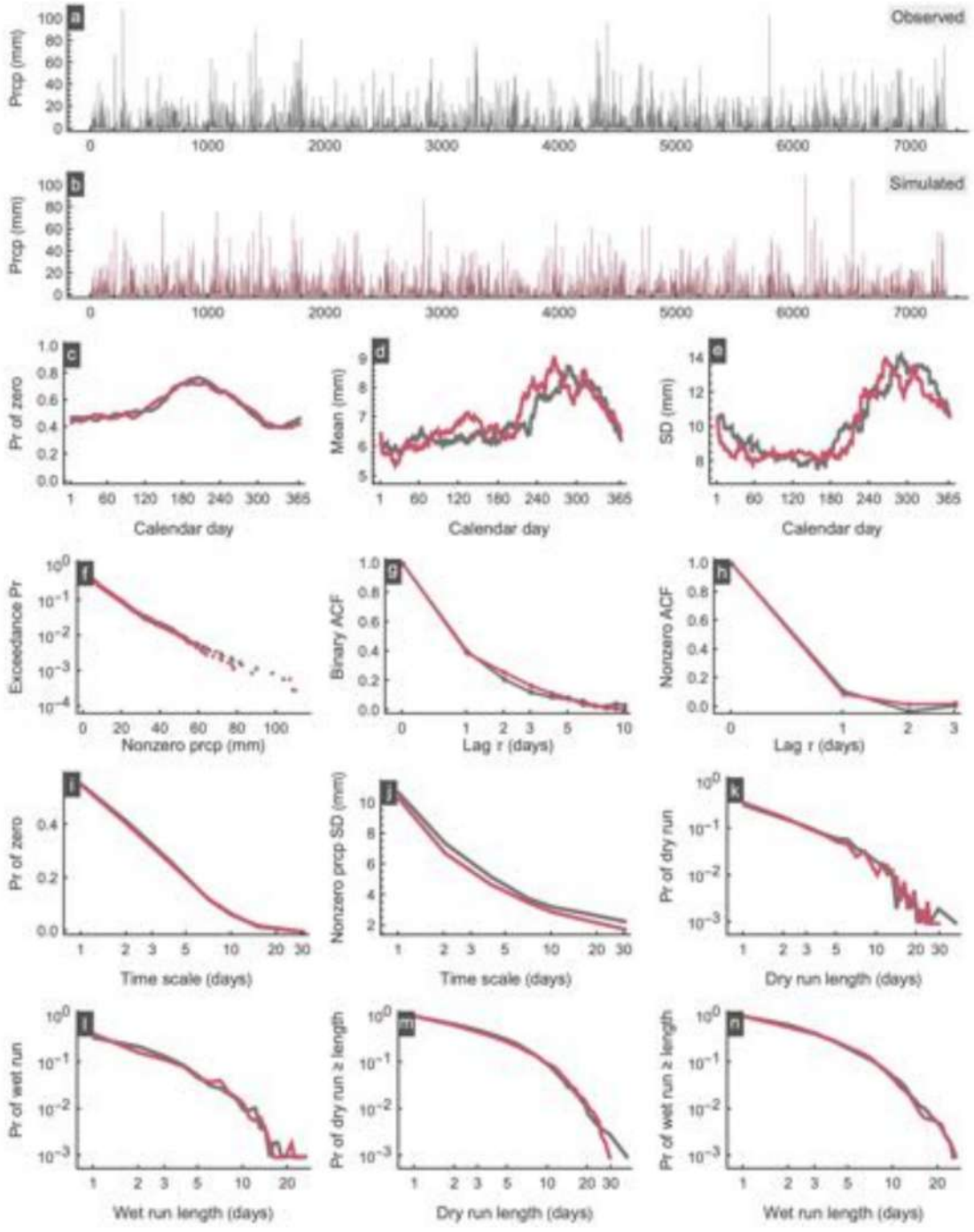

Figure A6. Simulation results for station PluvioMetro 05.

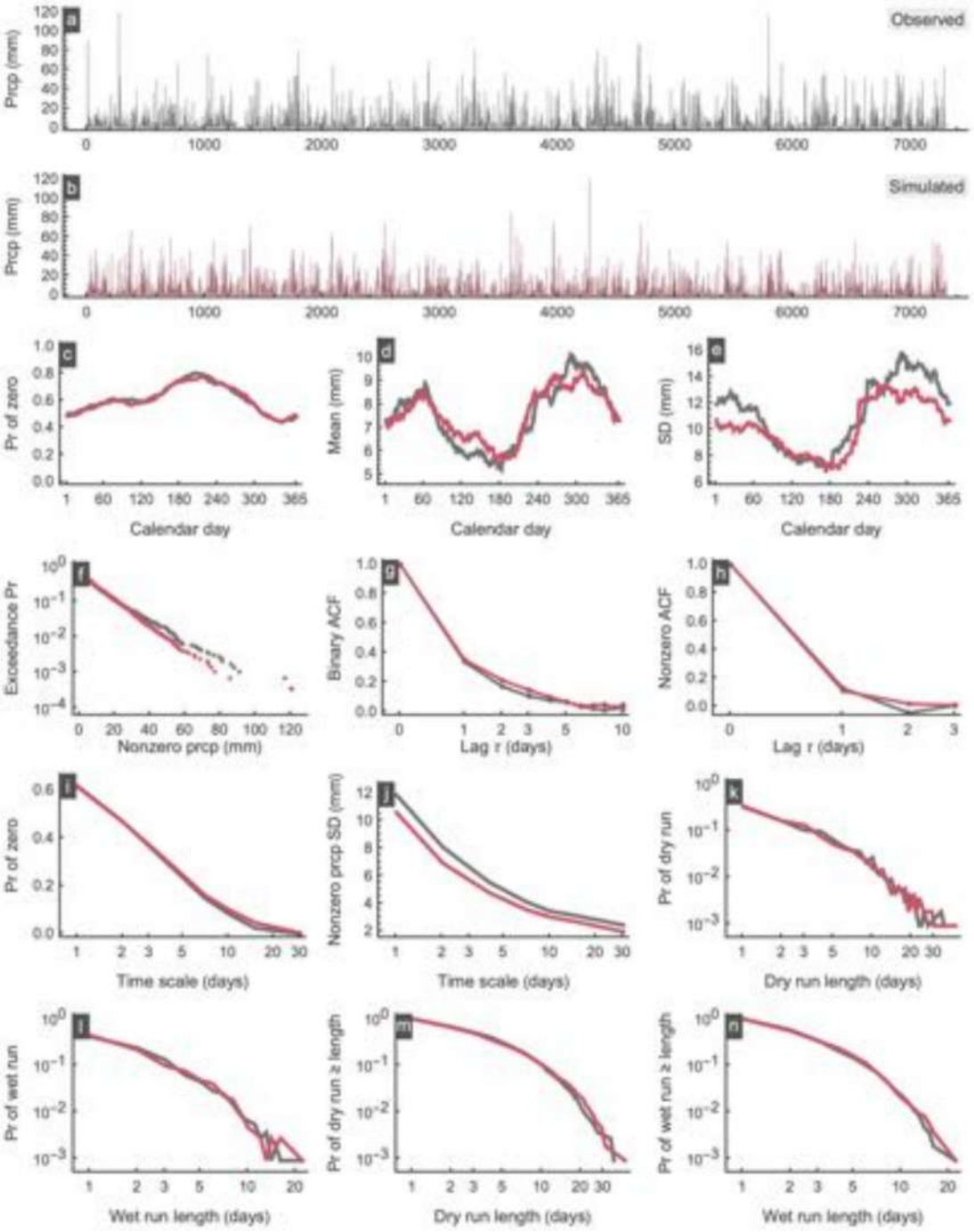

Figure A7. Simulation results for station PluvioMetro 06.

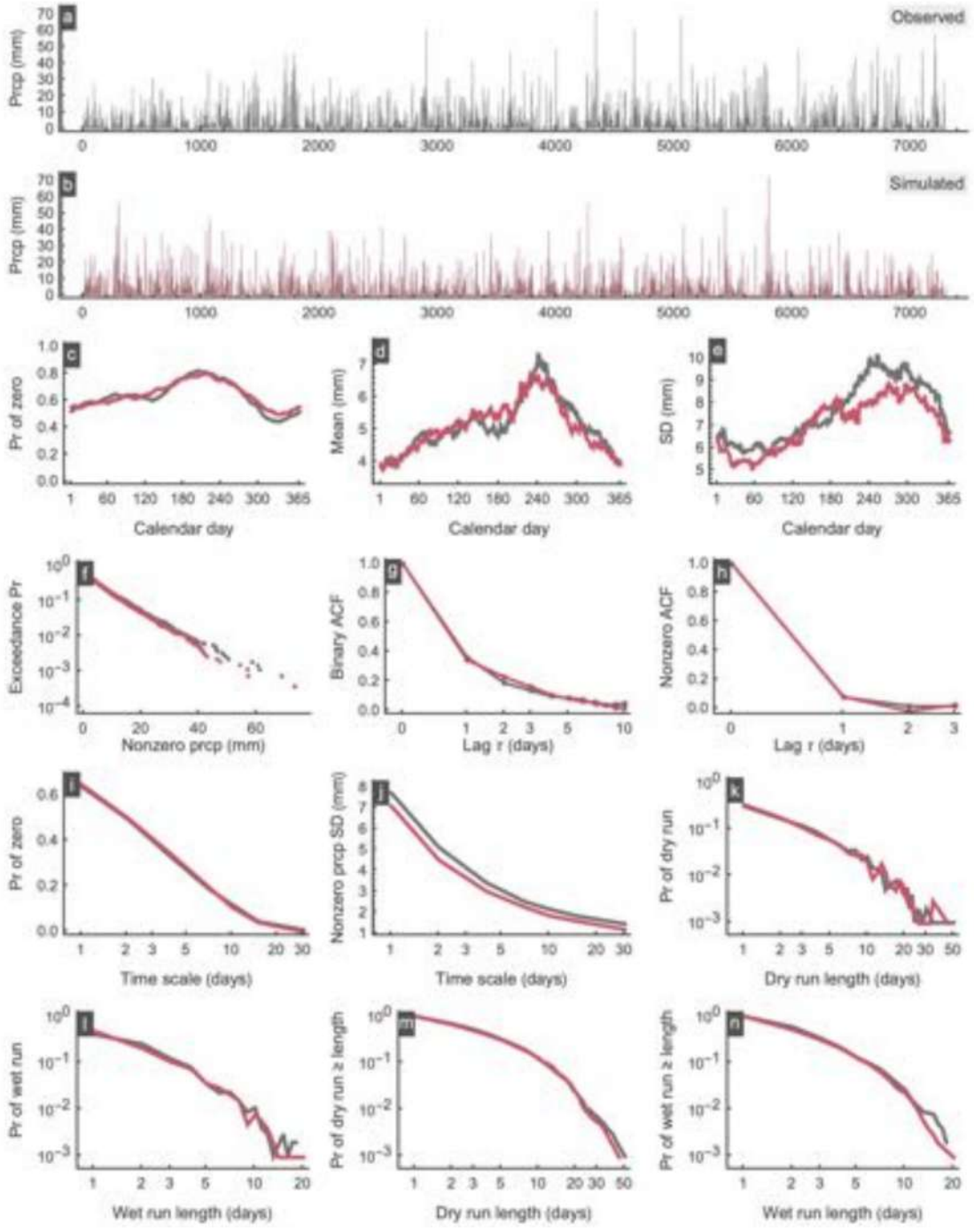

Figure A8. Simulation results for station PluvioMetro 07.

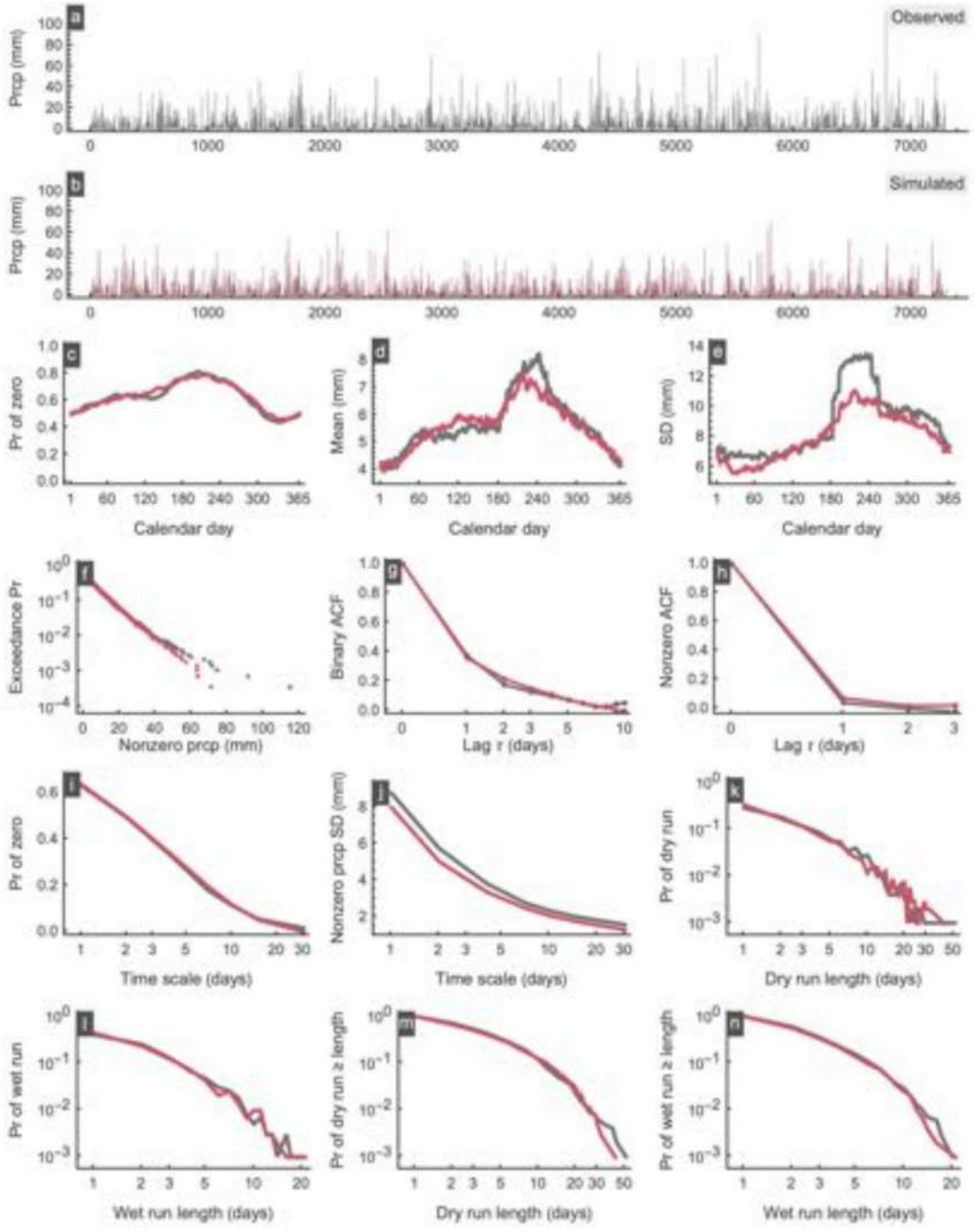

Figure A9. Simulation results for station PluvioMetro 08.

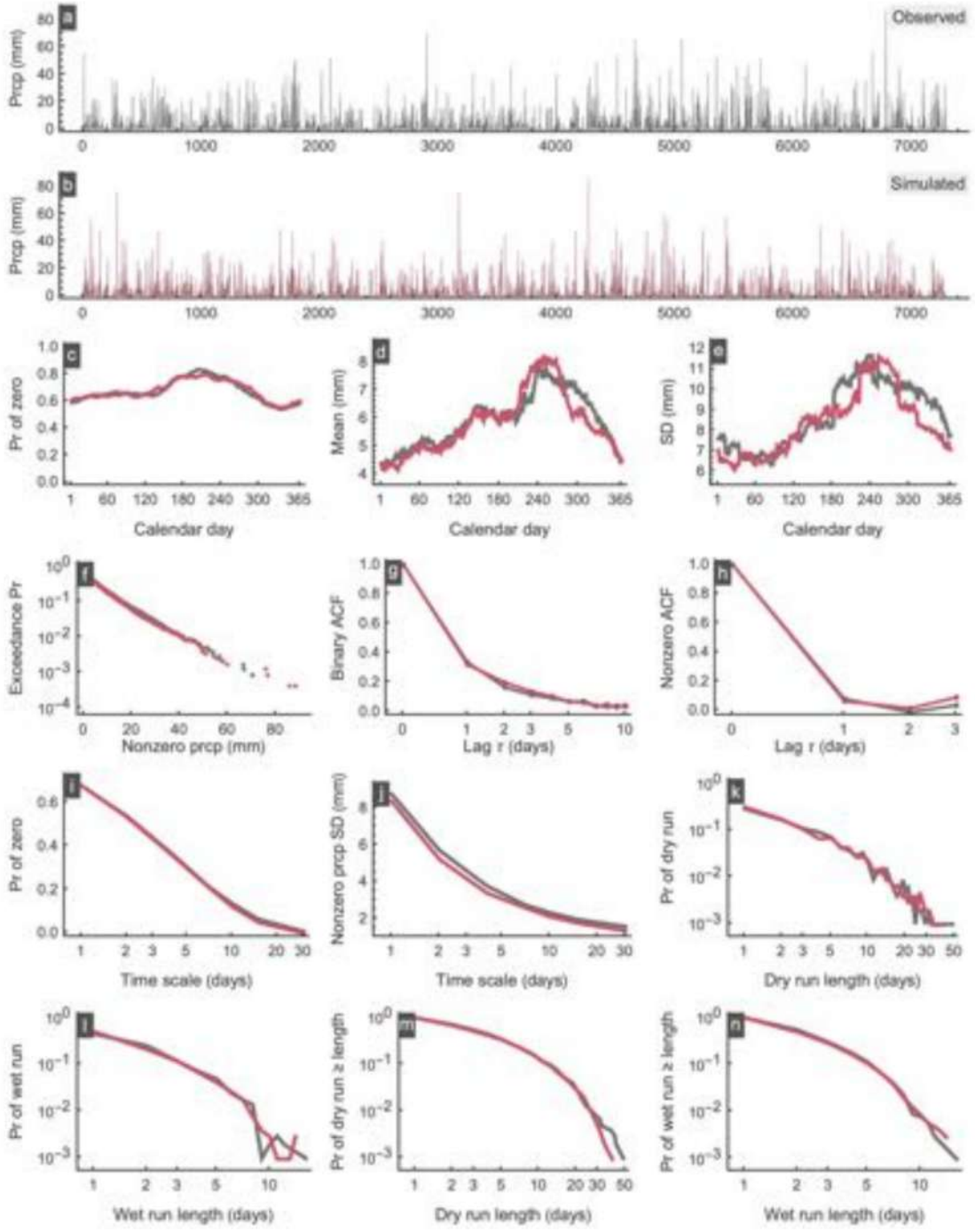

Figure A10. Simulation results for station PluvioMetro 11.

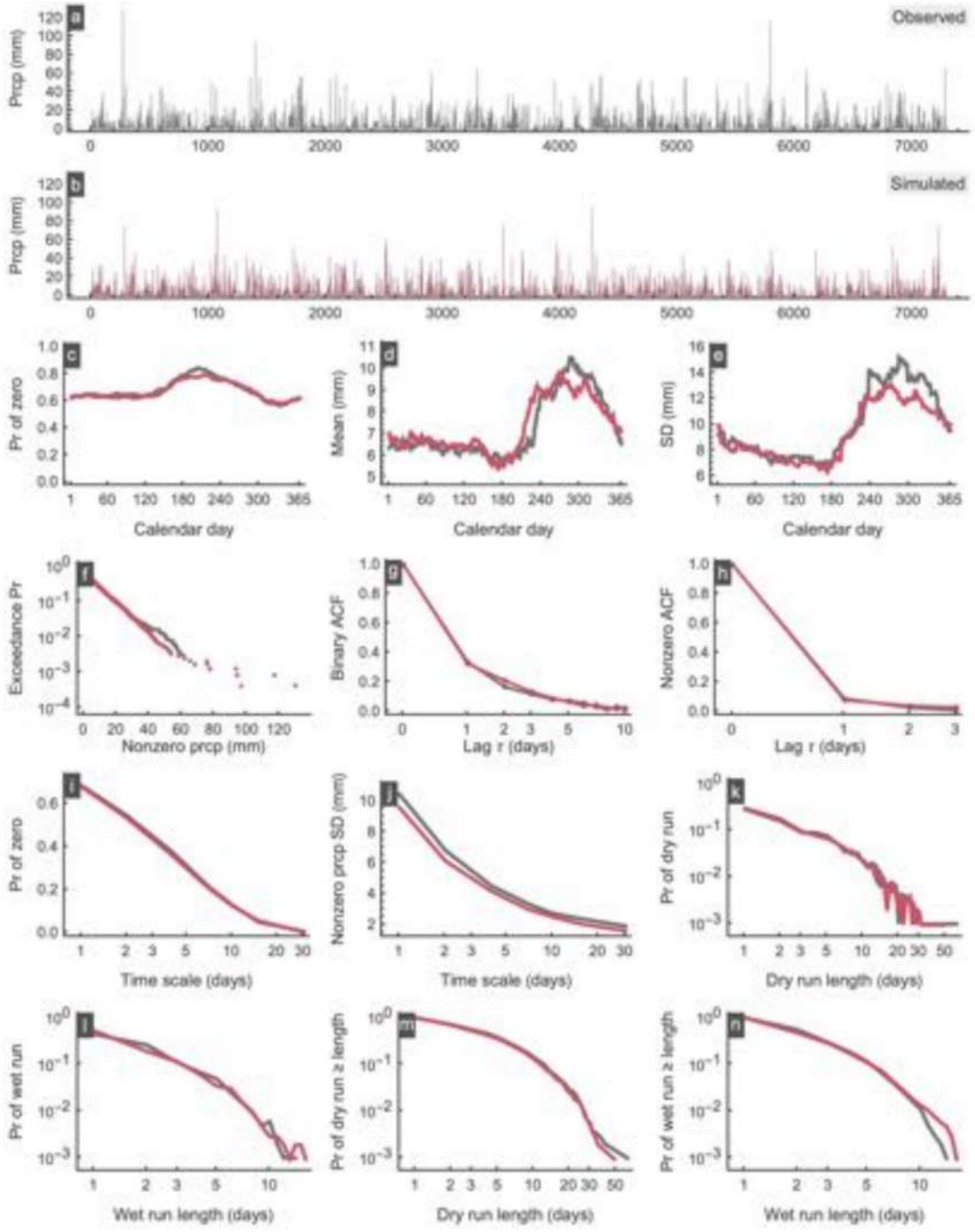

Figure A11. Simulation results for station PluvioMetro 13.

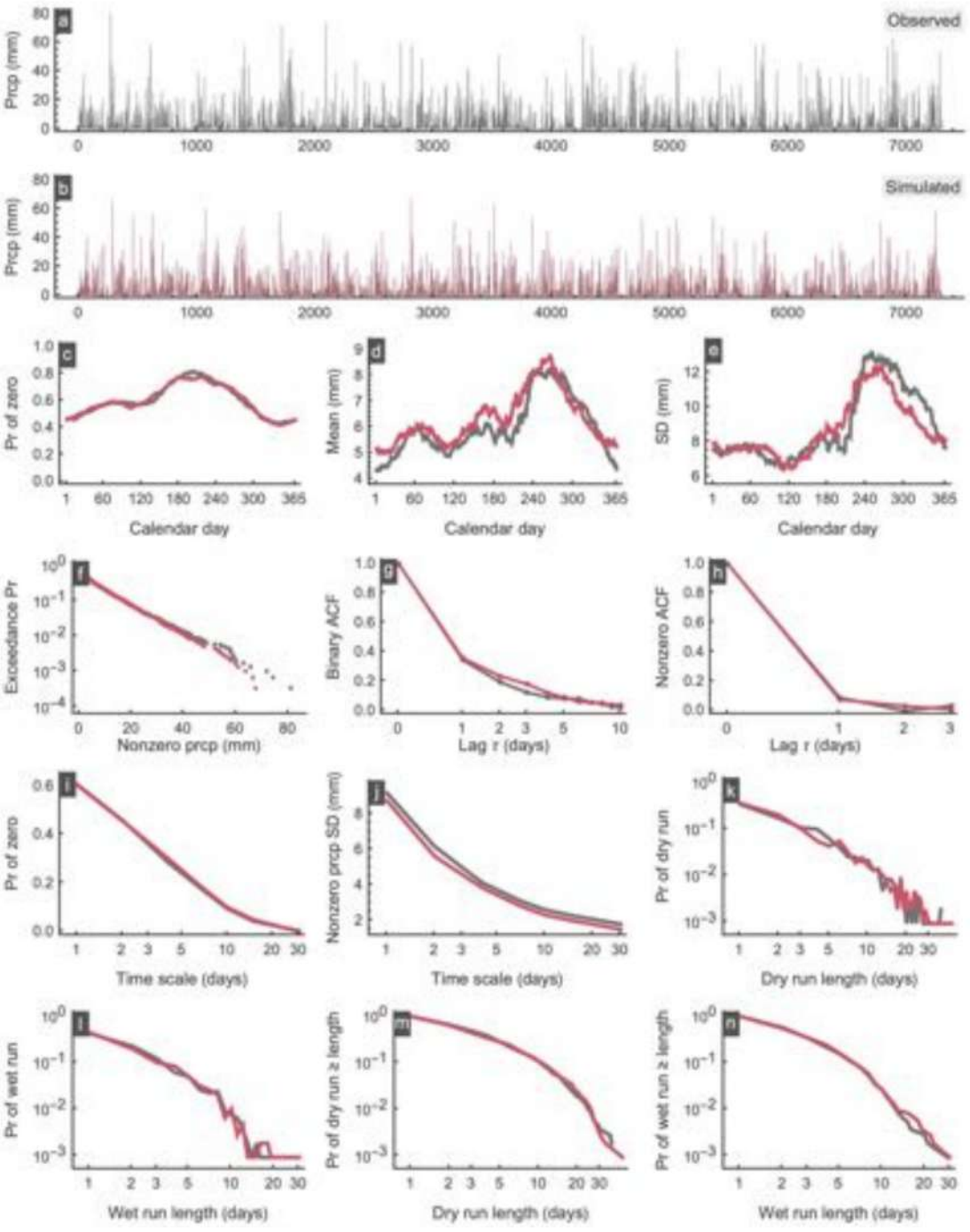

Figure A12. Simulation results for station PluvioMetro 14.

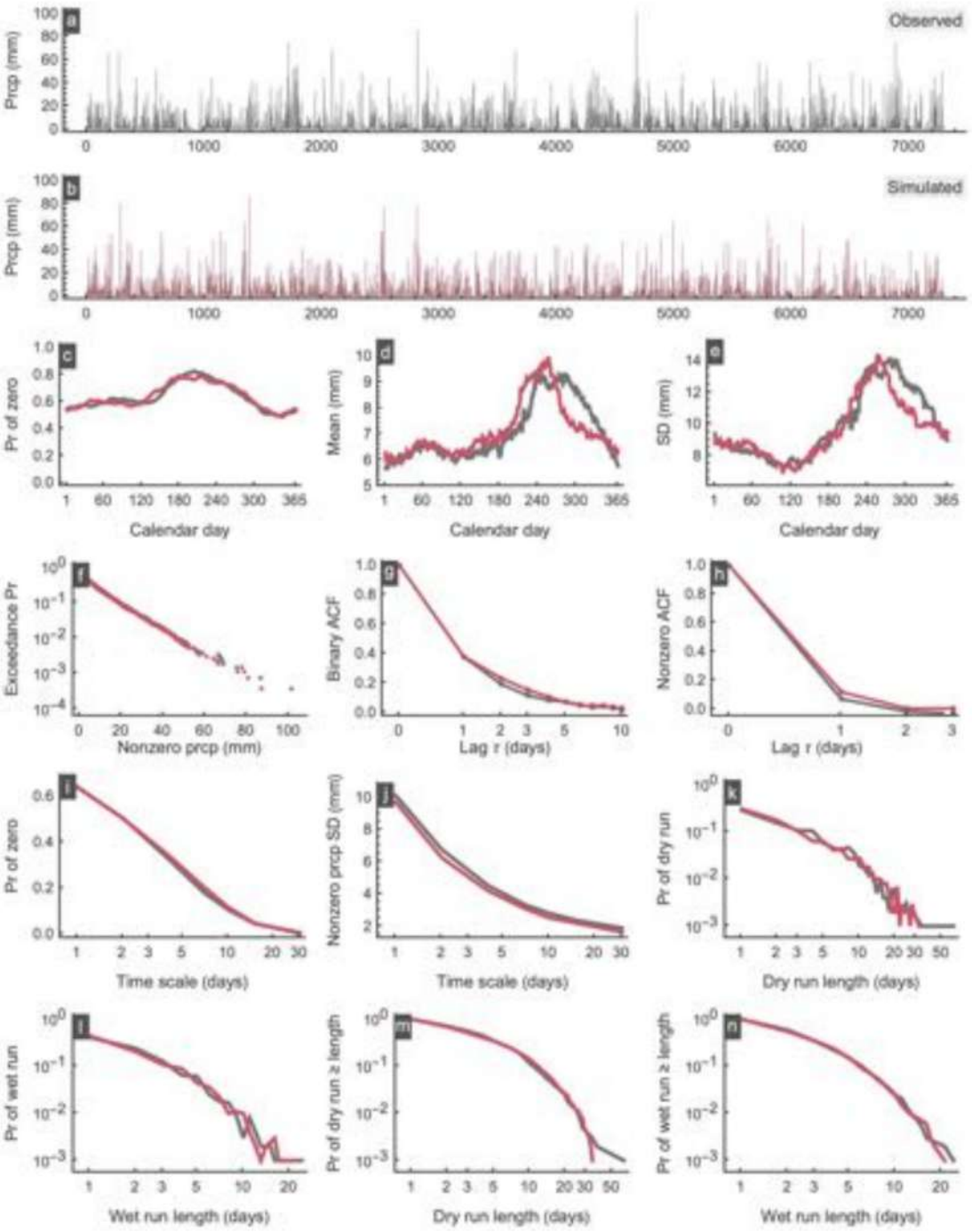

Figure A13. Simulation results for station PluvioMetro 15.

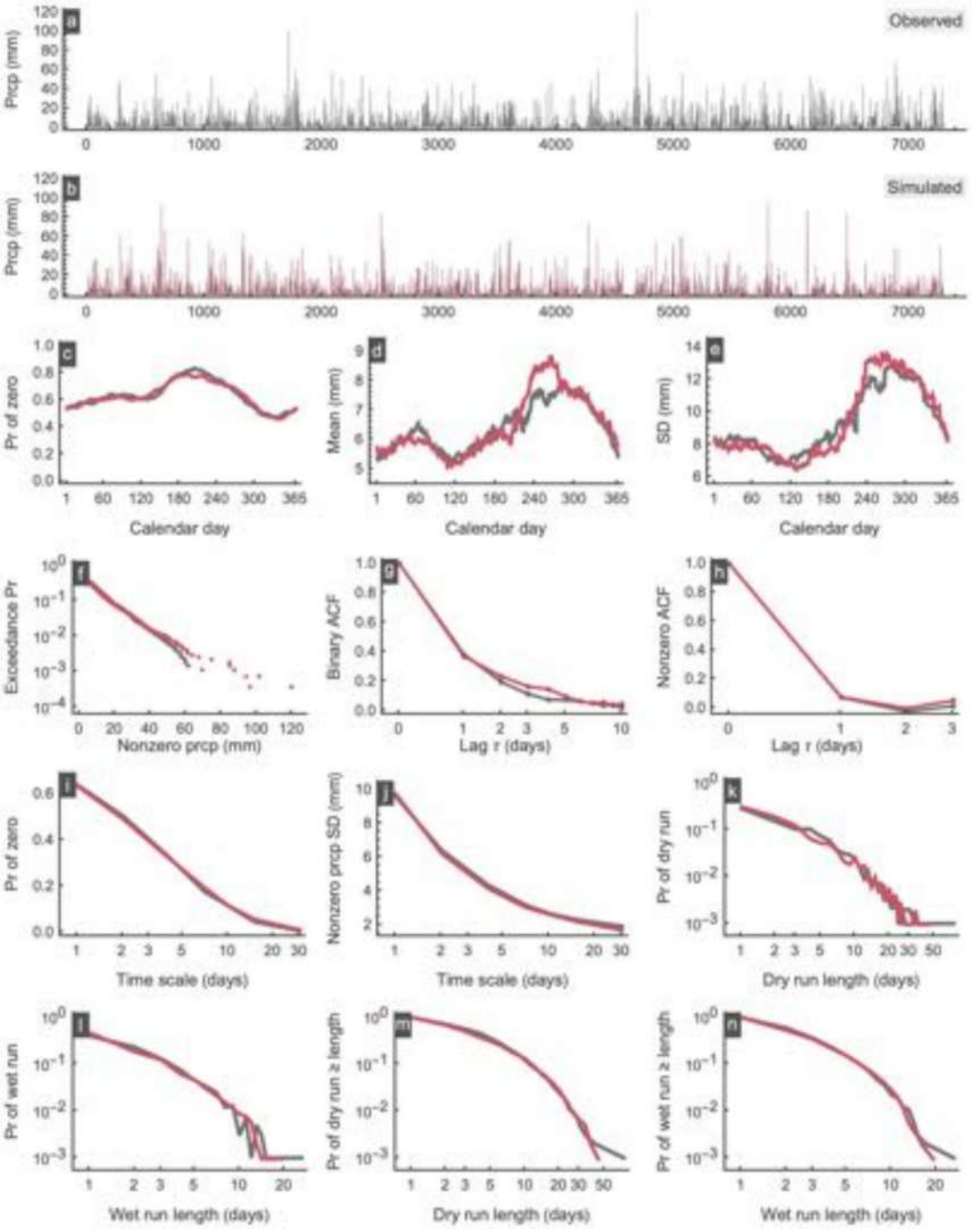

Figure A14. Simulation results for station PluvioMetro 16.

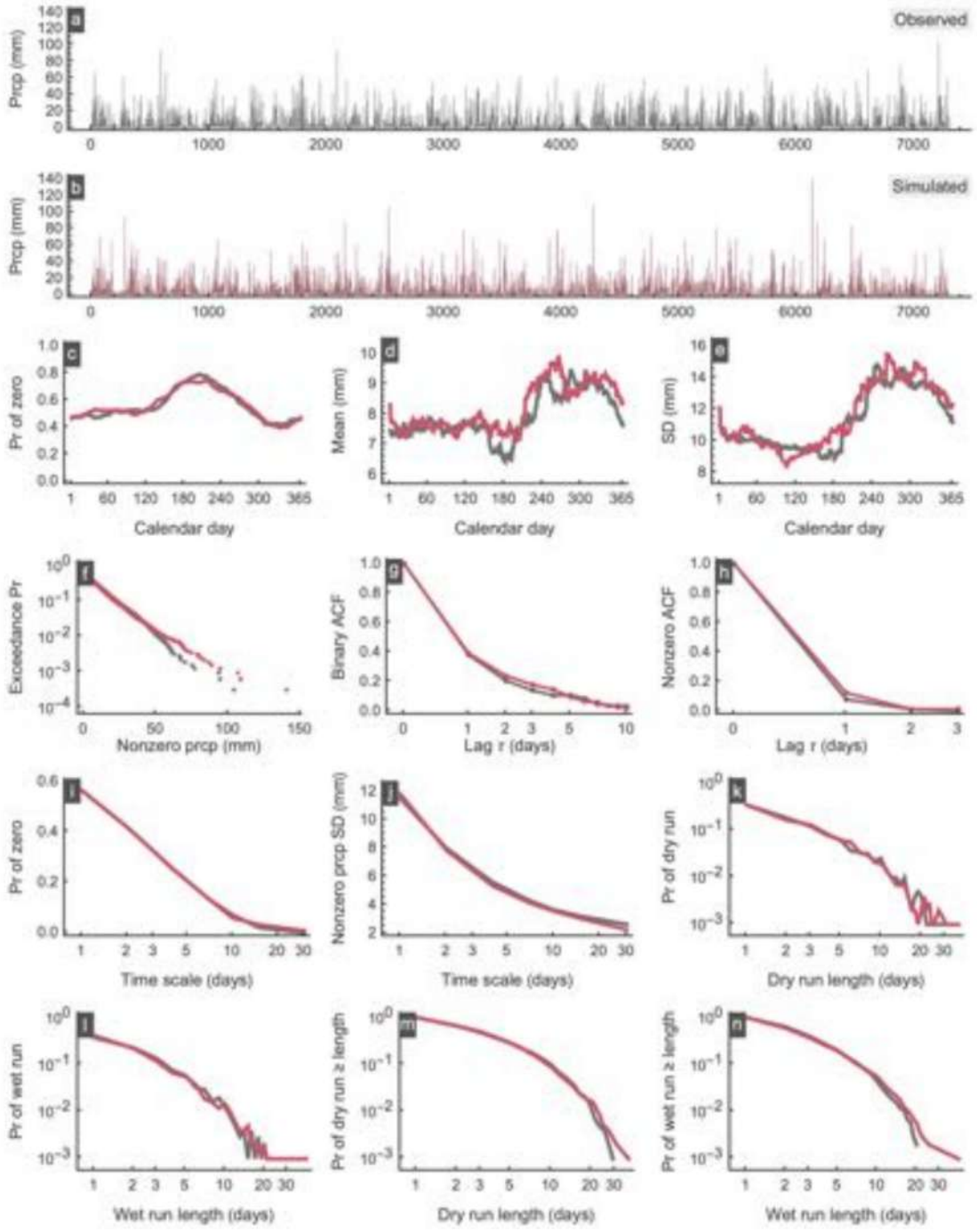

Figure A15. Simulation results for station PluvioMetro 17.

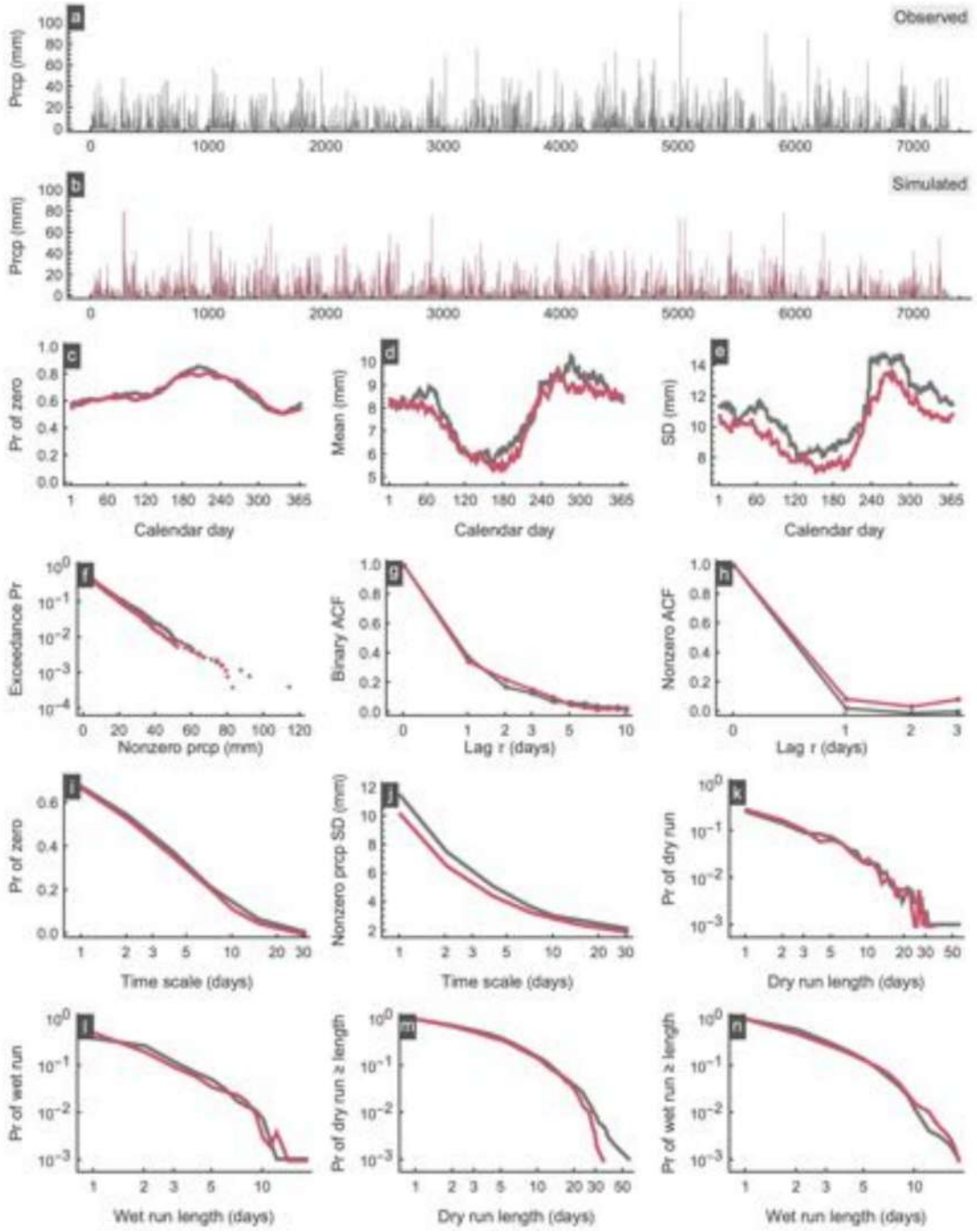

Figure A16. Simulation results for station PluvioMetro 18.

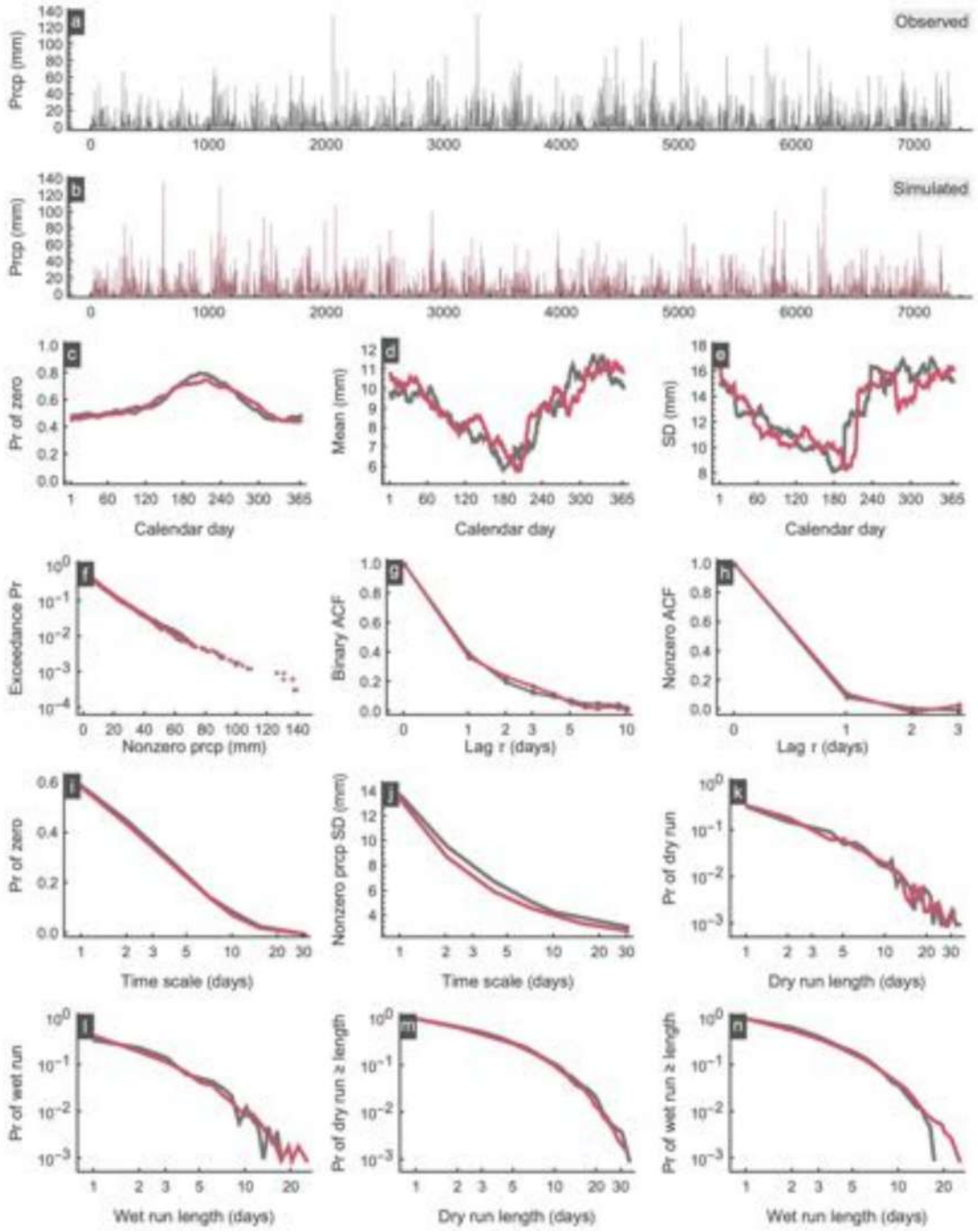

Figure A17. Simulation results for station PluvioMetro 19.

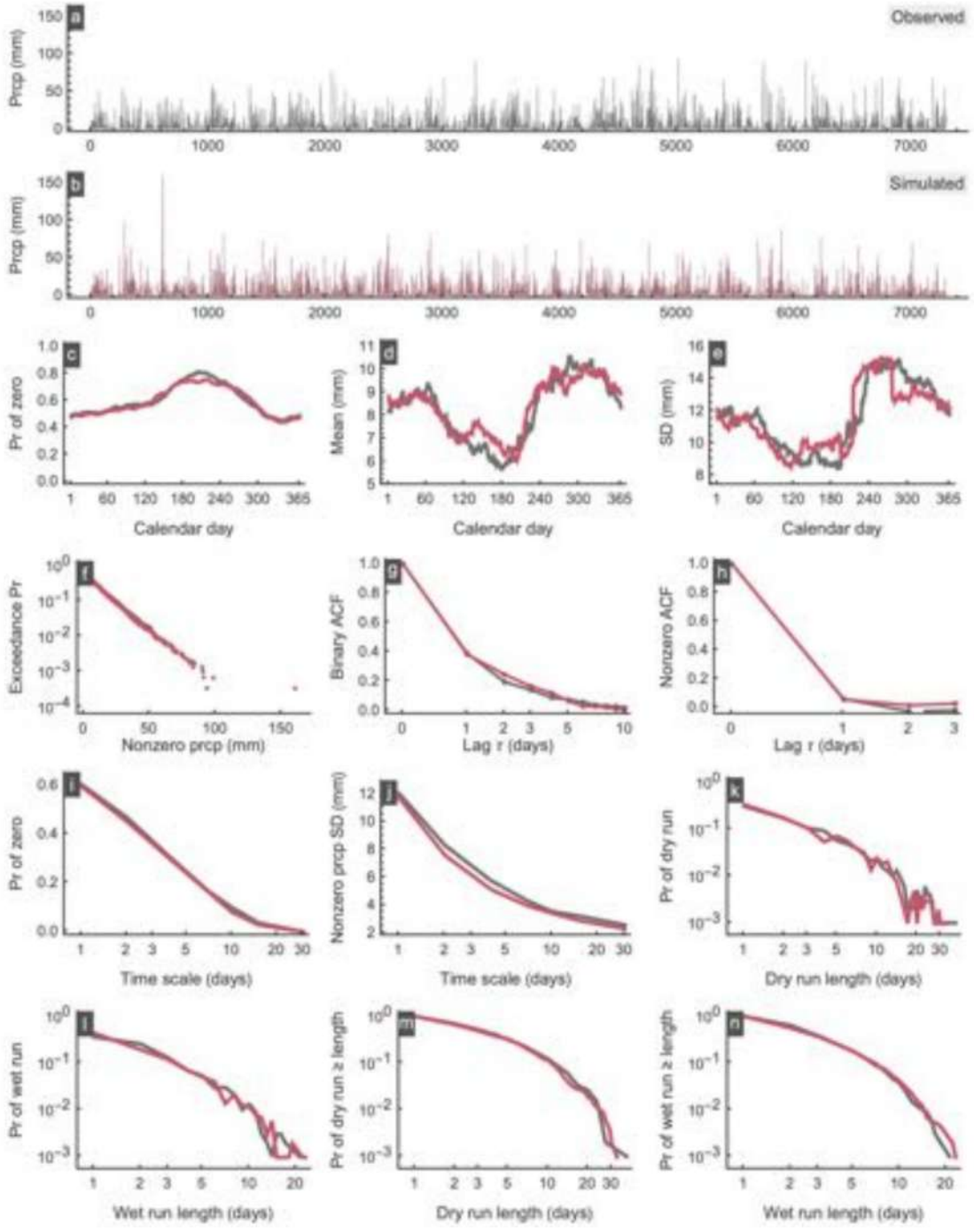

Figure A18. Simulation results for station PluvioMetro 21.

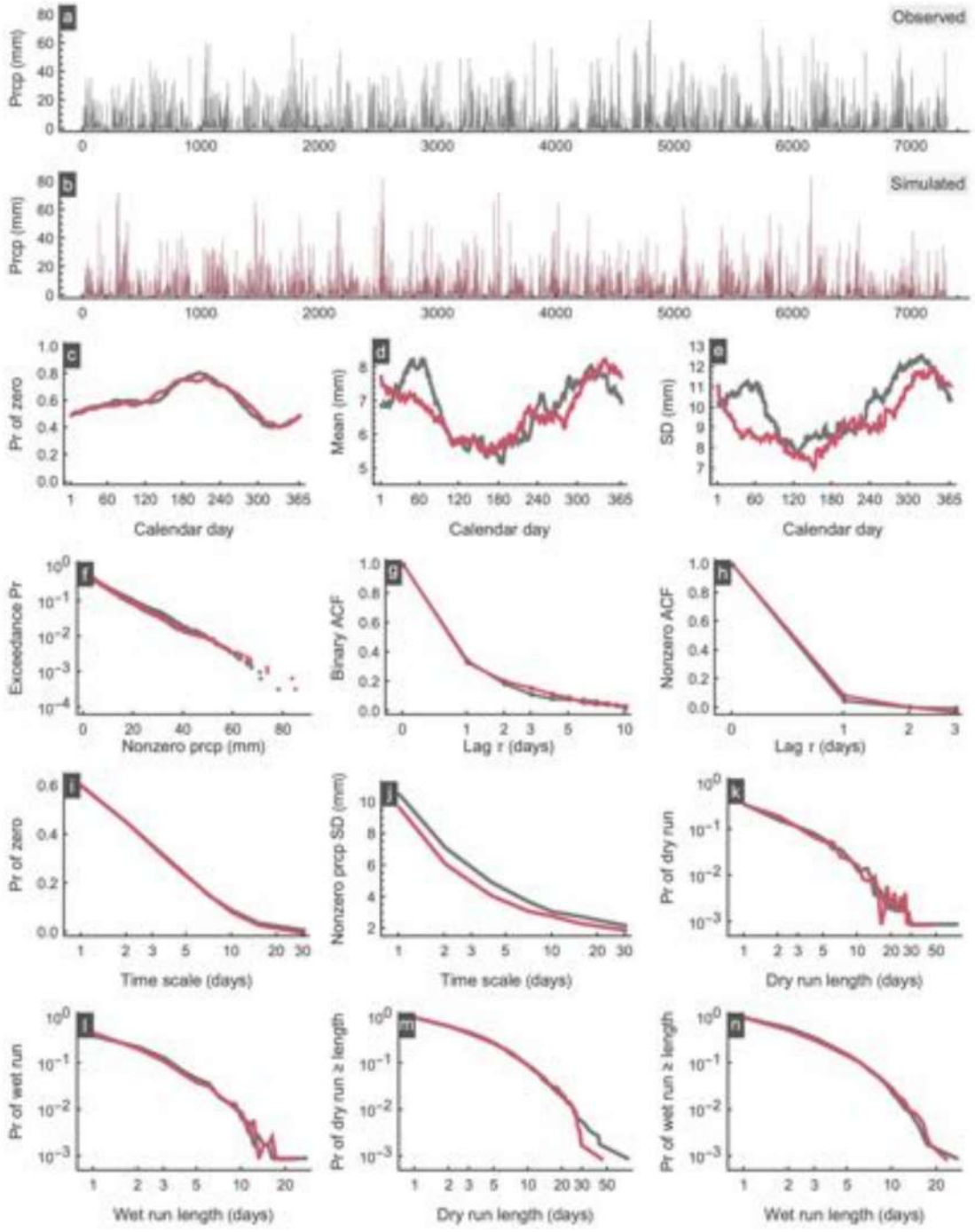

Figure A19. Simulation results for station PluvioMetro 22.

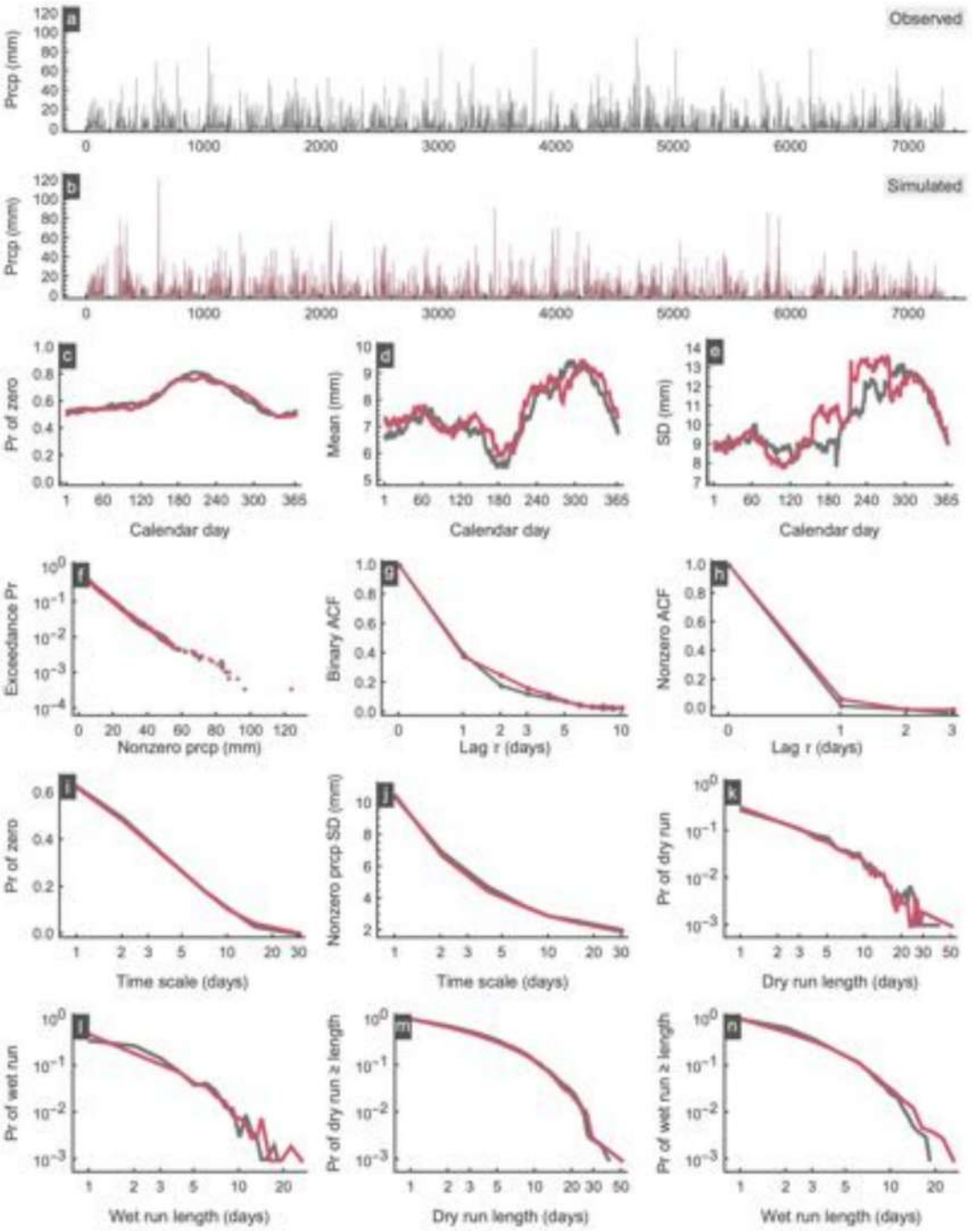

Figure A20. Simulation results for station PluvioMetro 24.

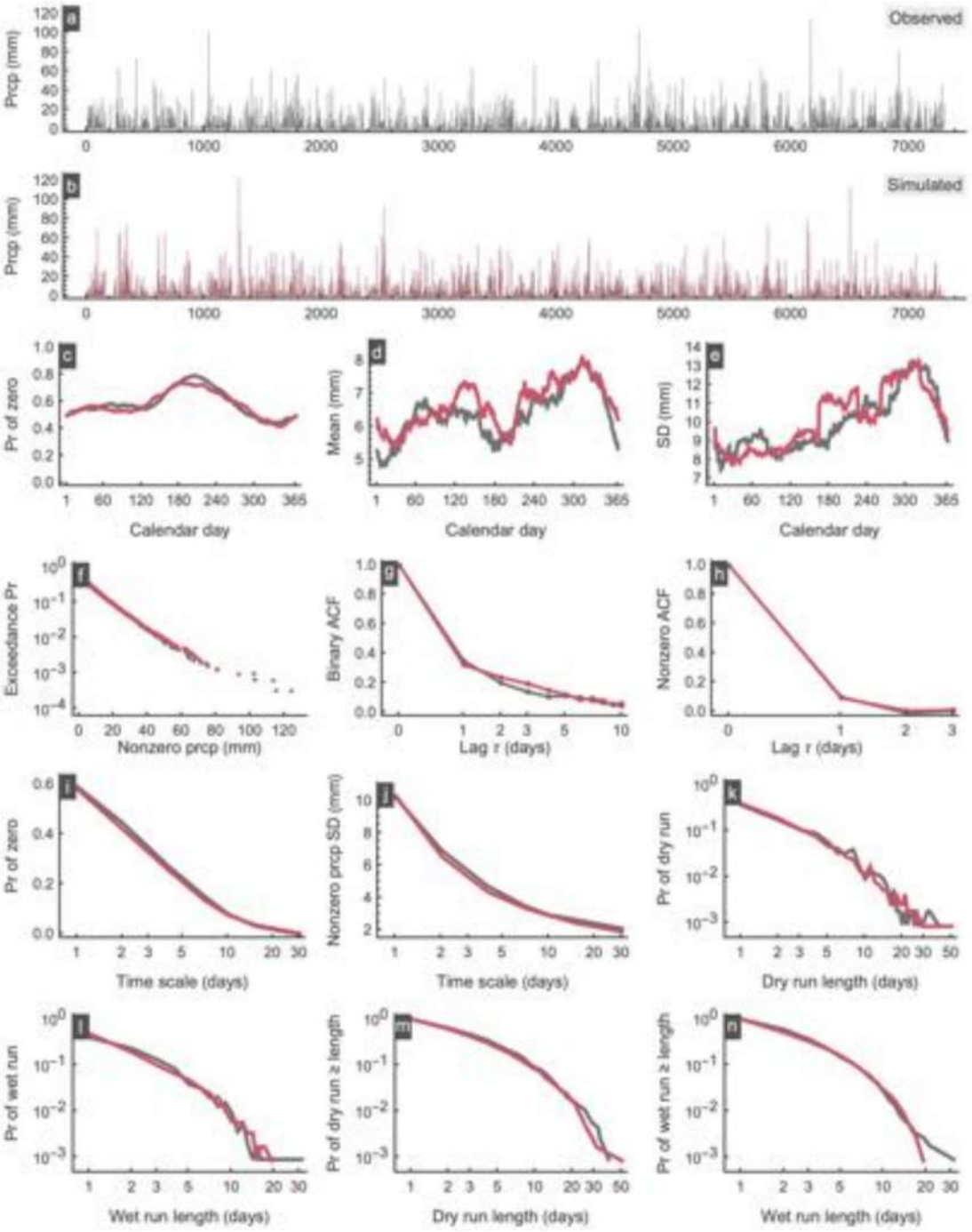

Figure A21. Simulation results for station PluvioMetro 26.

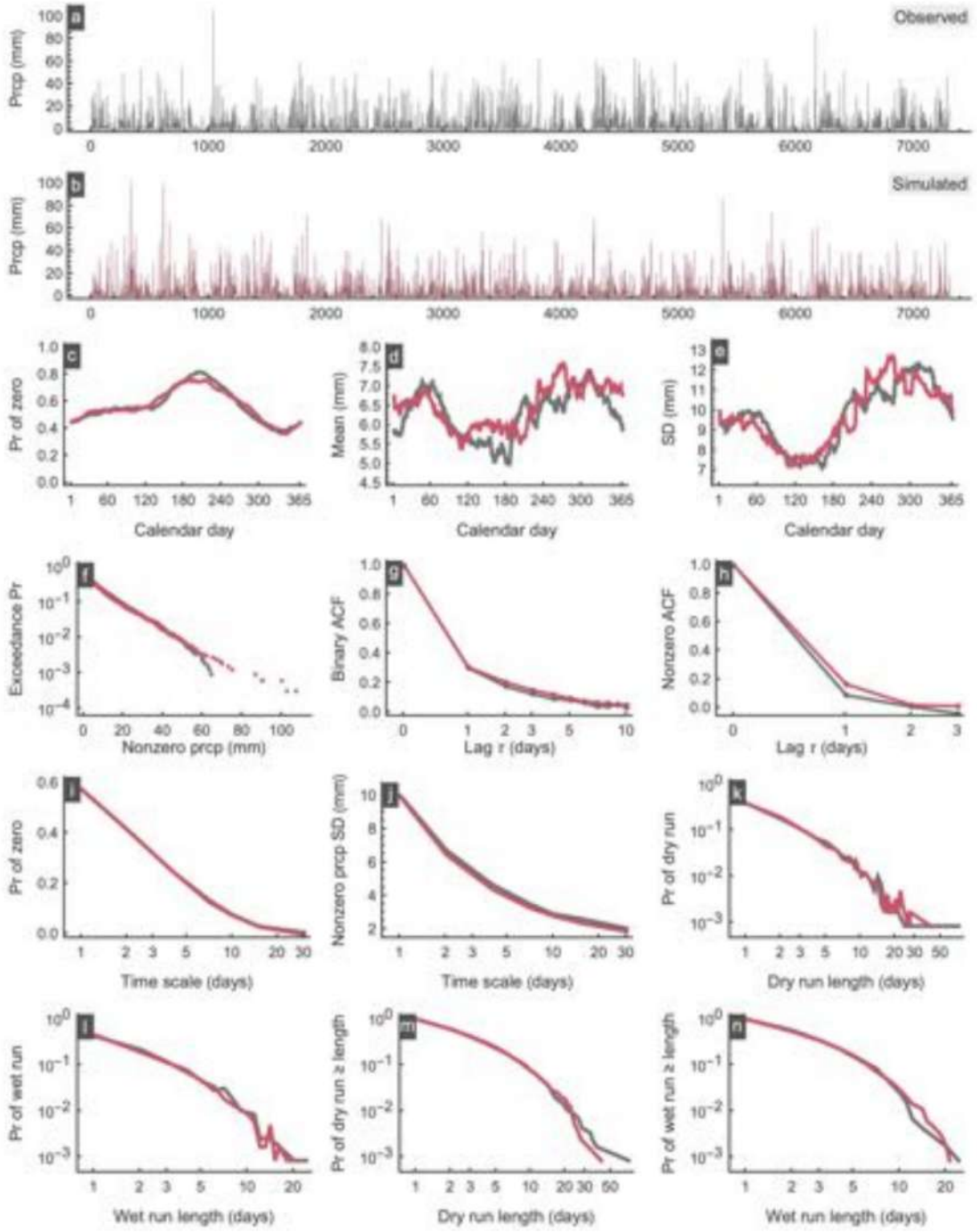

Figure A22. Simulation results for station PluvioMetro 27.

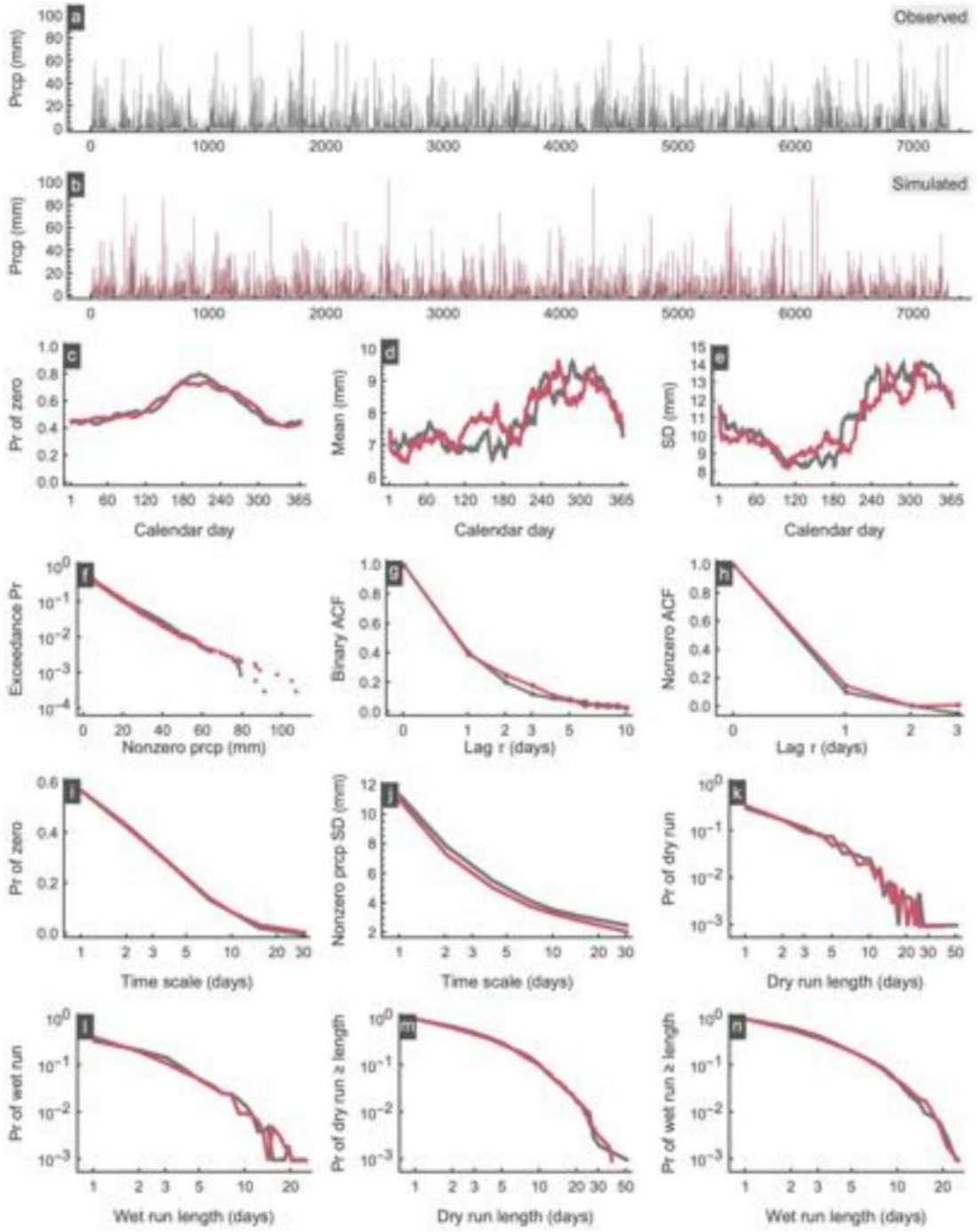

Figure A23. Simulation results for station PluvioMetro 28.

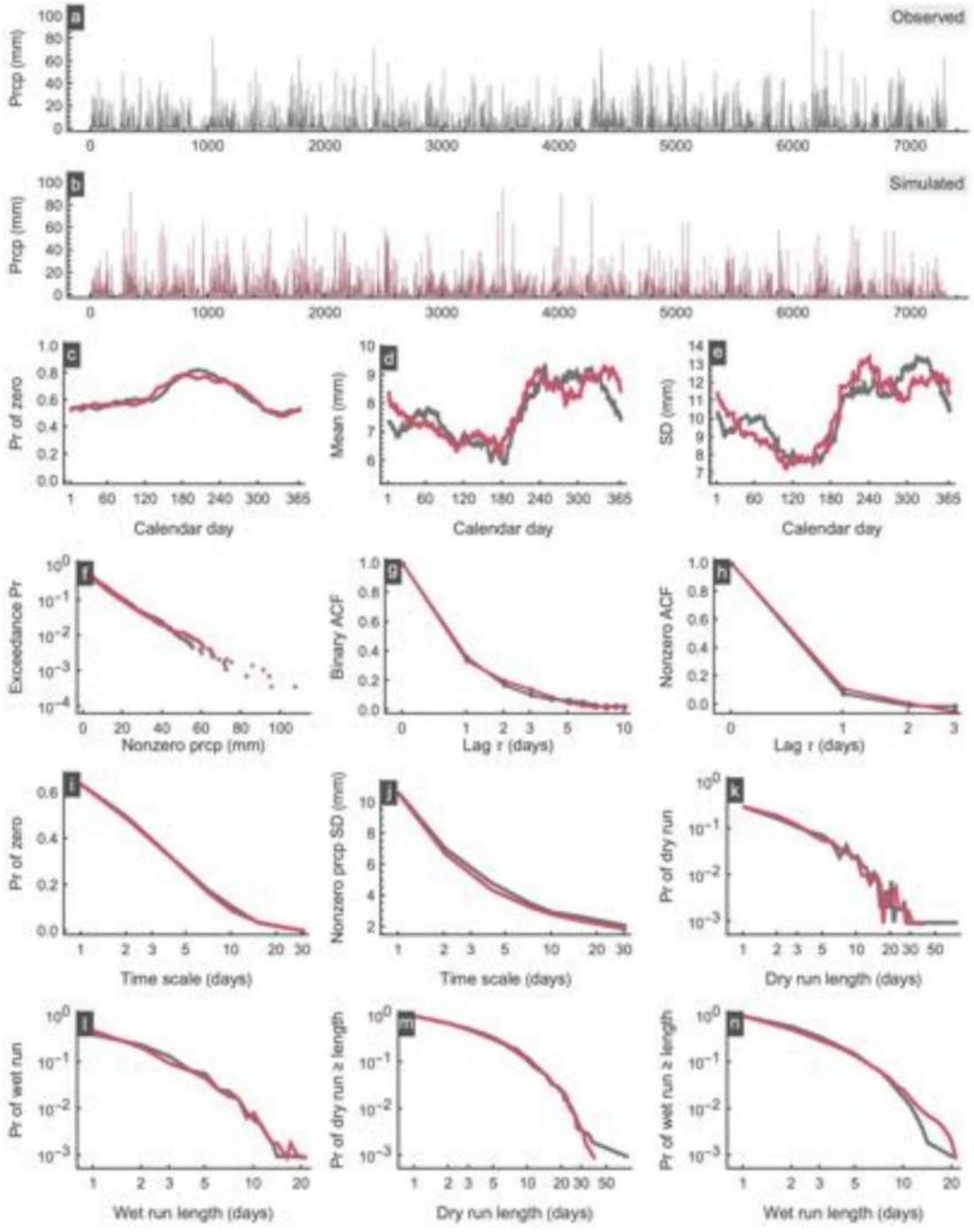

Figure A24. Simulation results for station PluvioMetro 29.

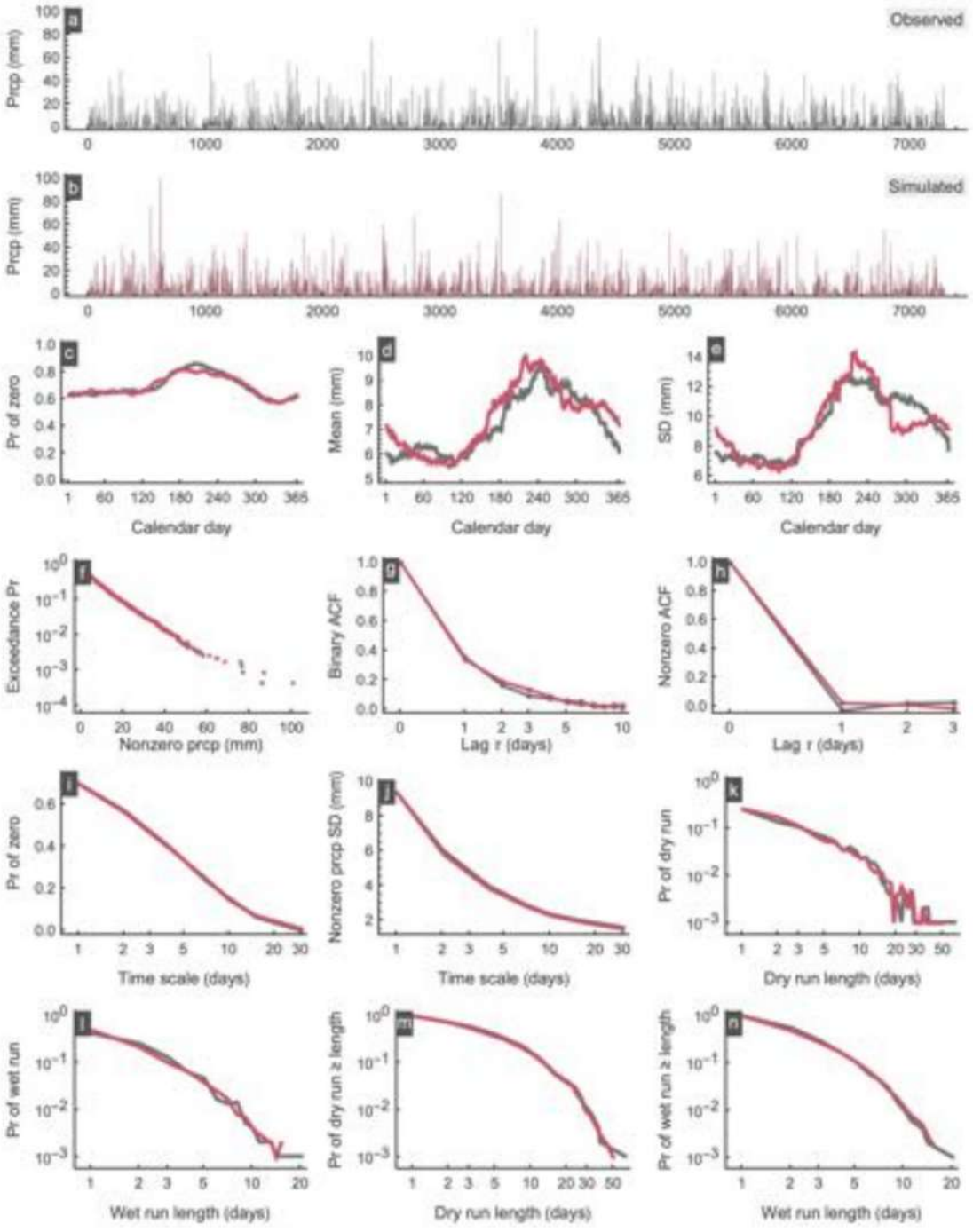

Figure A25. Simulation results for station PluvioMetro 30.

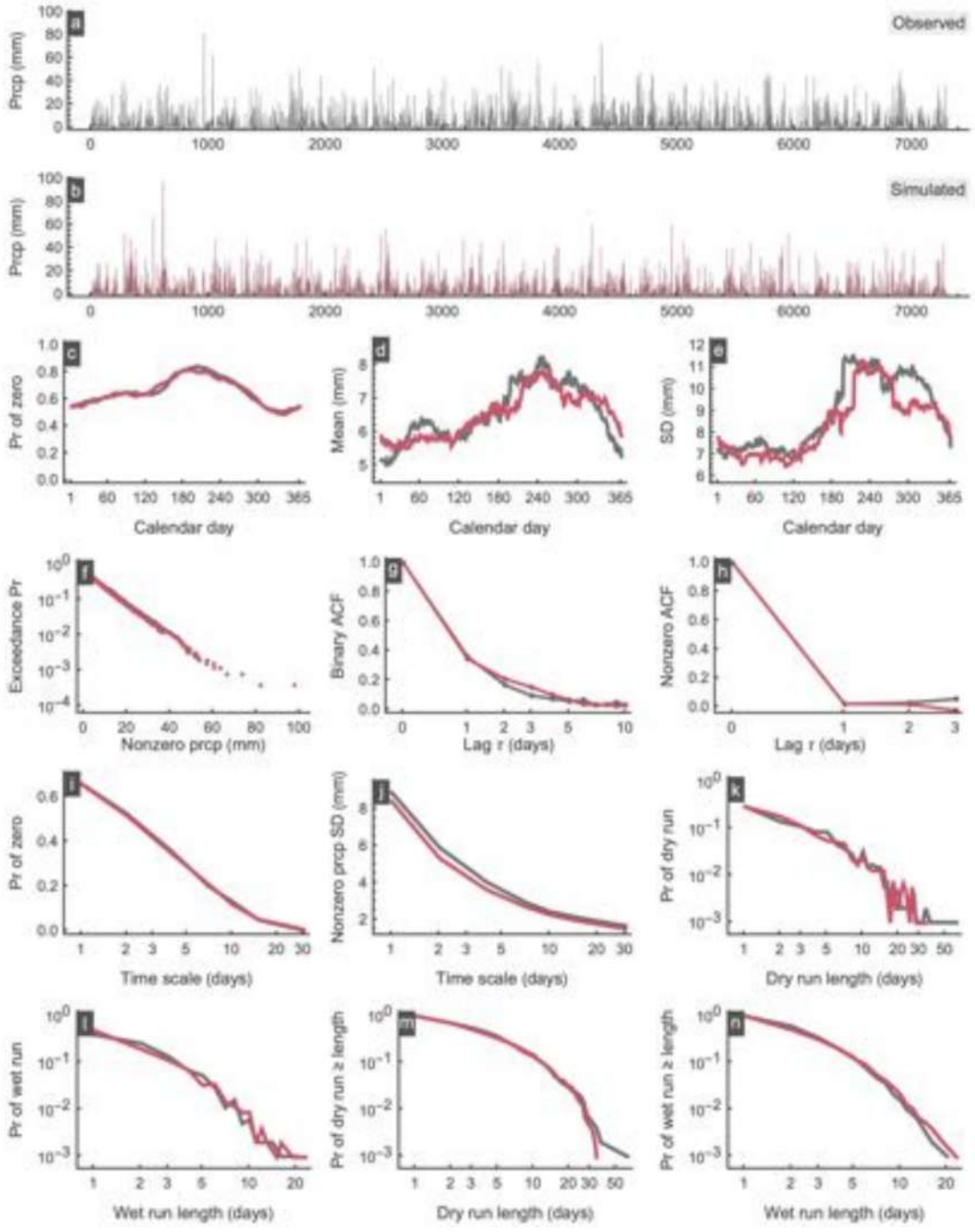

Figure A26. Simulation results for station PluvioMetro 31.

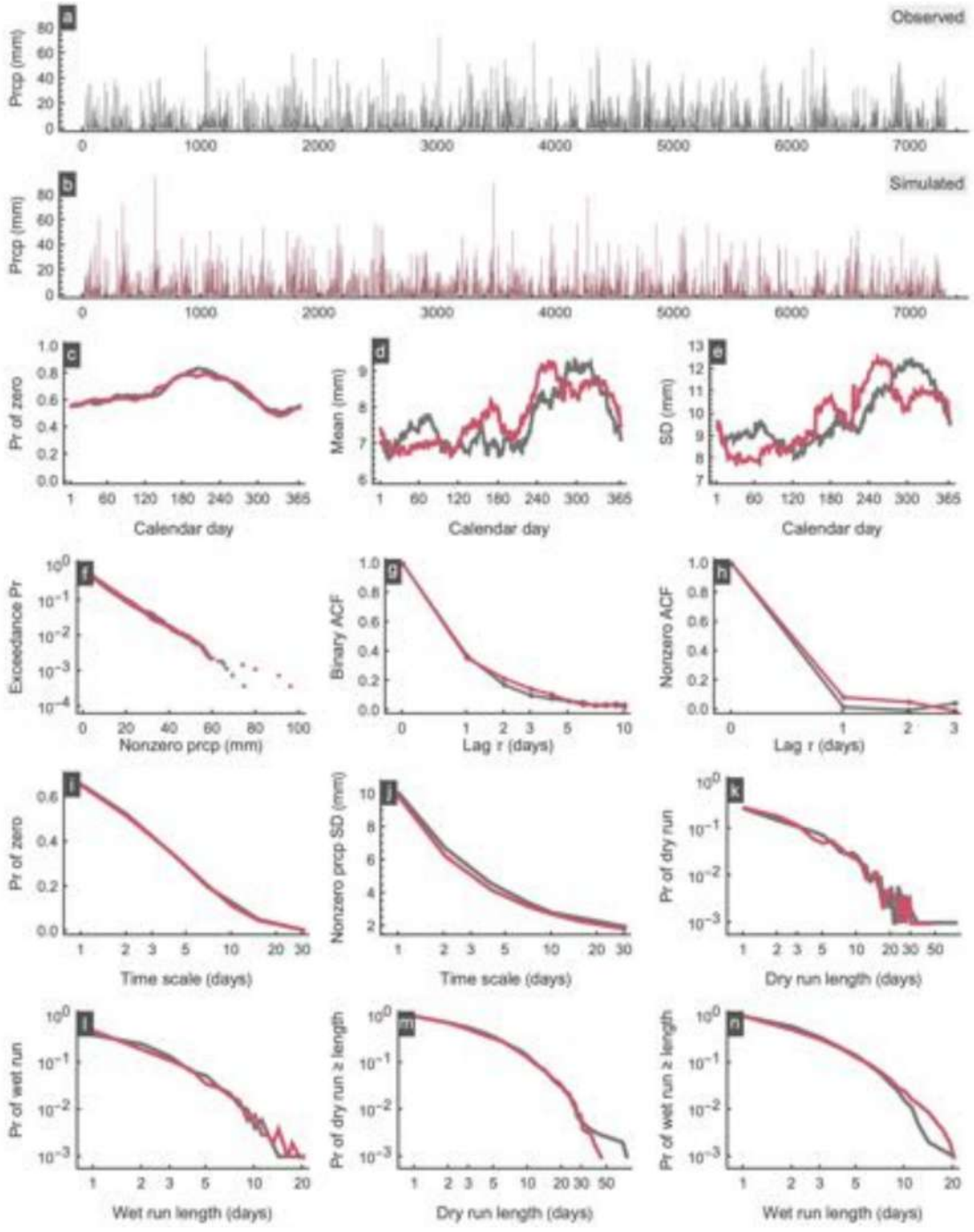

Figure A27. Simulation results for station PluvioMetro 32.

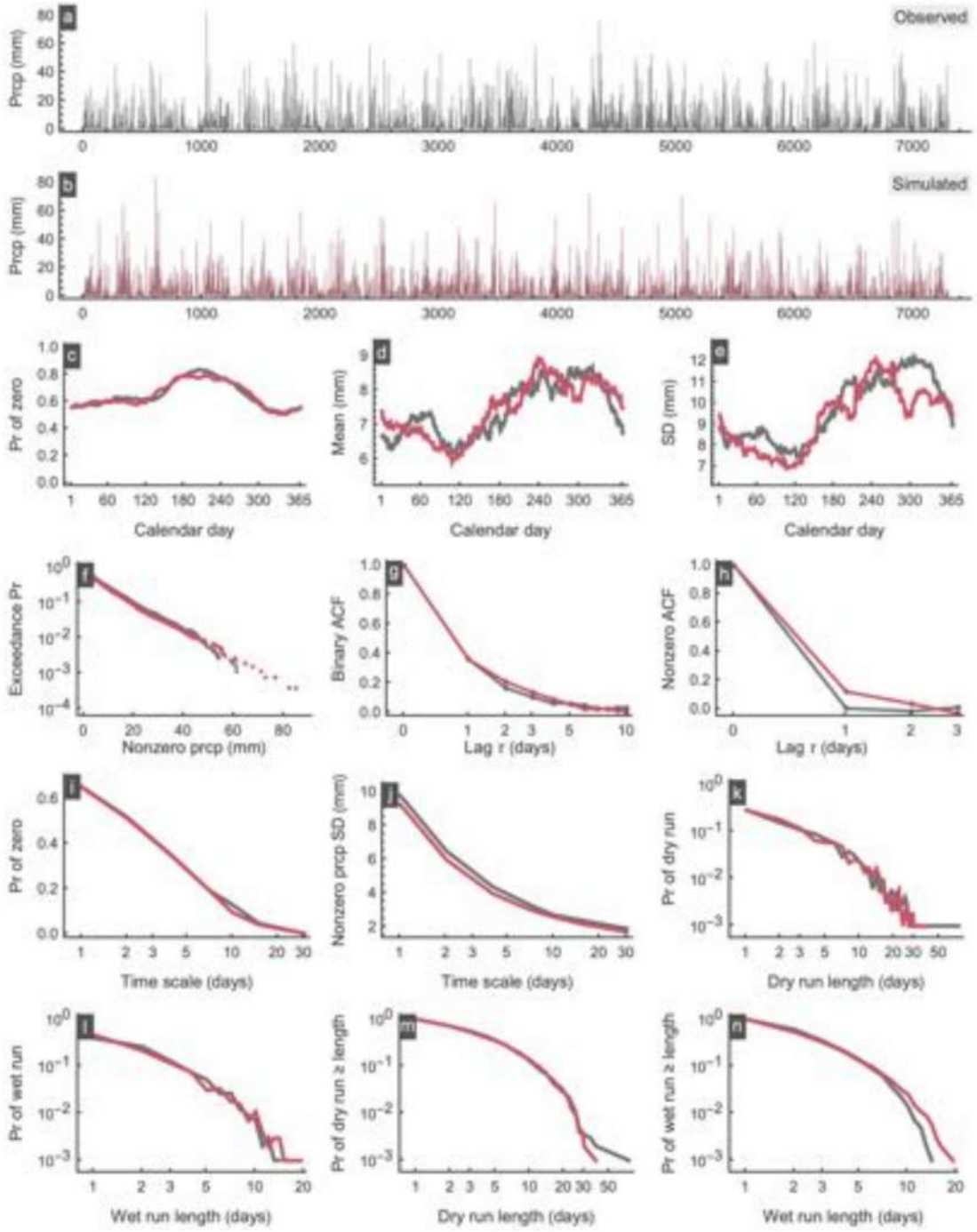

Figure A28. Simulation results for station PluvioMetro 33.

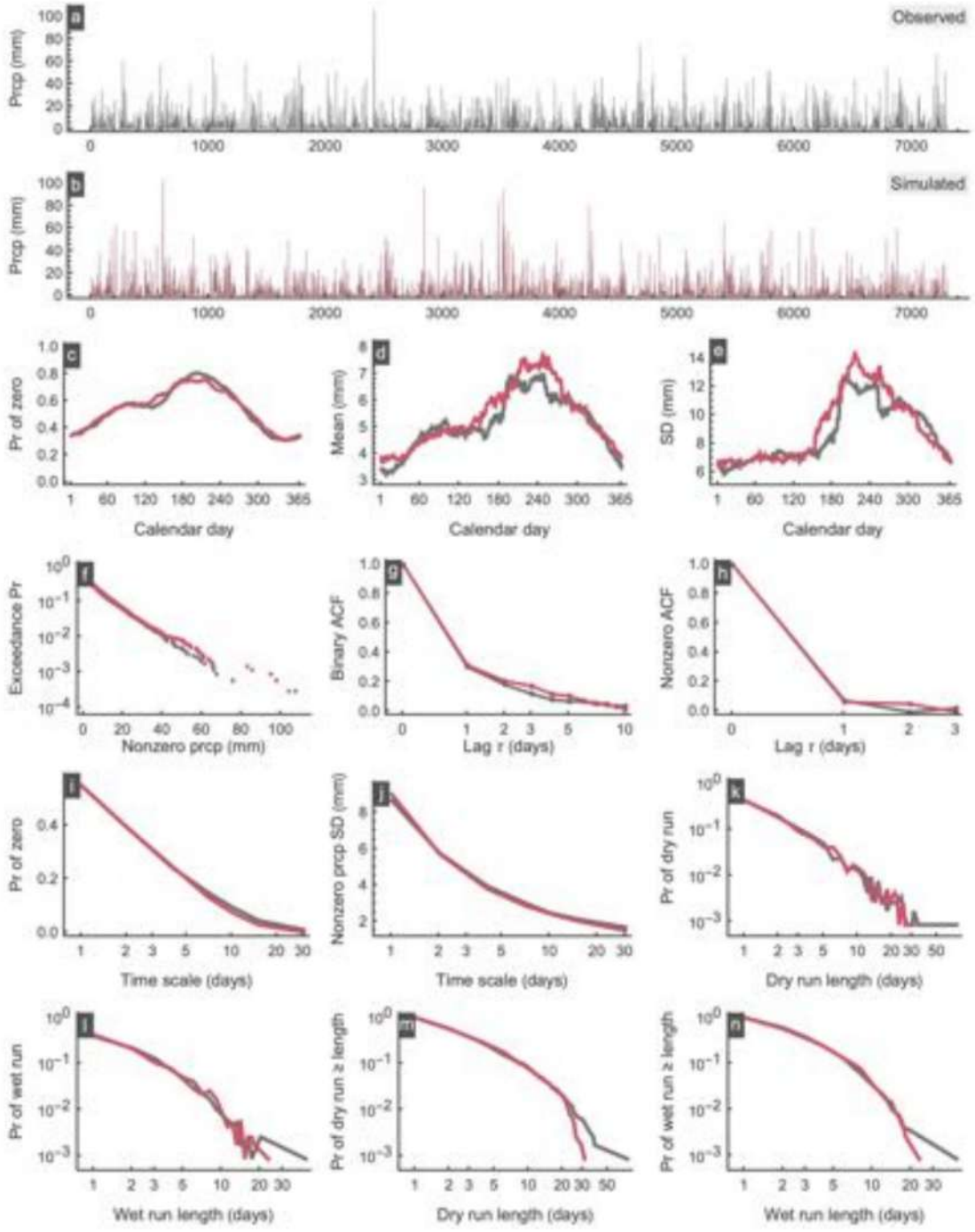

Figure A29. Simulation results for station PluvioMetro 34.

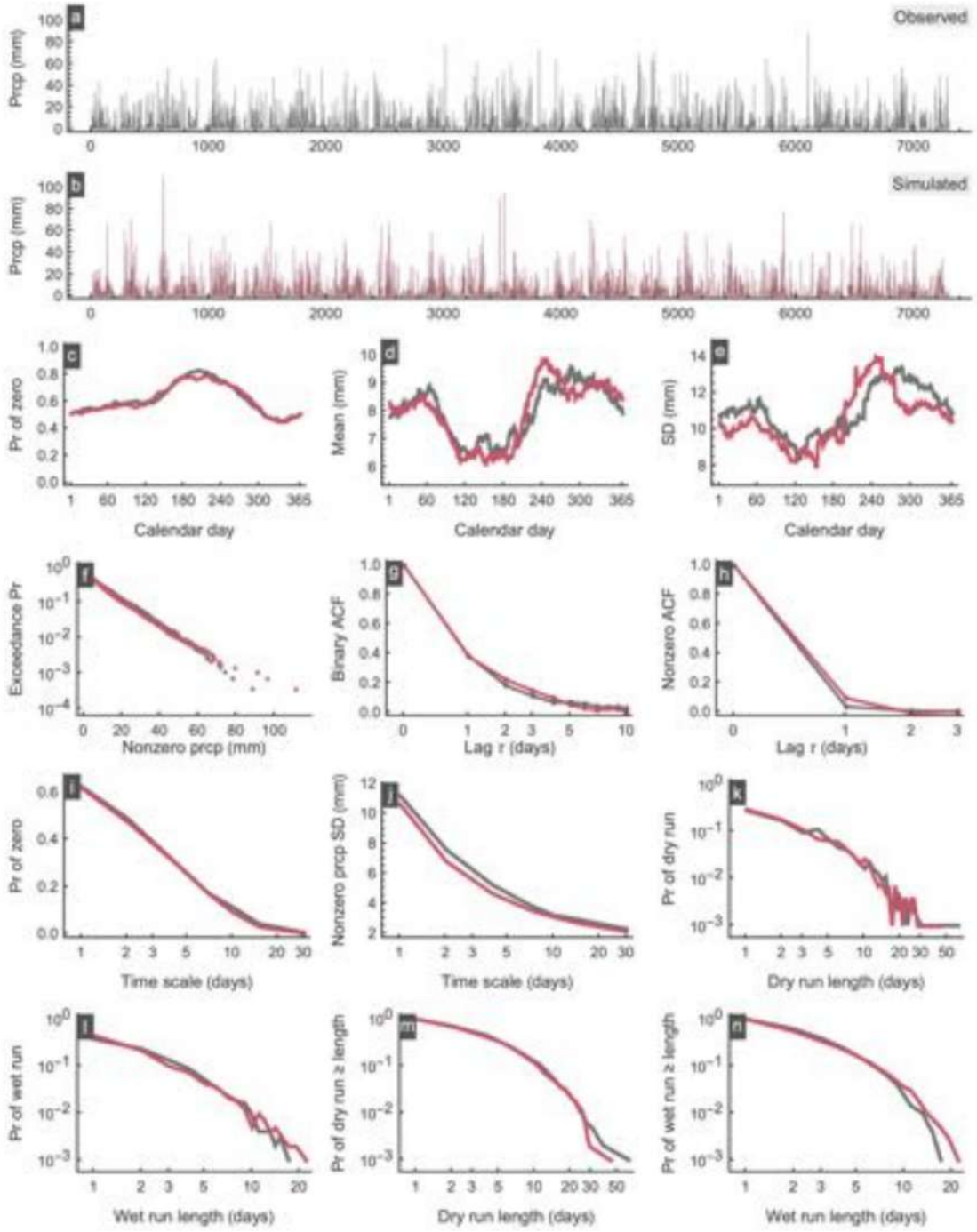

Figure A30. Simulation results for station PluvioMetro 38.

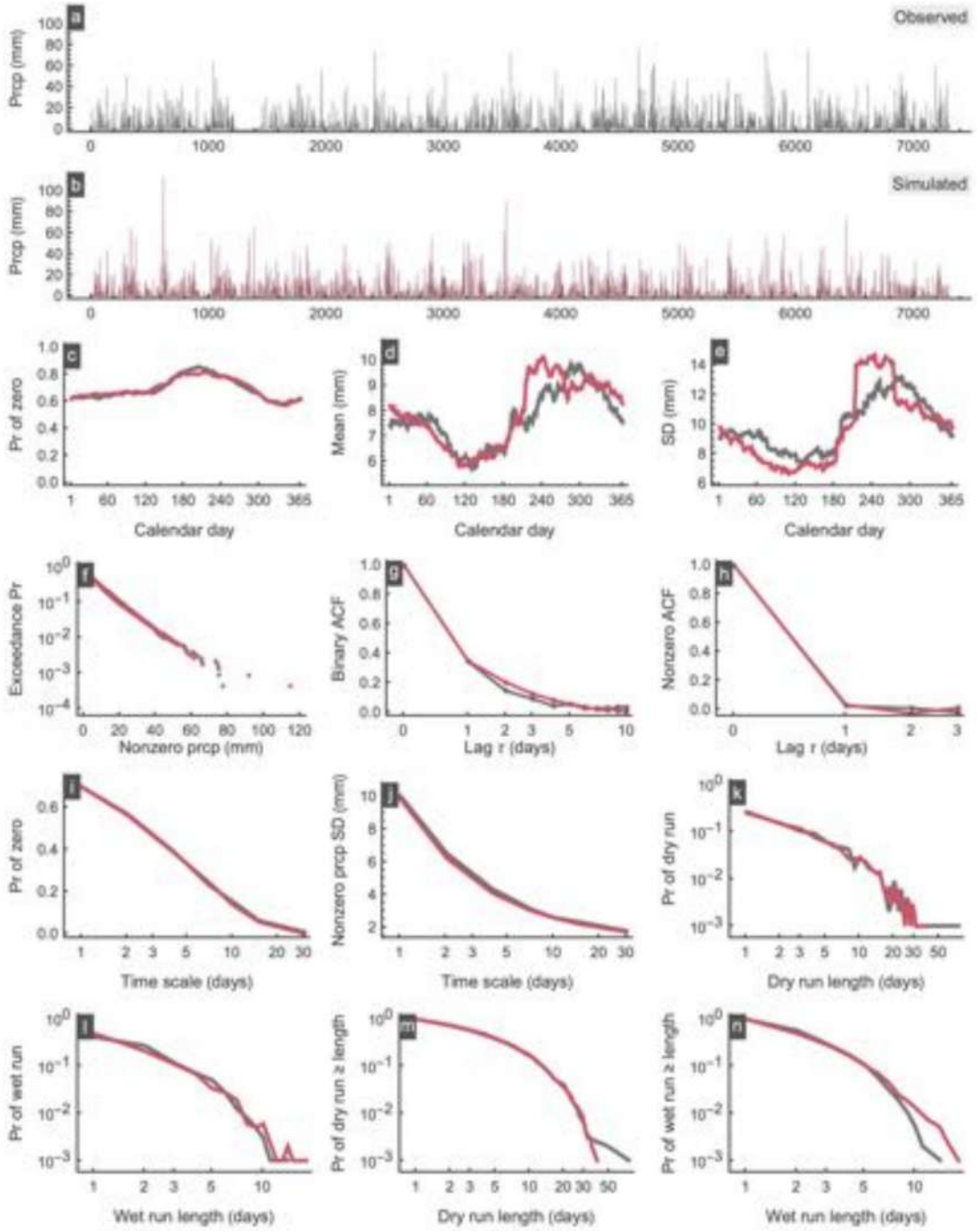

Figure A31. Simulation results for station PluvioMetro 39.

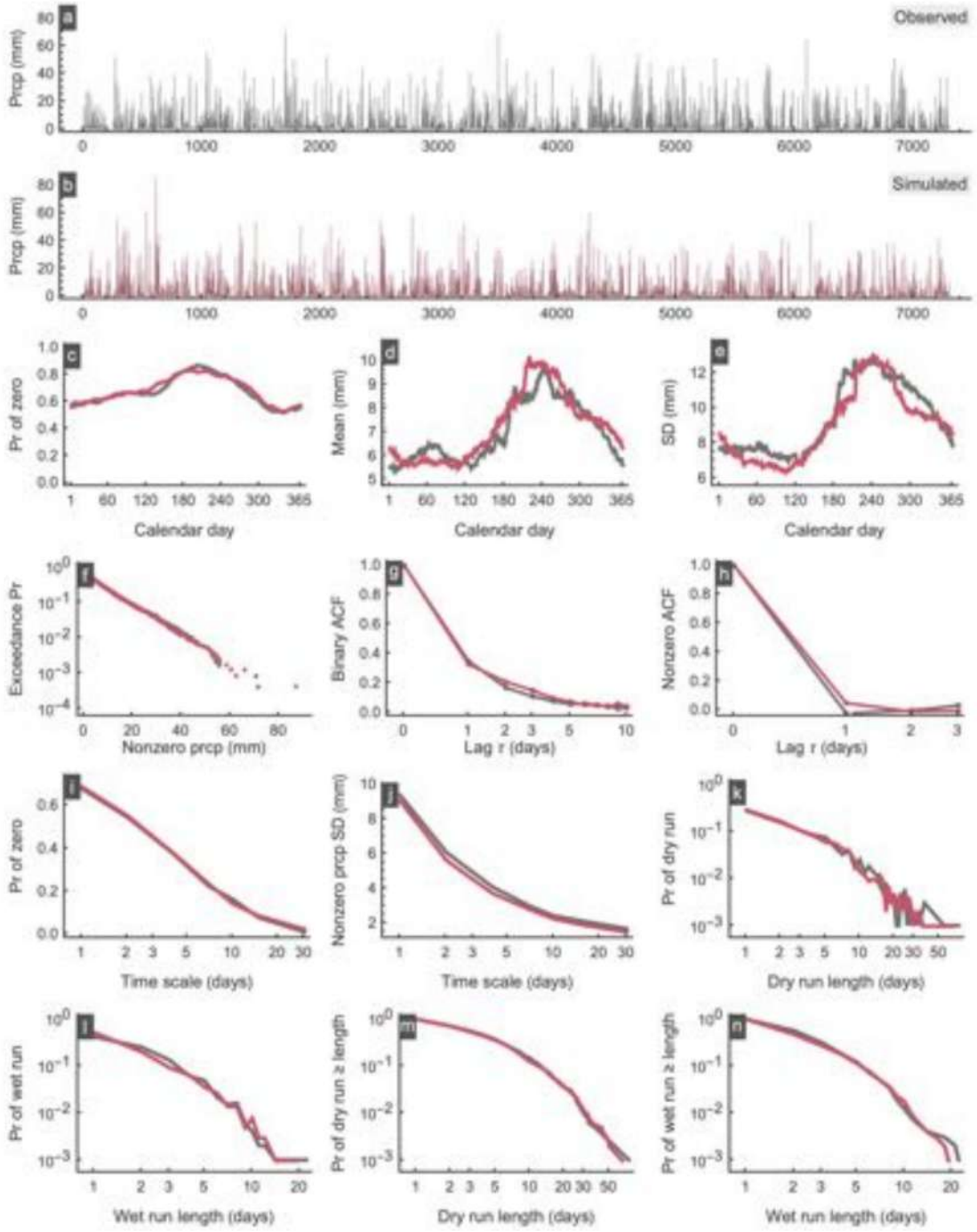

Figure A32. Simulation results for station PluvioMetro 40.

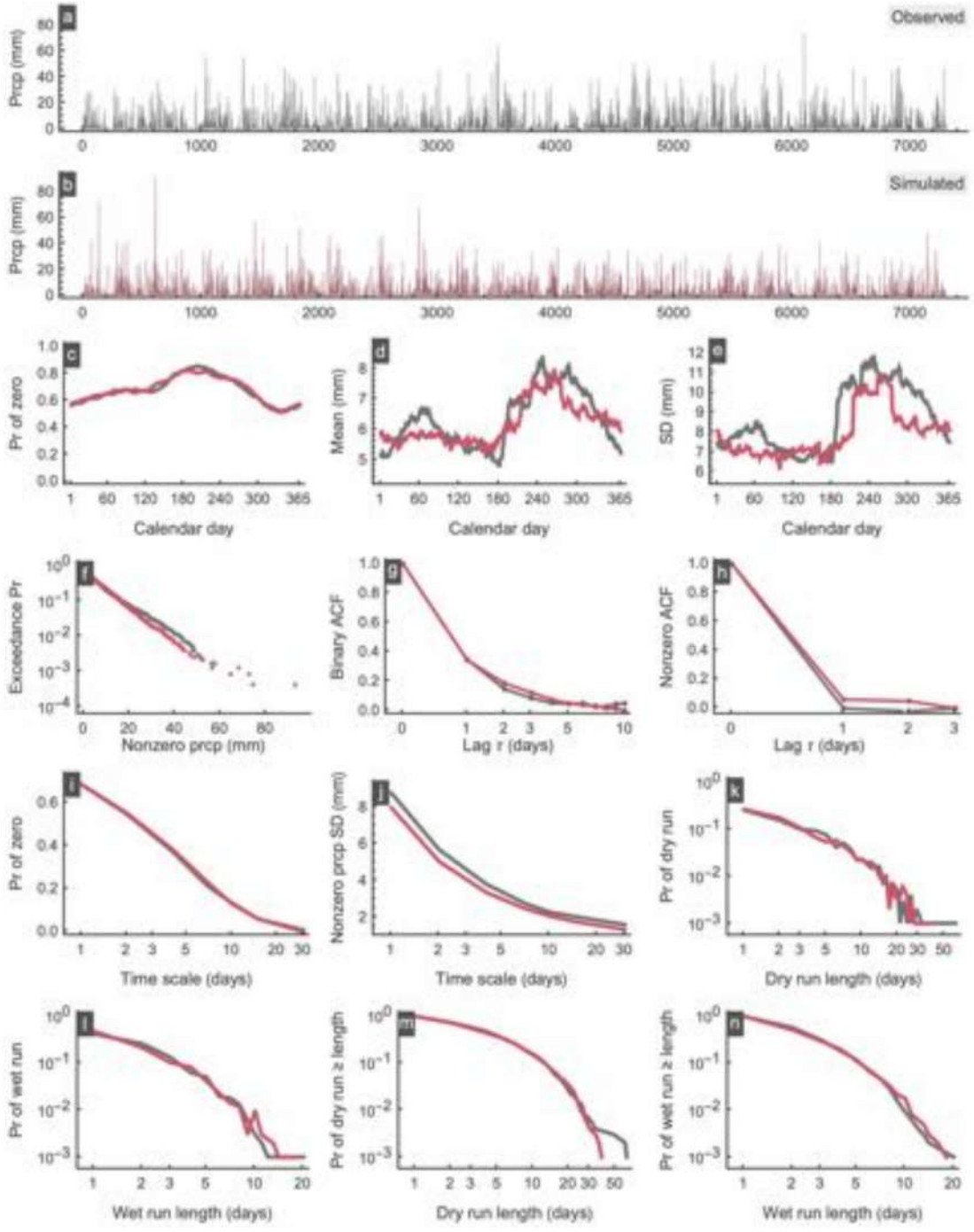

Figure A33. Simulation results for station PluvioMetro 41.

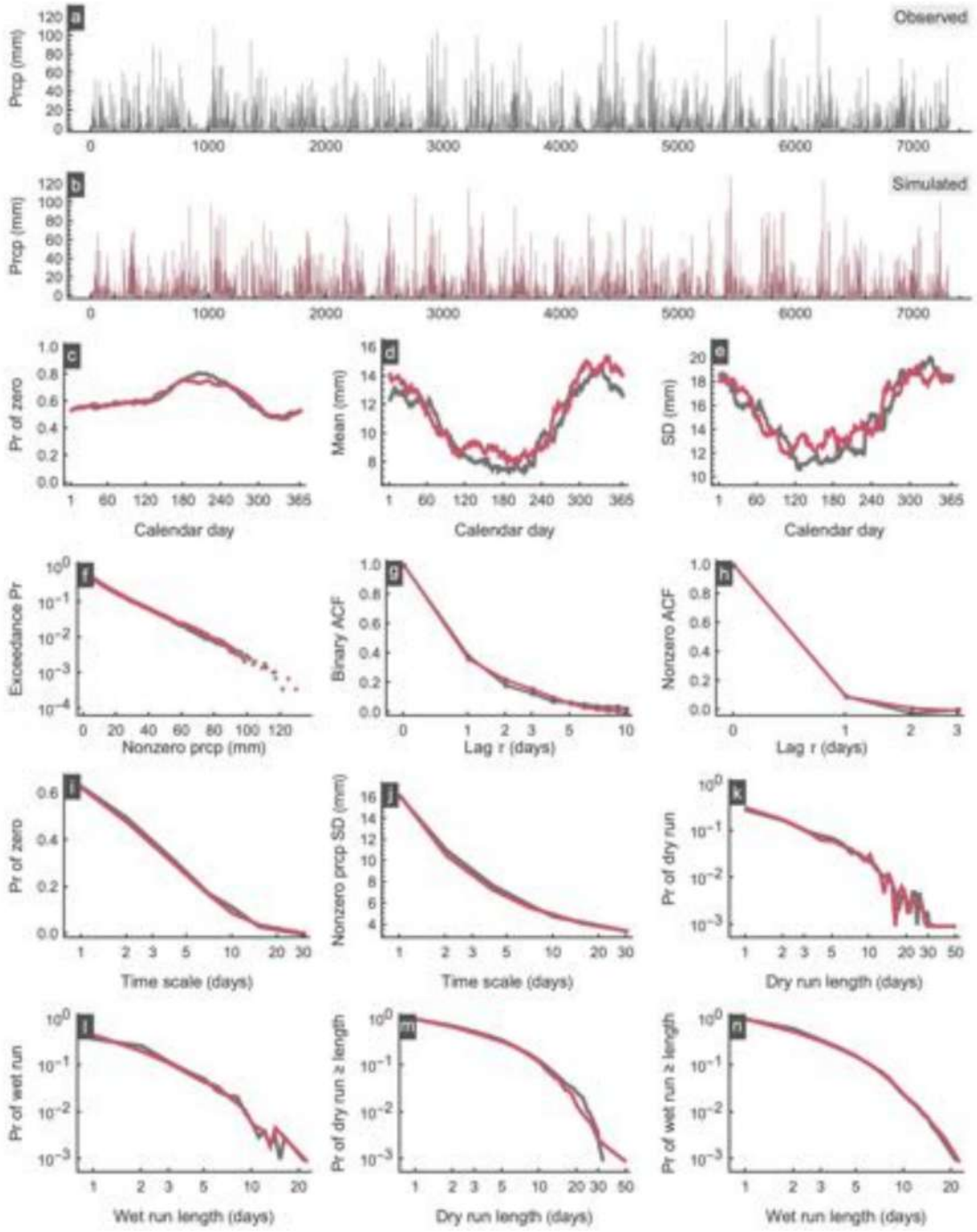

Figure A34. Simulation results for station PluvioMetro 42.

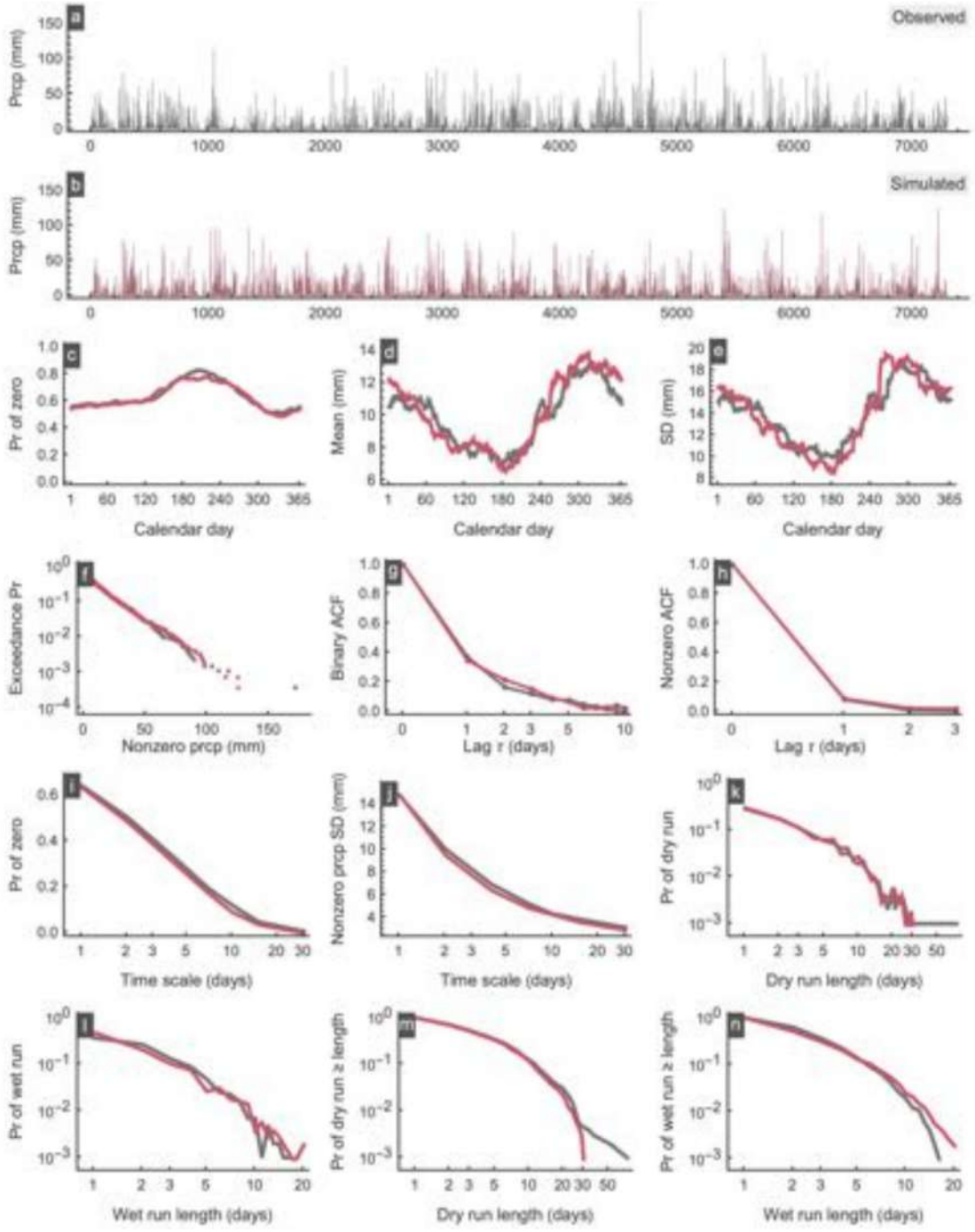

Figure A35. Simulation results for station PluvioMetro 43.

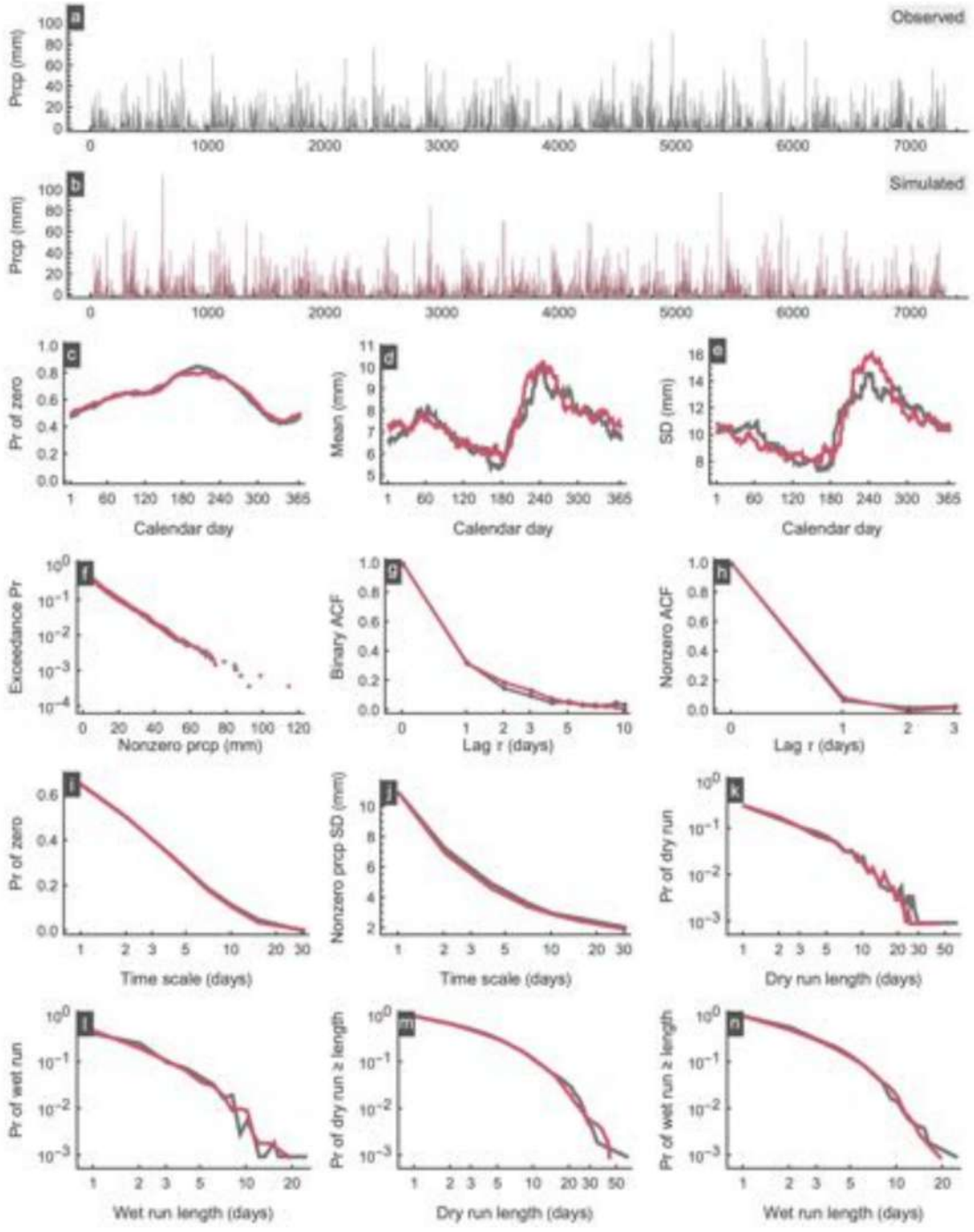

Figure A36. Simulation results for station PluvioMetro 44.

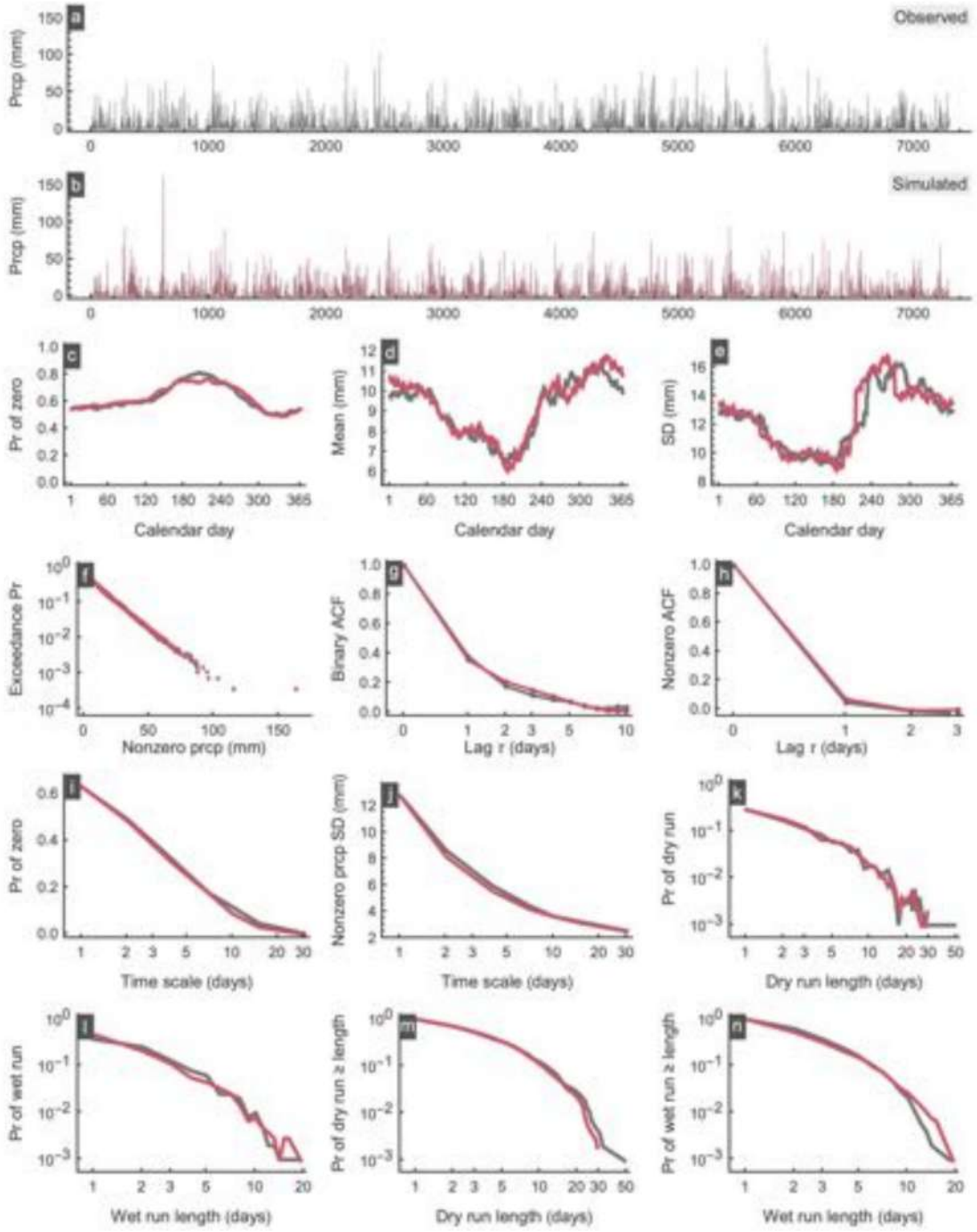

Figure A37. Simulation results for station PluvioMetro 45.

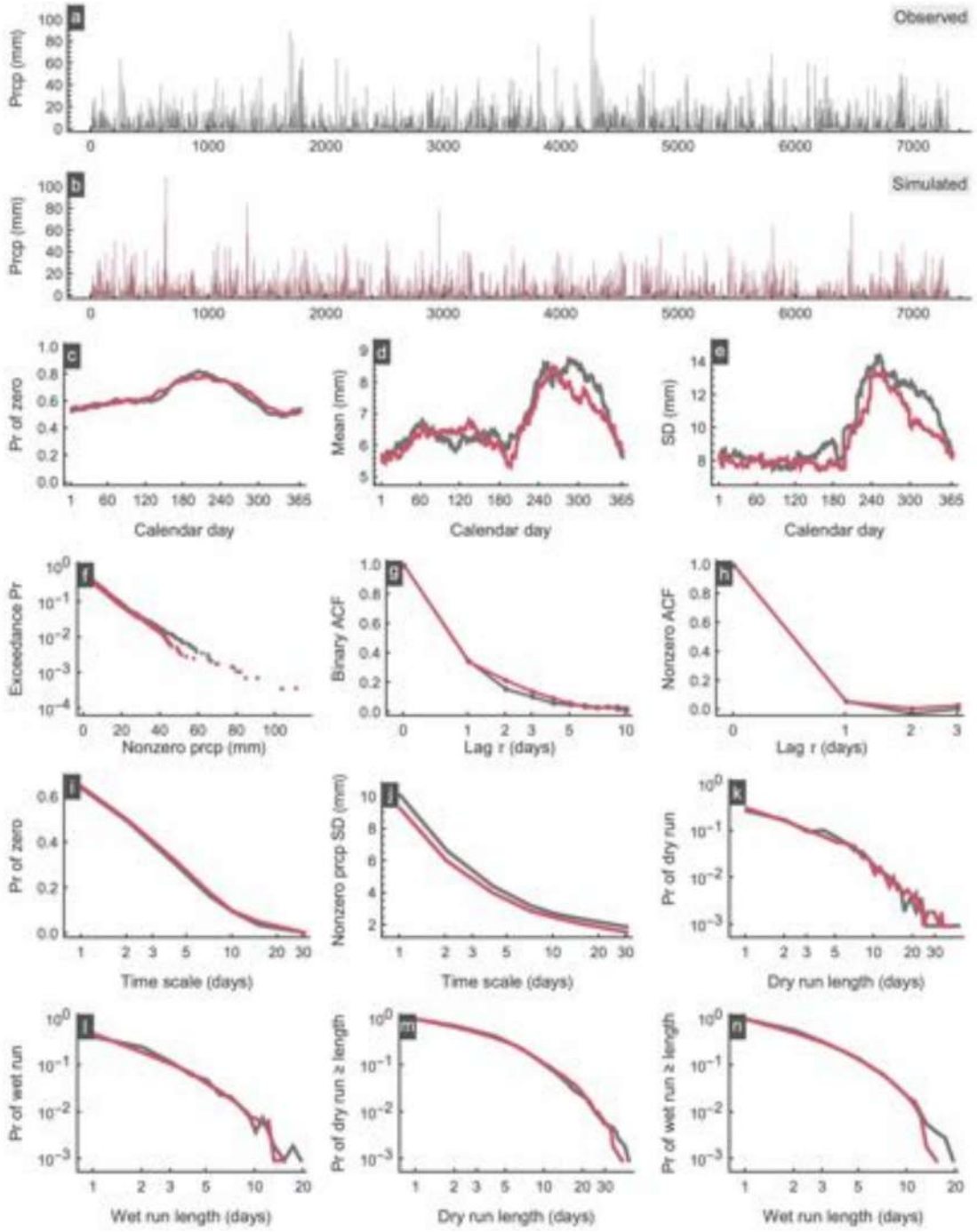

Figure A38. Simulation results for station PluvioMetro 46.

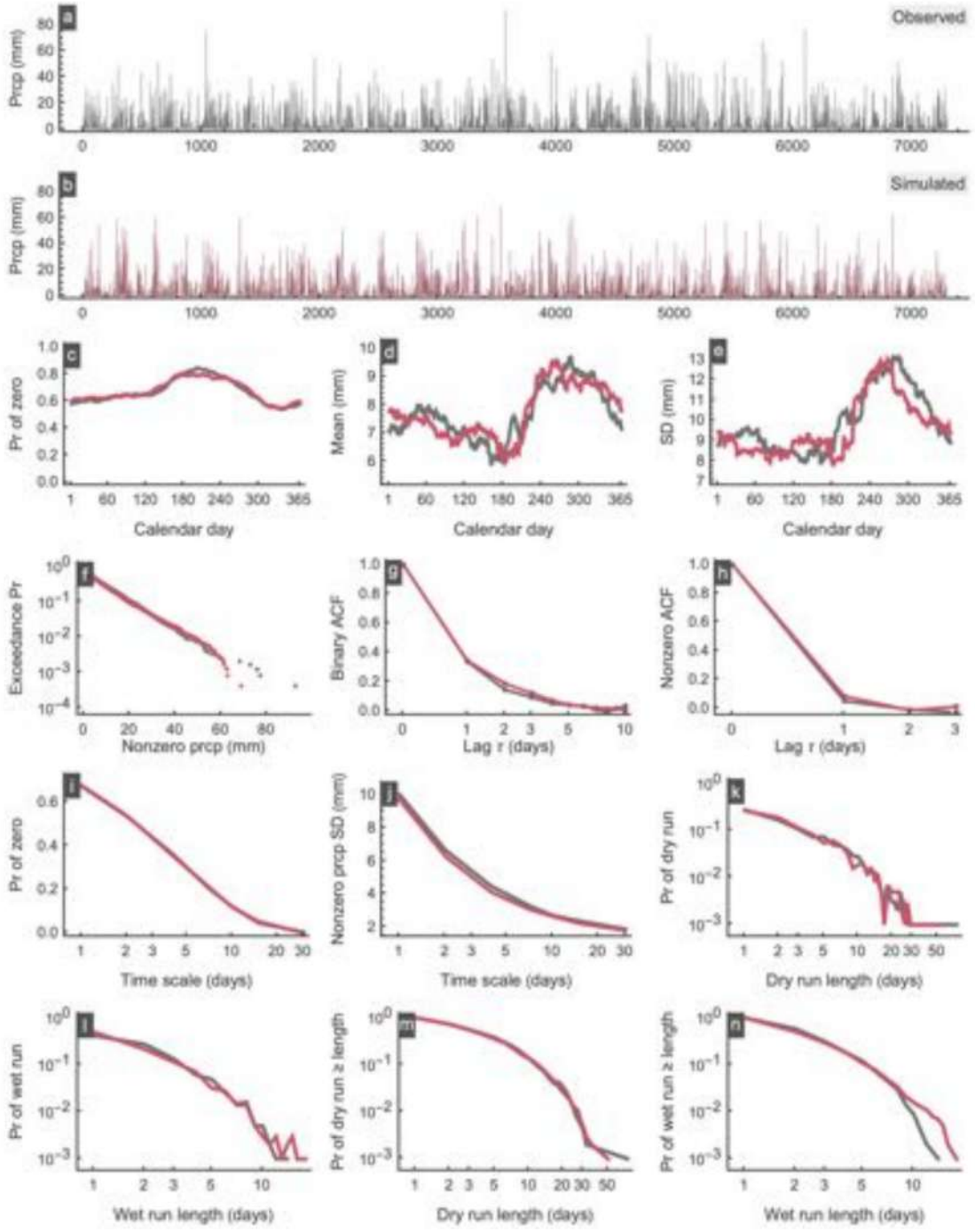

Figure A39. Simulation results for station PluvioMetro 47.

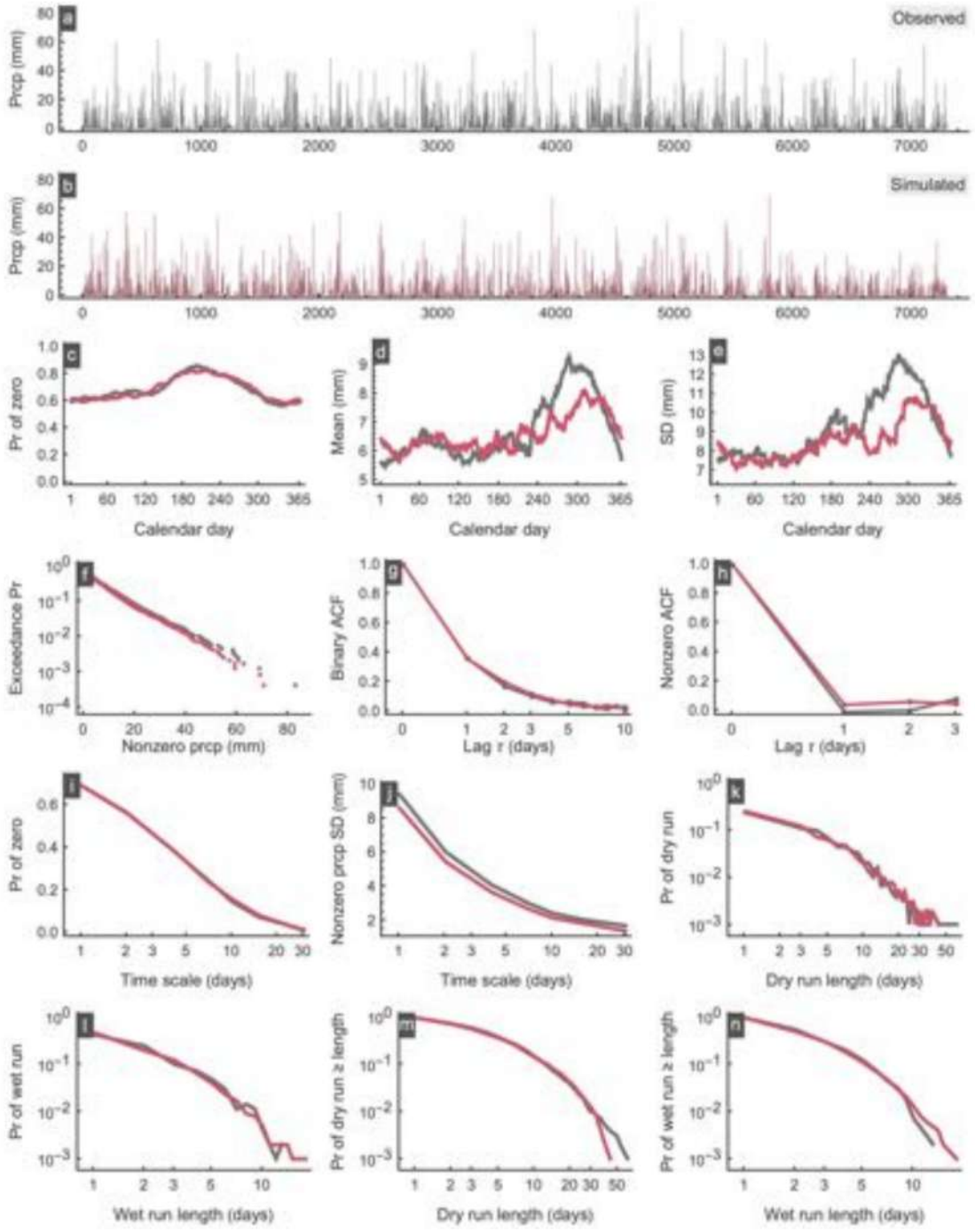

Figure A40. Simulation results for station PluvioMetro 48.

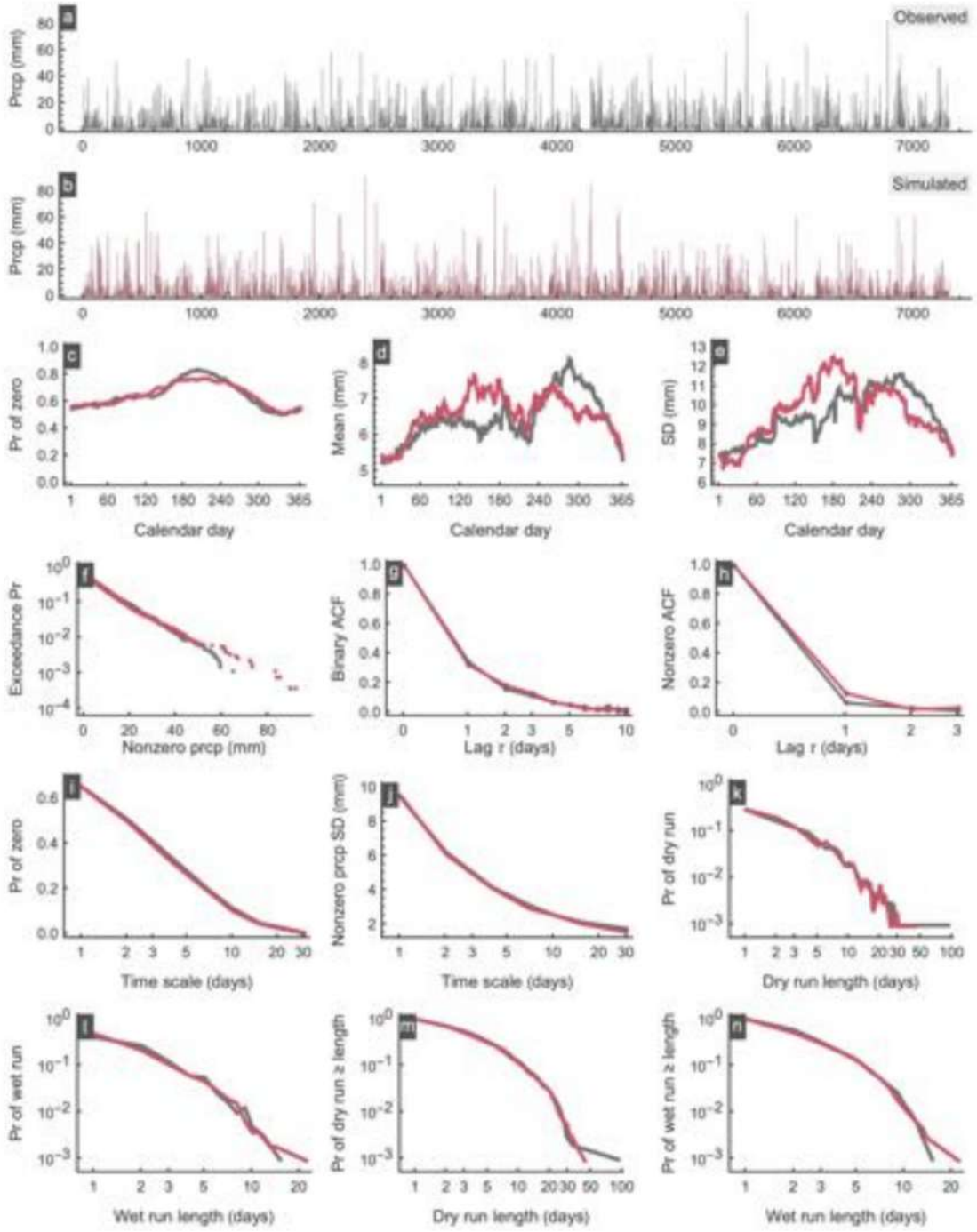

Figure A41. Simulation results for station PluvioMetro 49.

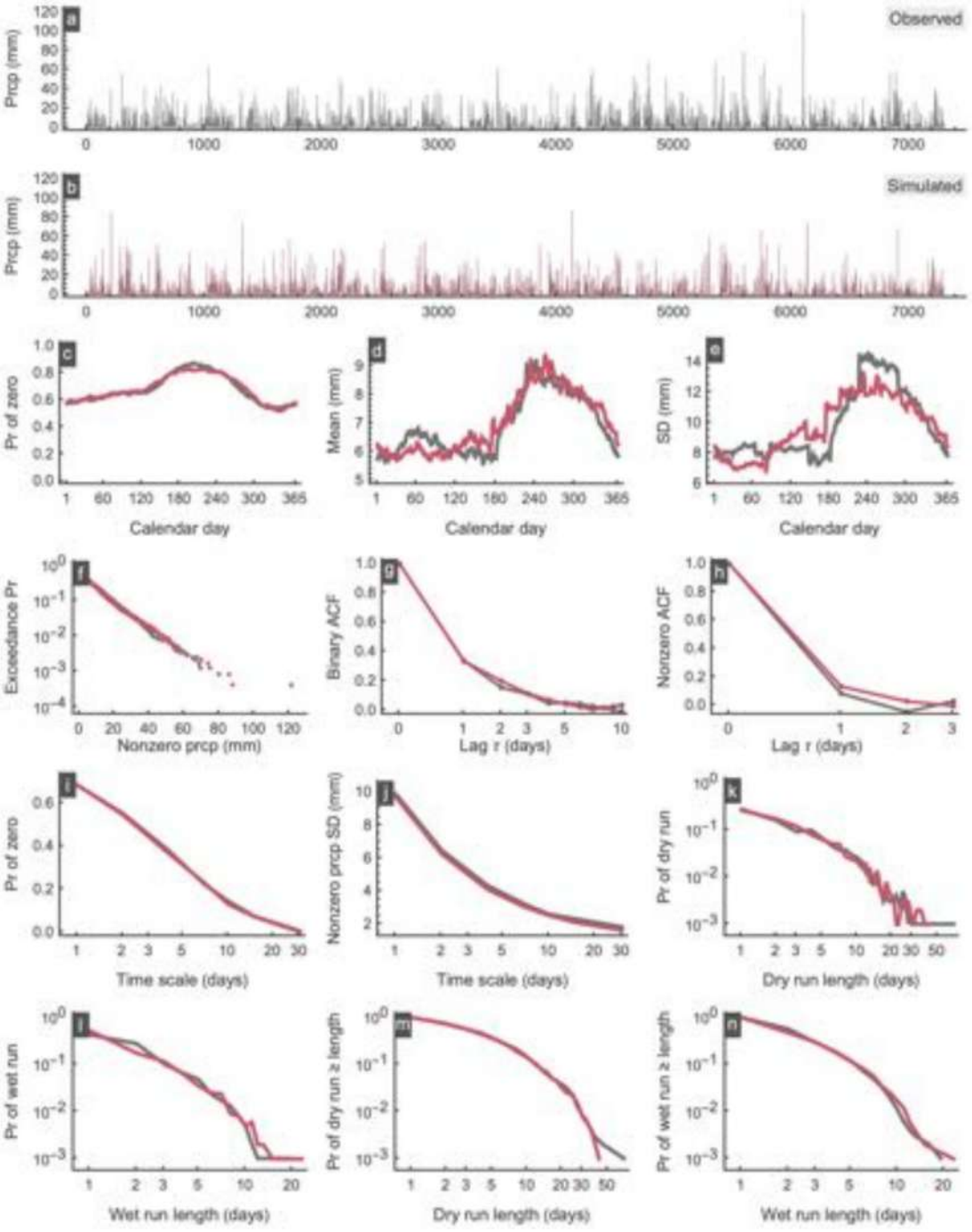

Figure A42. Simulation results for station PluvioMetro 50.

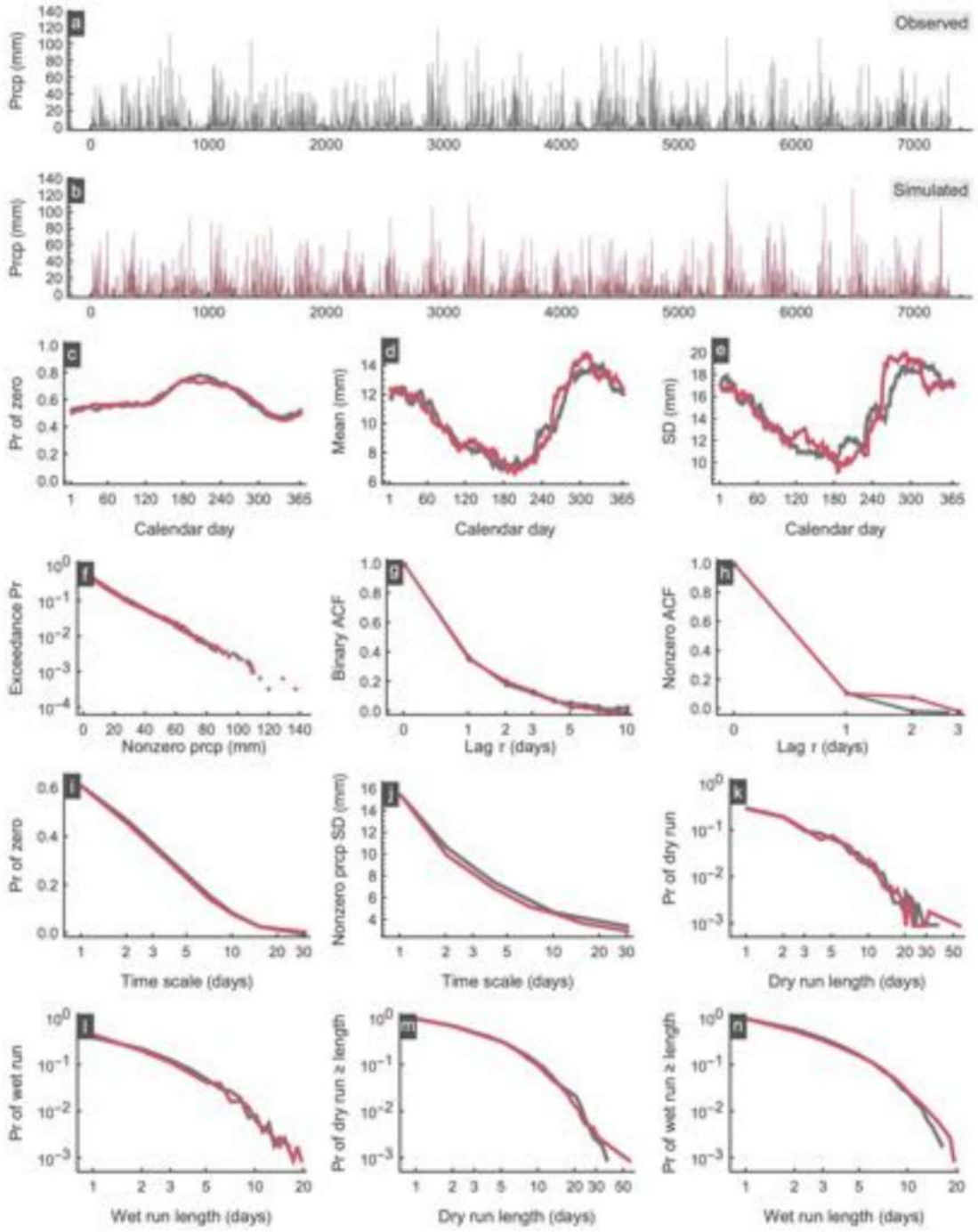

Figure A43. Simulation results for station PluvioMetro 51.

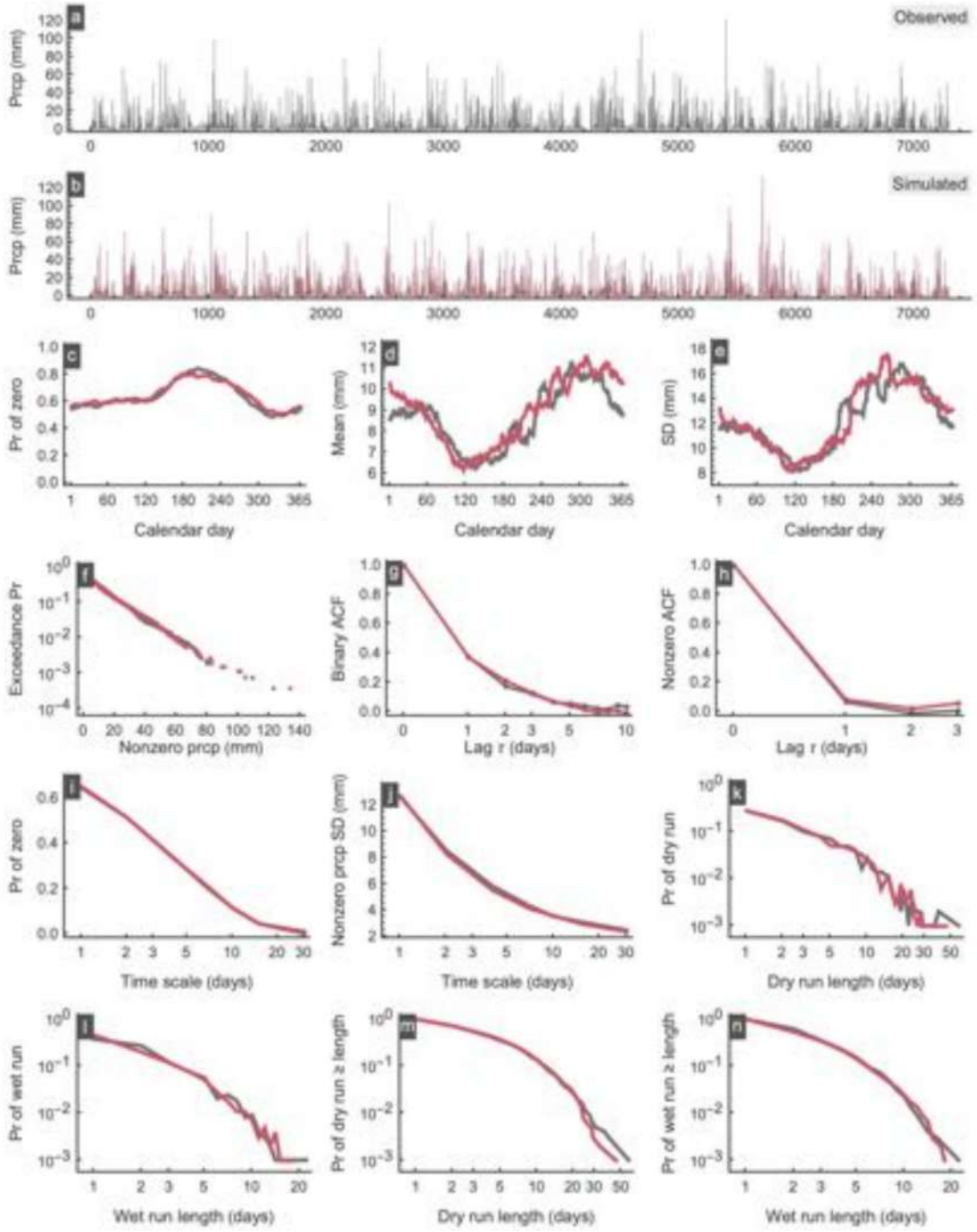

Figure A44. Simulation results for station PluvioMetro 52.

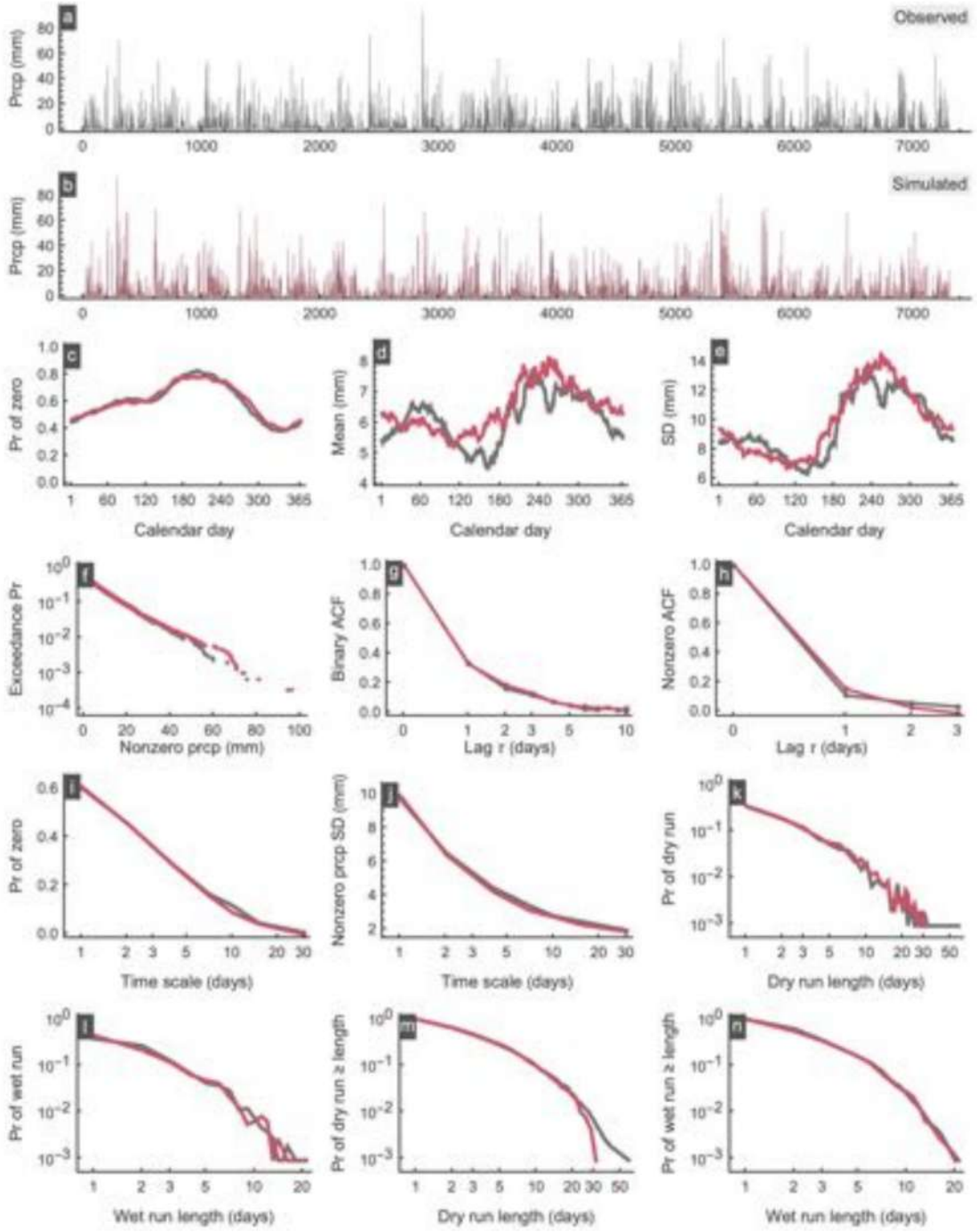

Figure A45. Simulation results for station PluvioMetro 53.

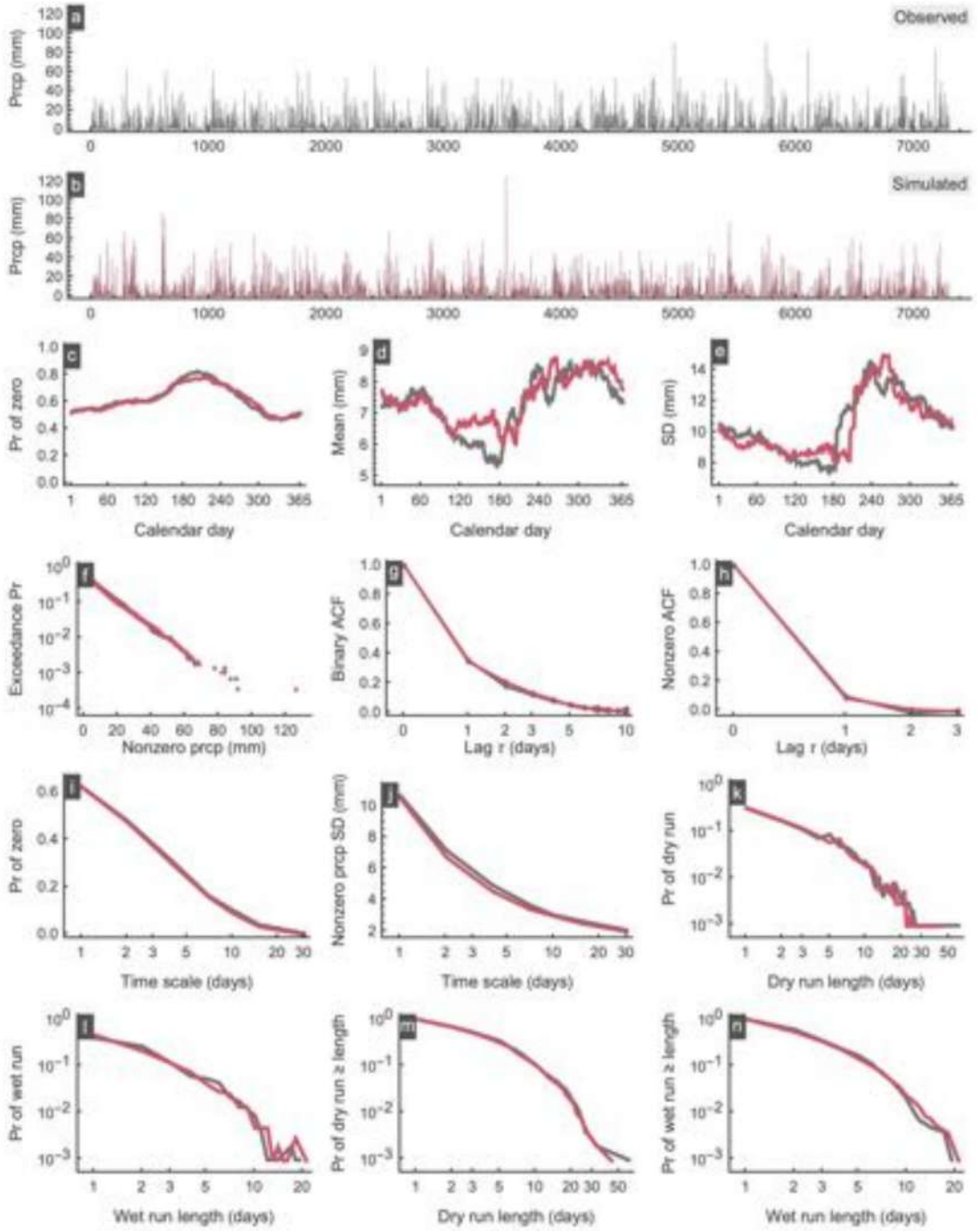

Figure A46. Simulation results for station PluvioMetro 54.

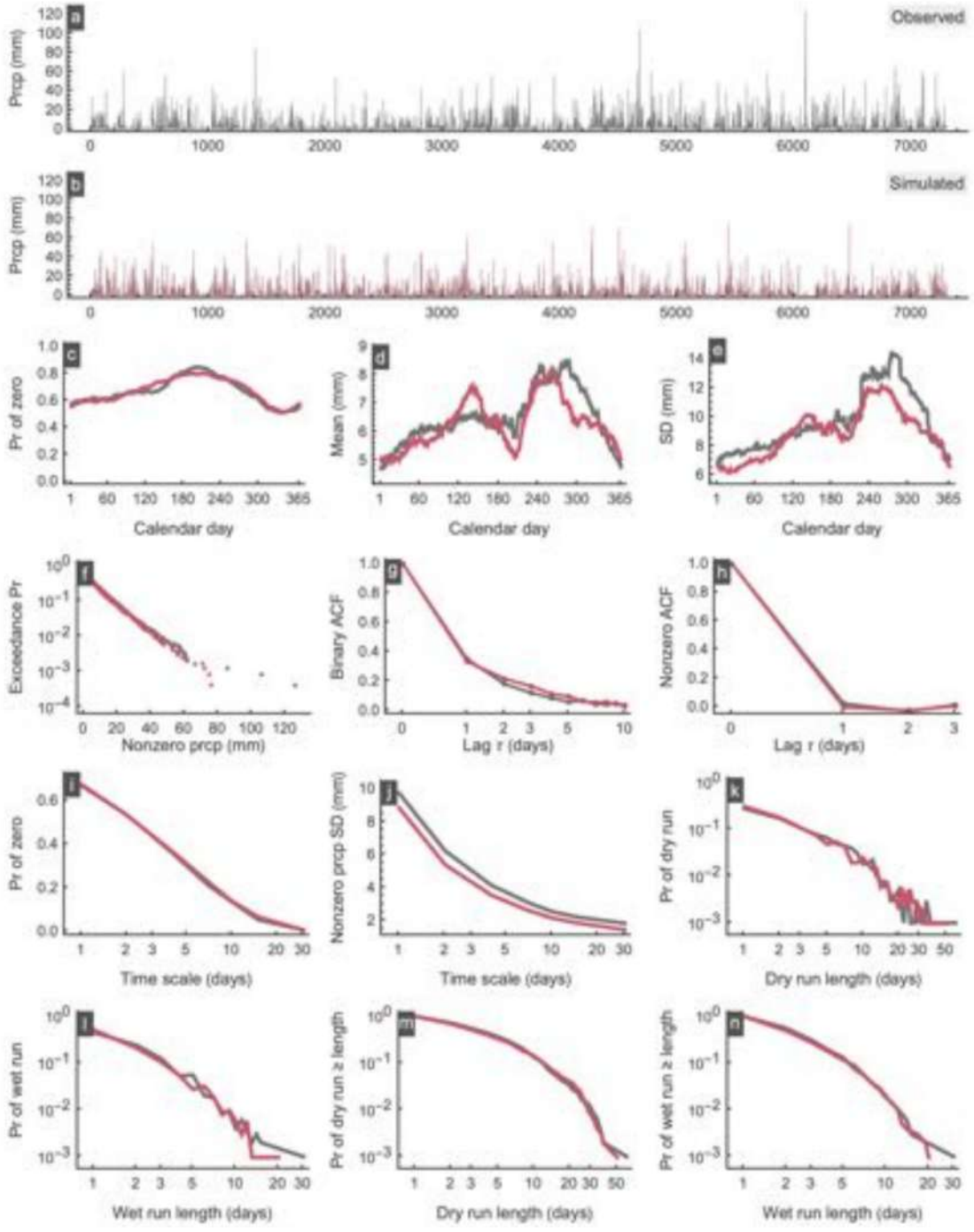

Figure A47. Simulation results for station PluvioMetro 55.

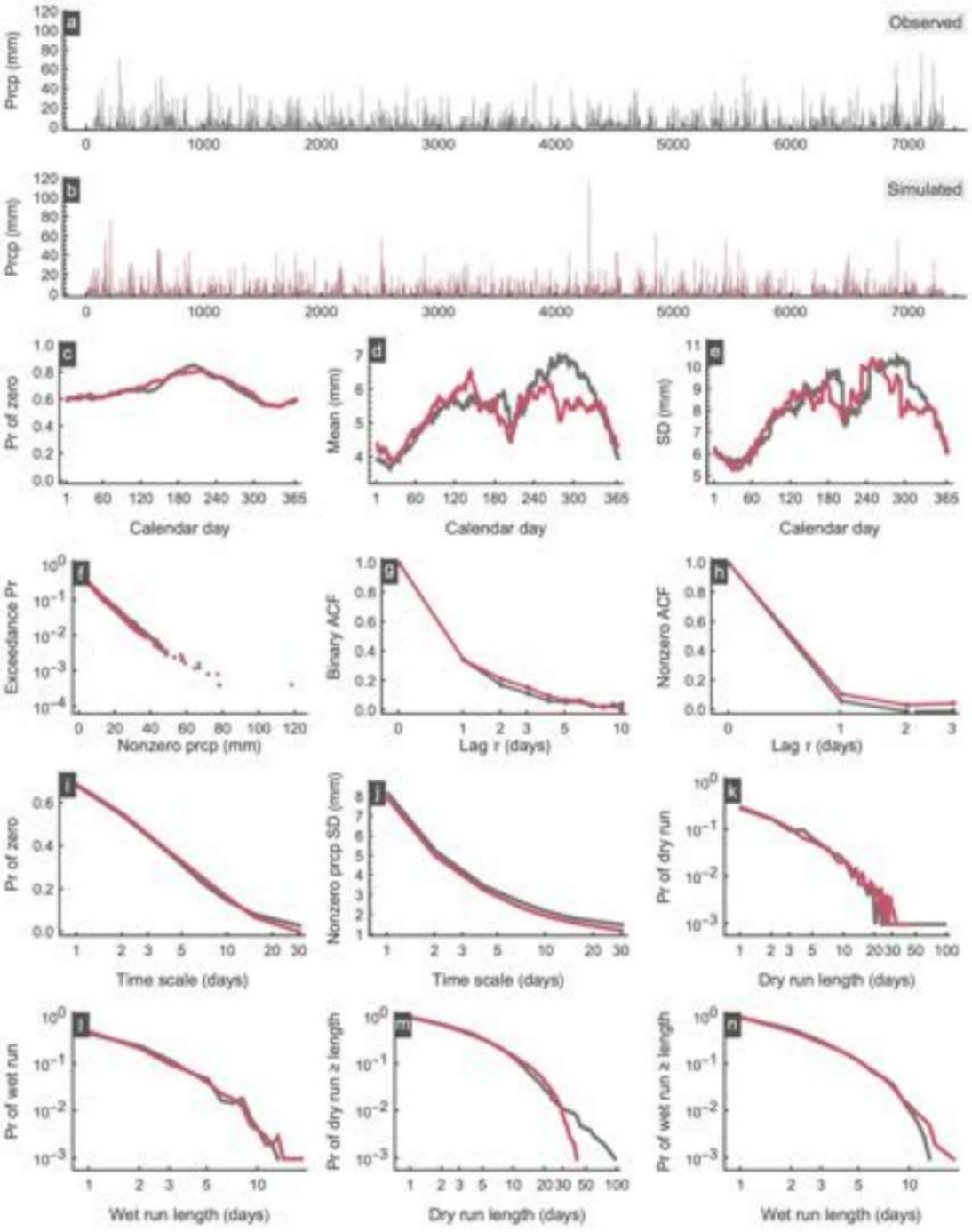

Figure A48. Simulation results for station PluvioMetro 56.

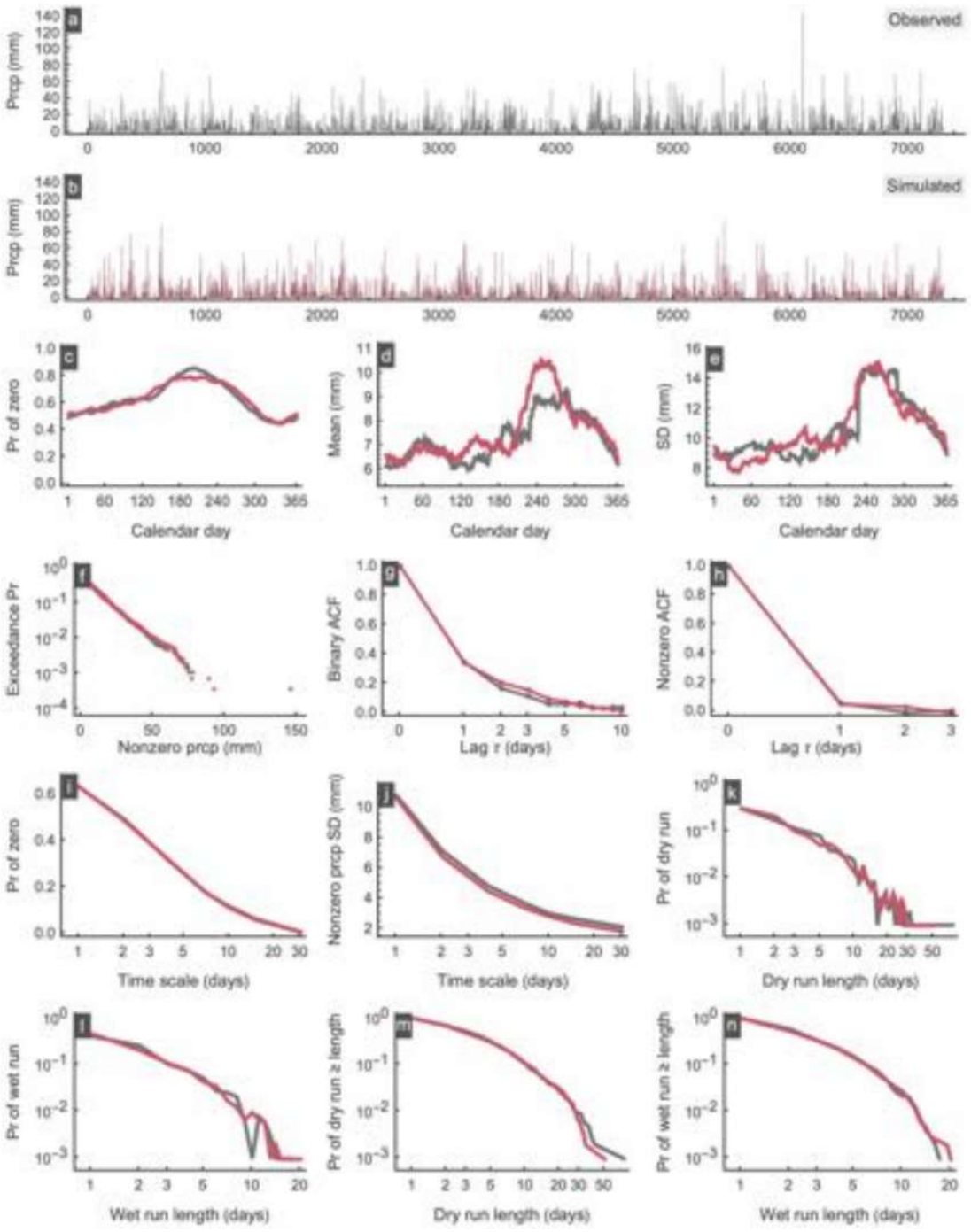

Figure A49. Simulation results for station PluvioMetro 57.

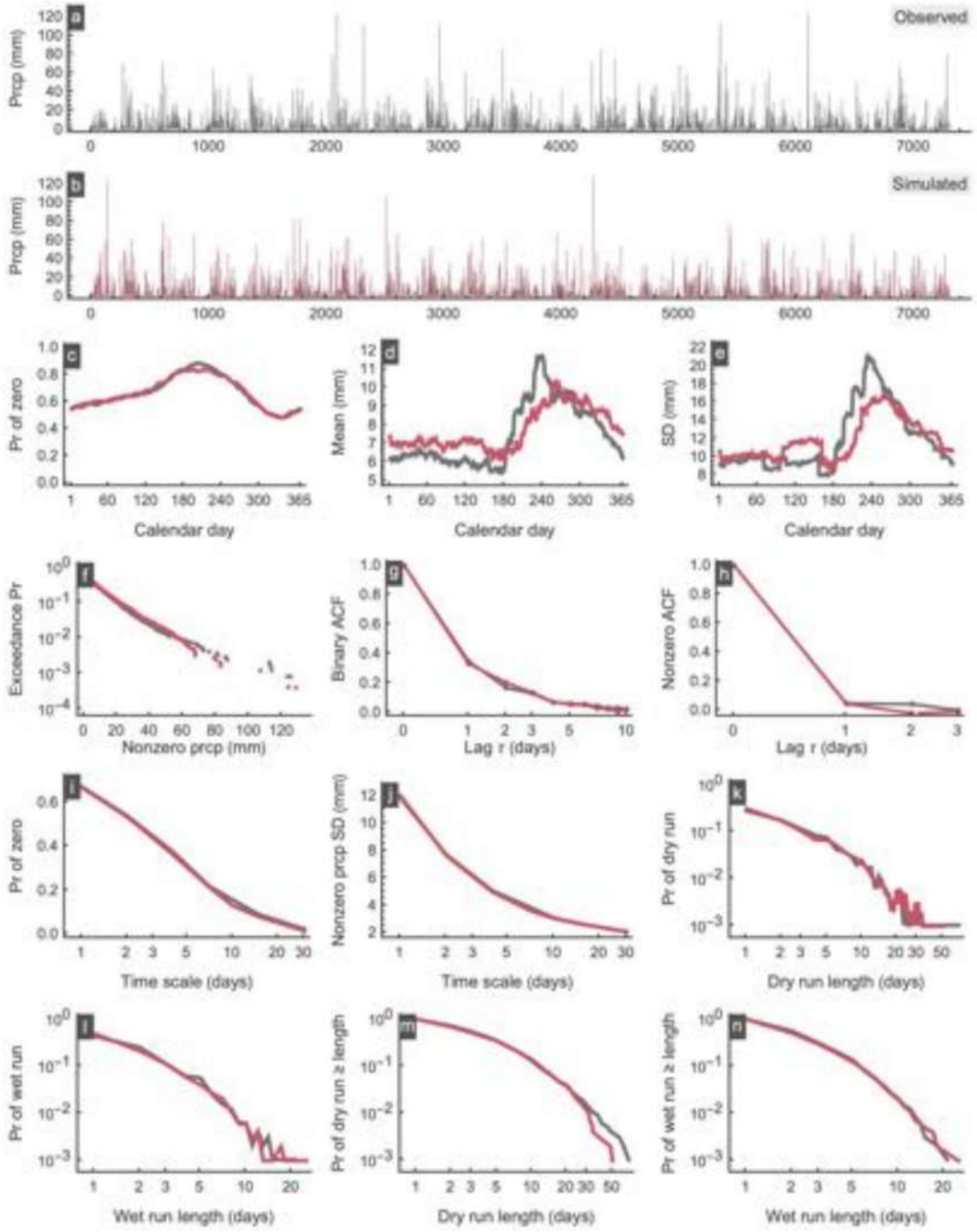

Figure A50. Simulation results for station PluvioMetro 58.

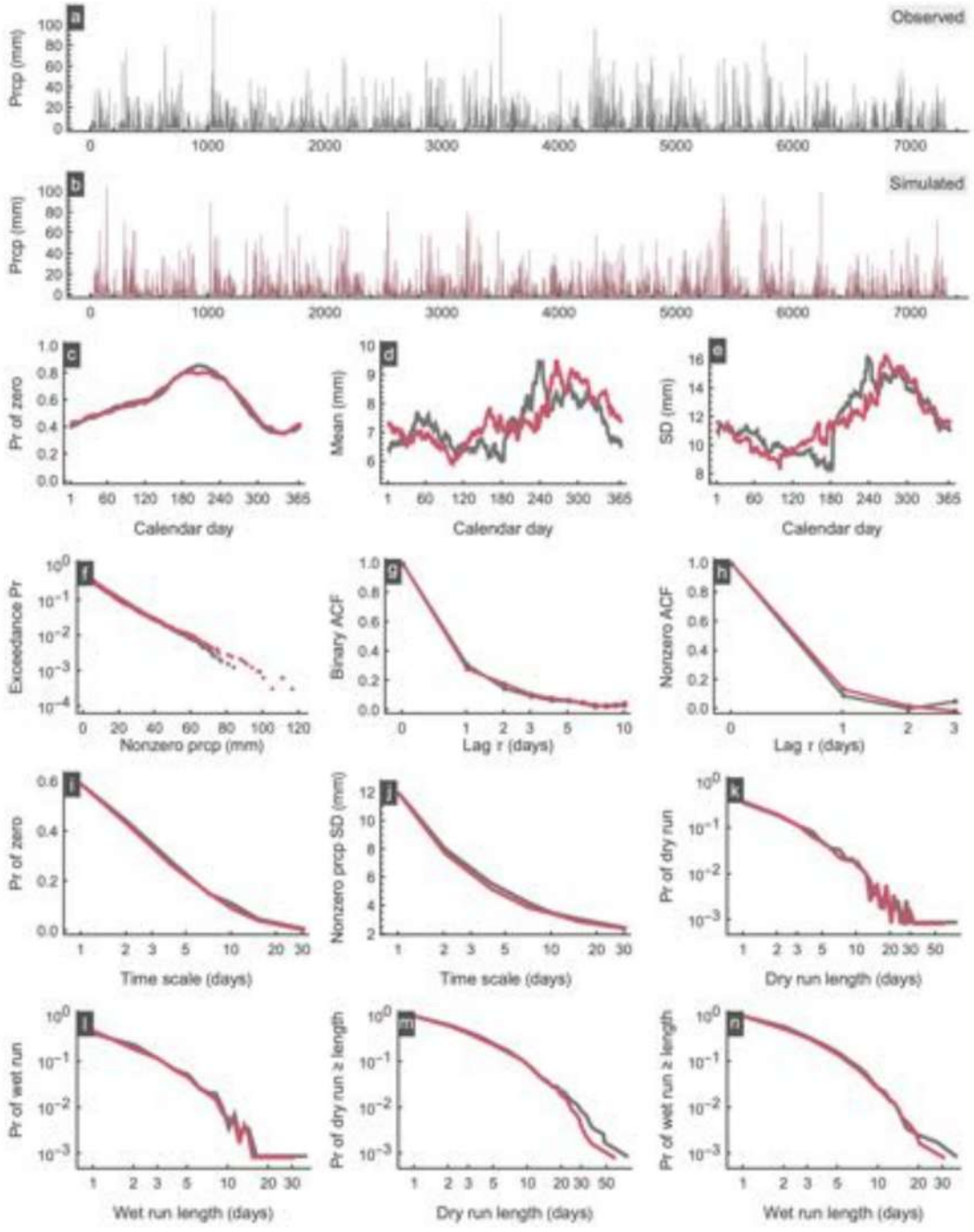

Figure A51. Simulation results for station PluvioMetro 59.

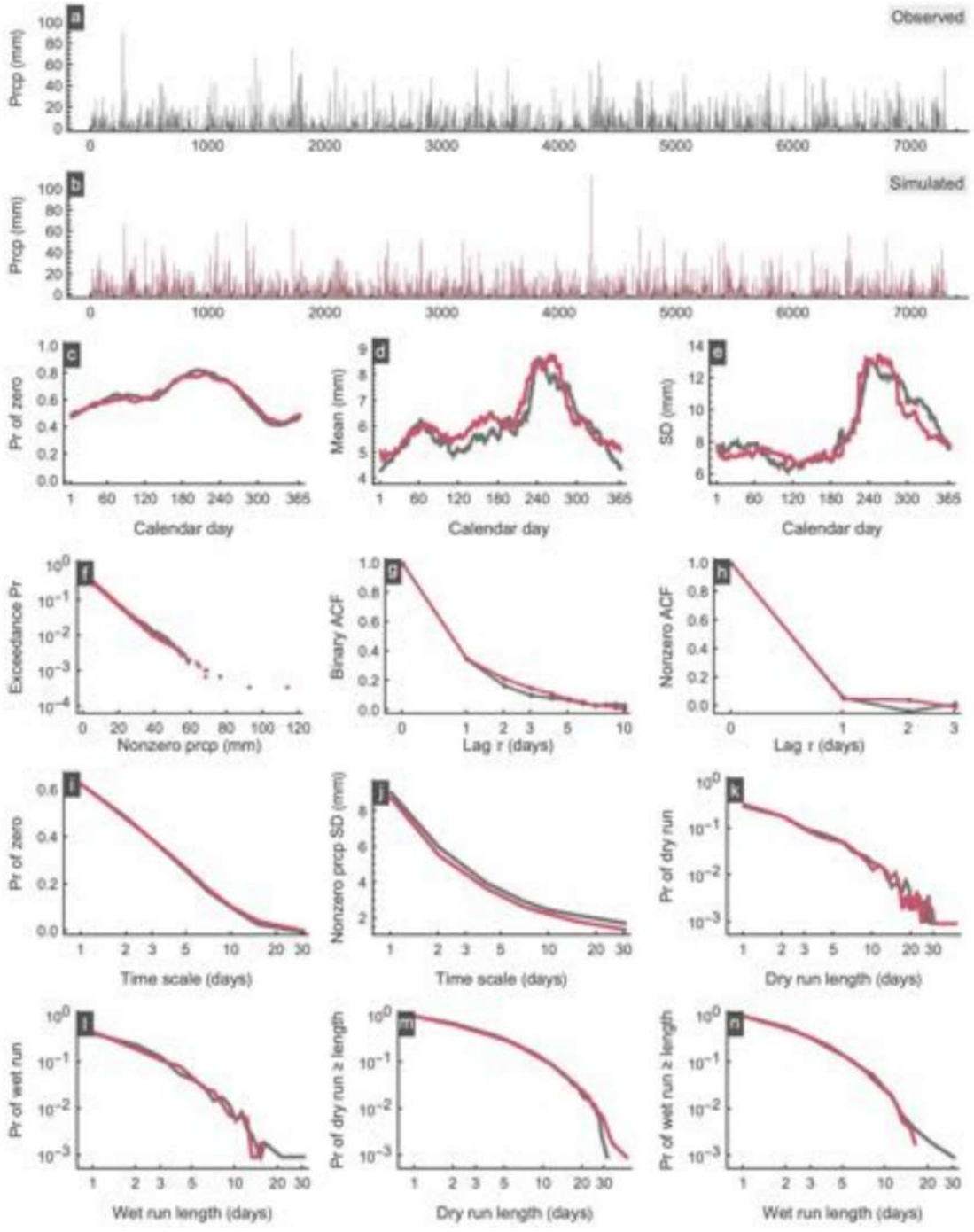

Figure A52. Simulation results for station PluvioMetro 60.

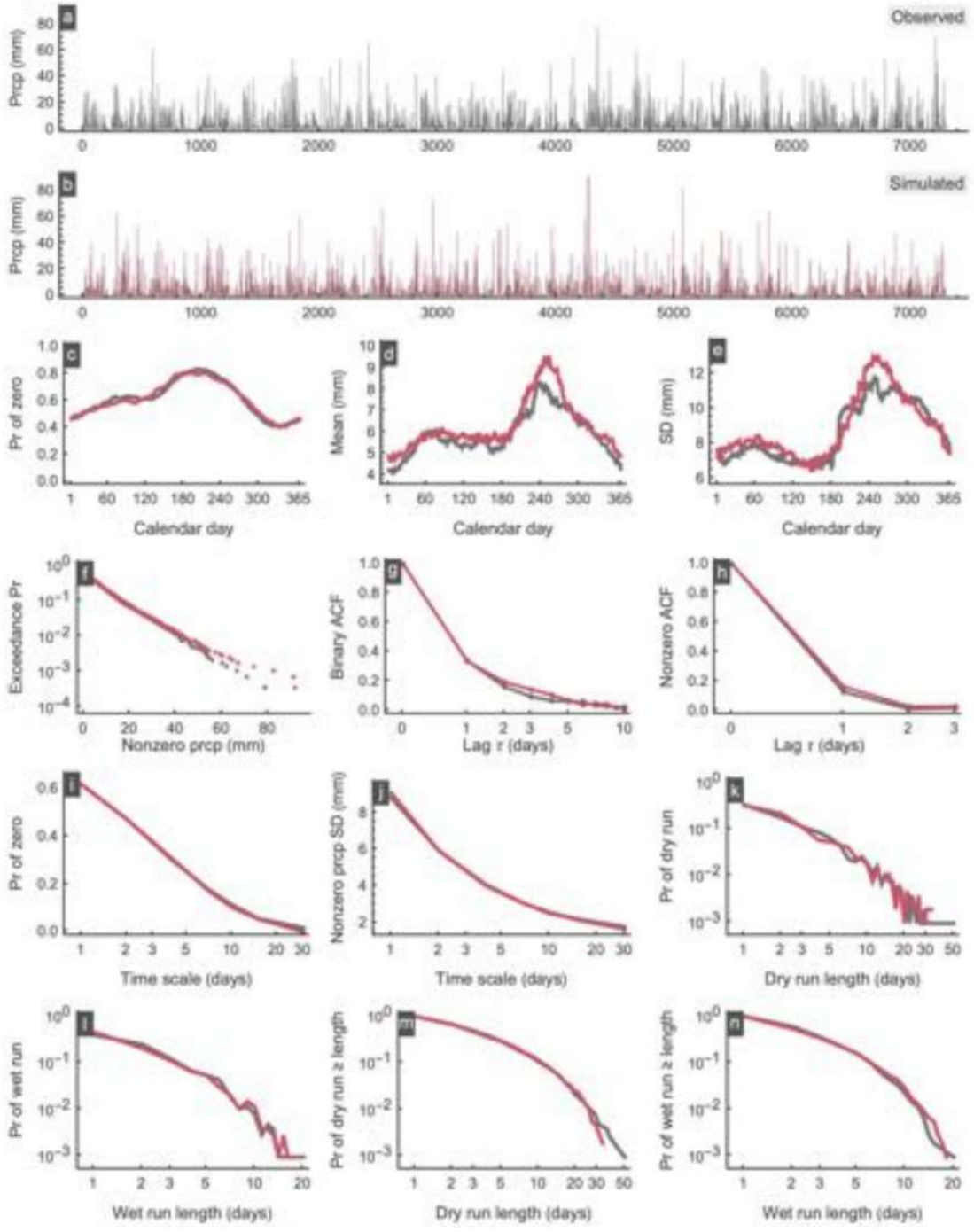

Figure A53. Simulation results for station PluvioMetro 61.

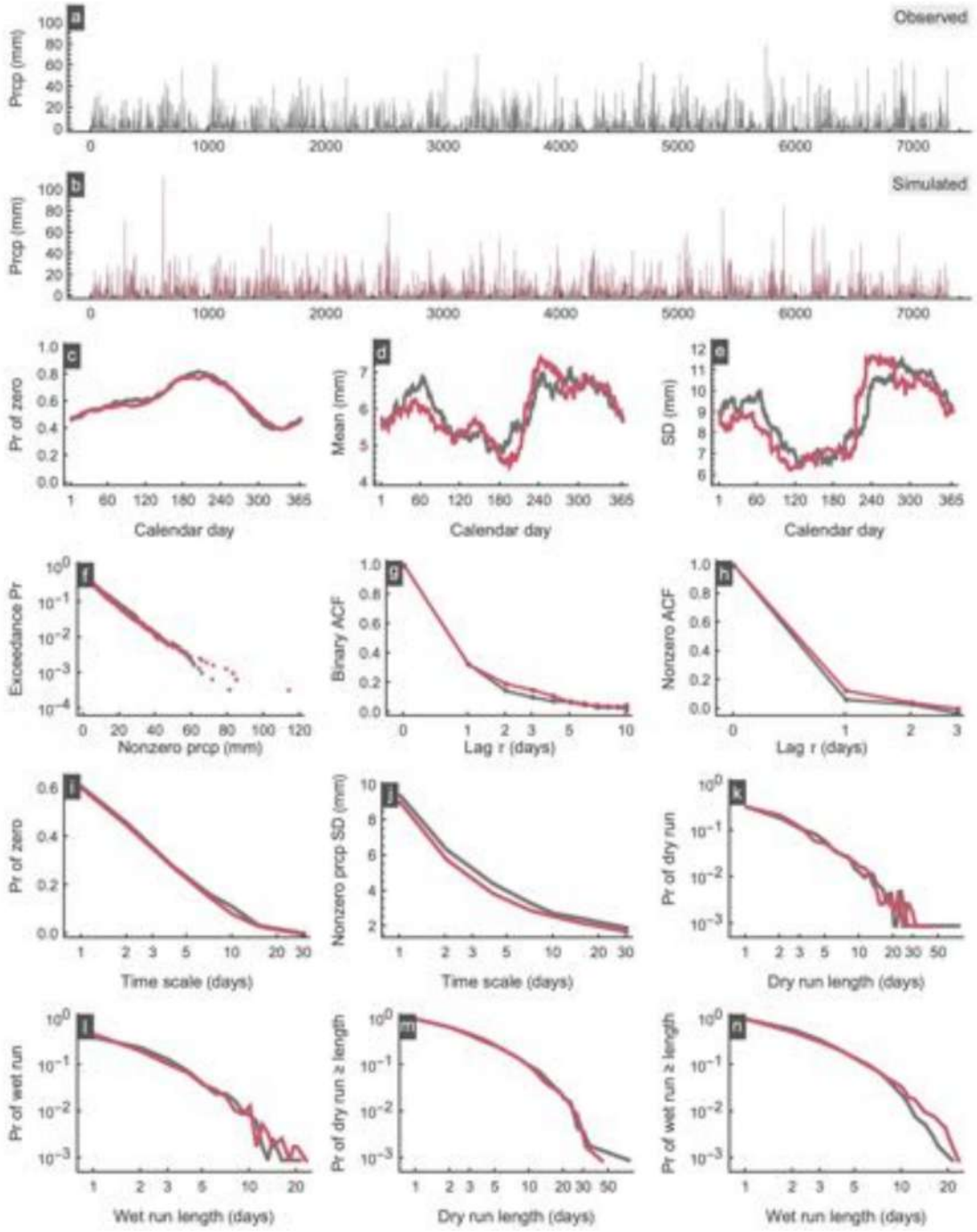

Figure A54. Simulation results for station PluvioMetro 62.

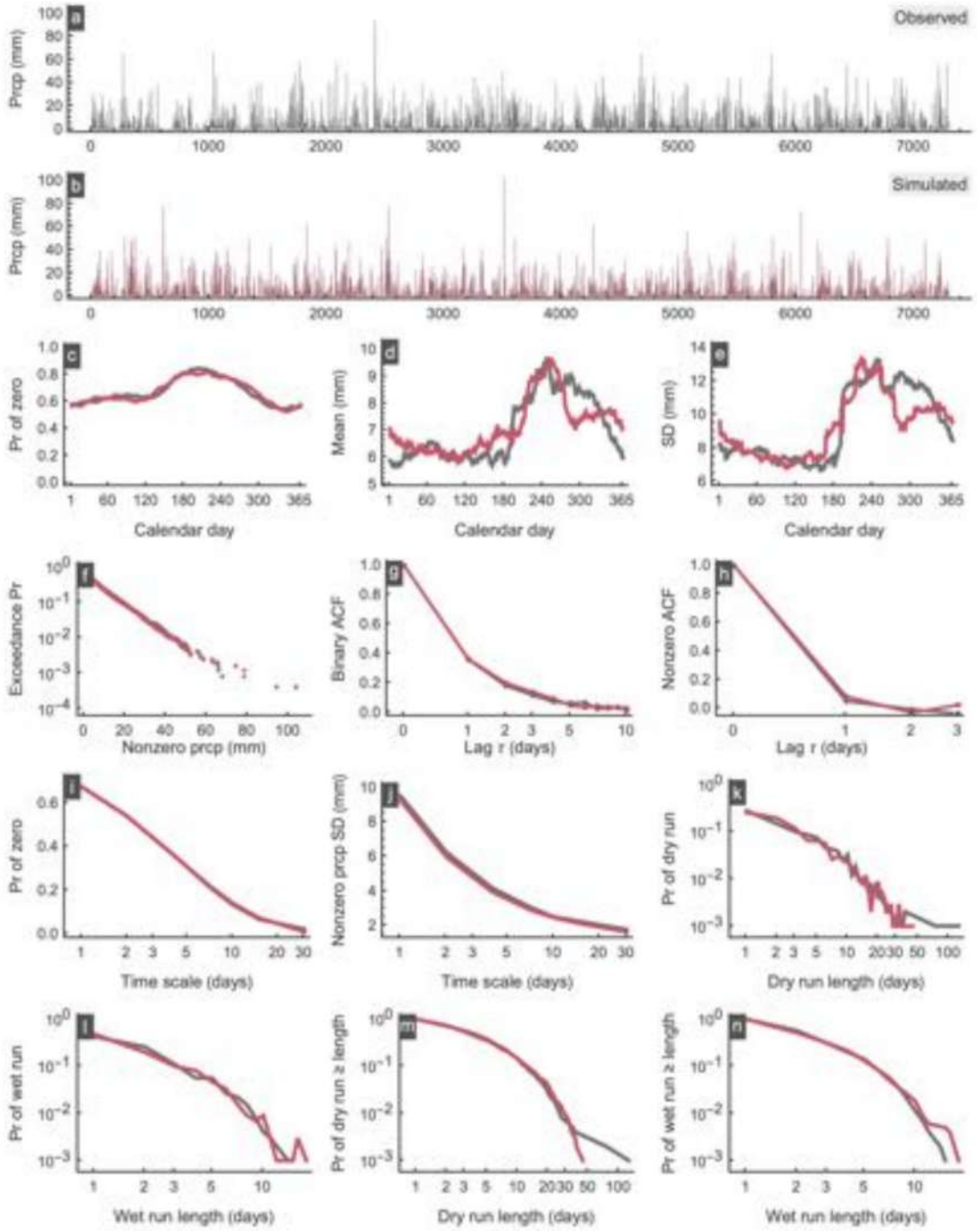

Figure A55. Simulation results for station PluvioMetro 63.

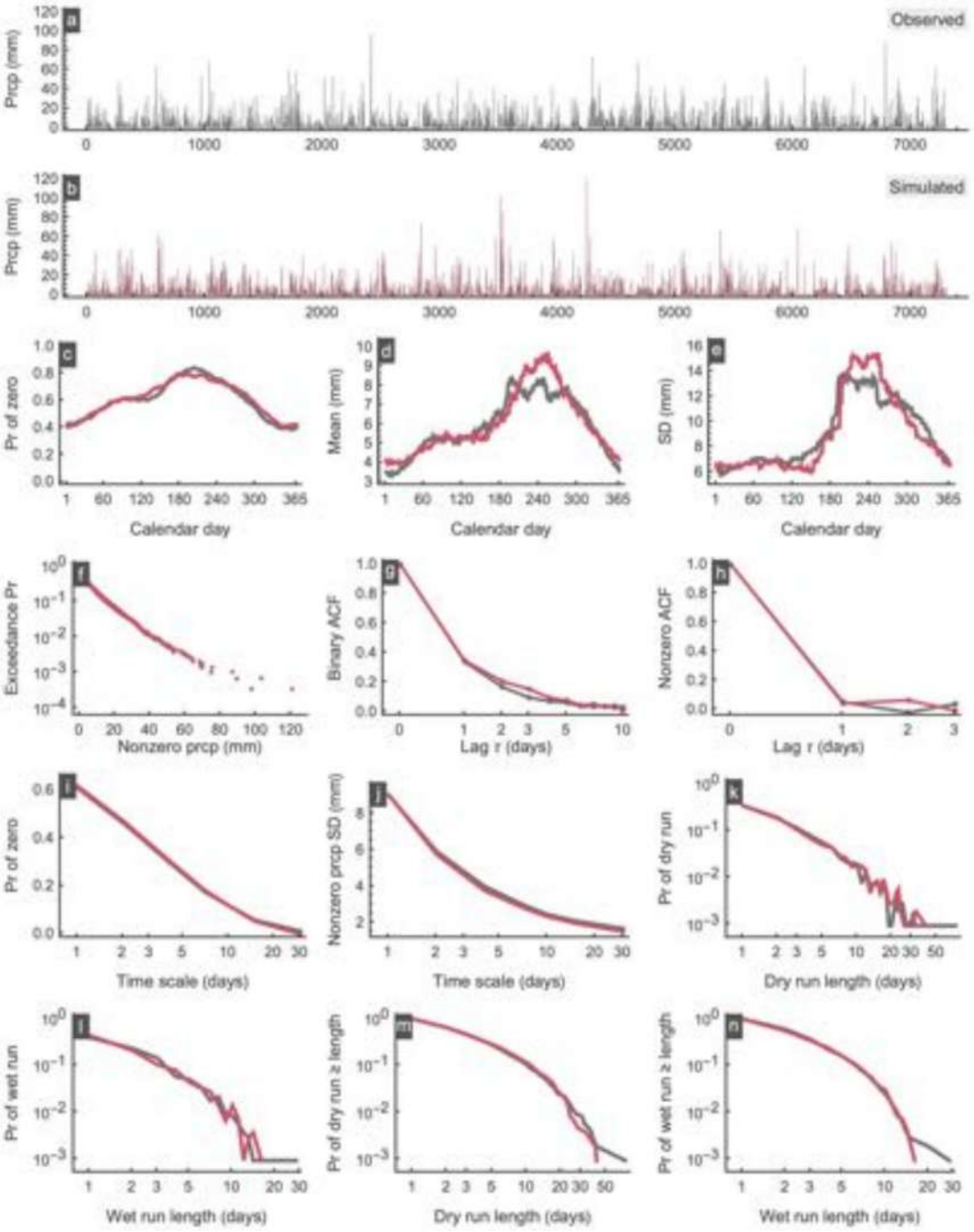

Figure A56. Simulation results for station PluvioMetro 64.

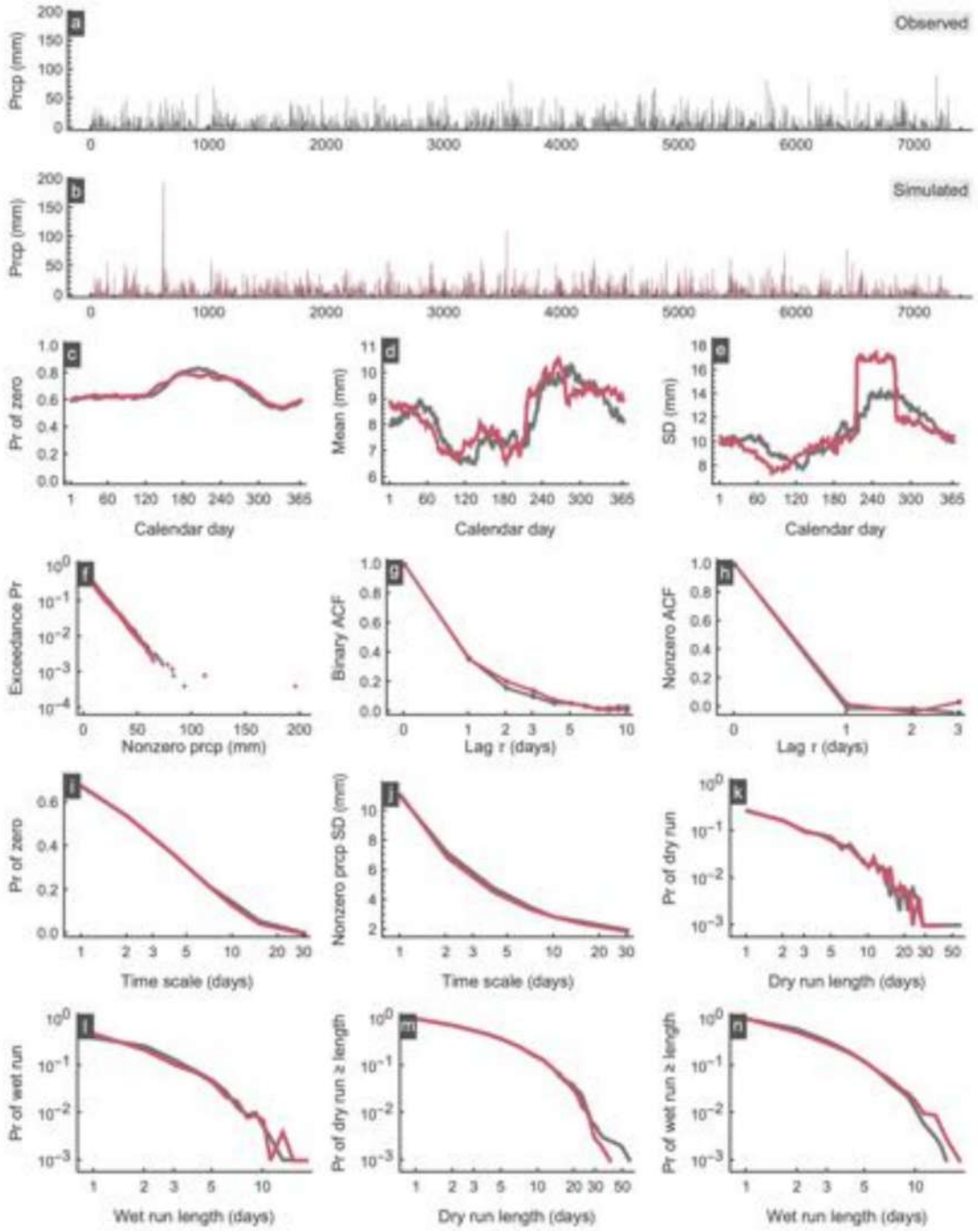

Figure A57. Simulation results for station PluvioMetro 65.

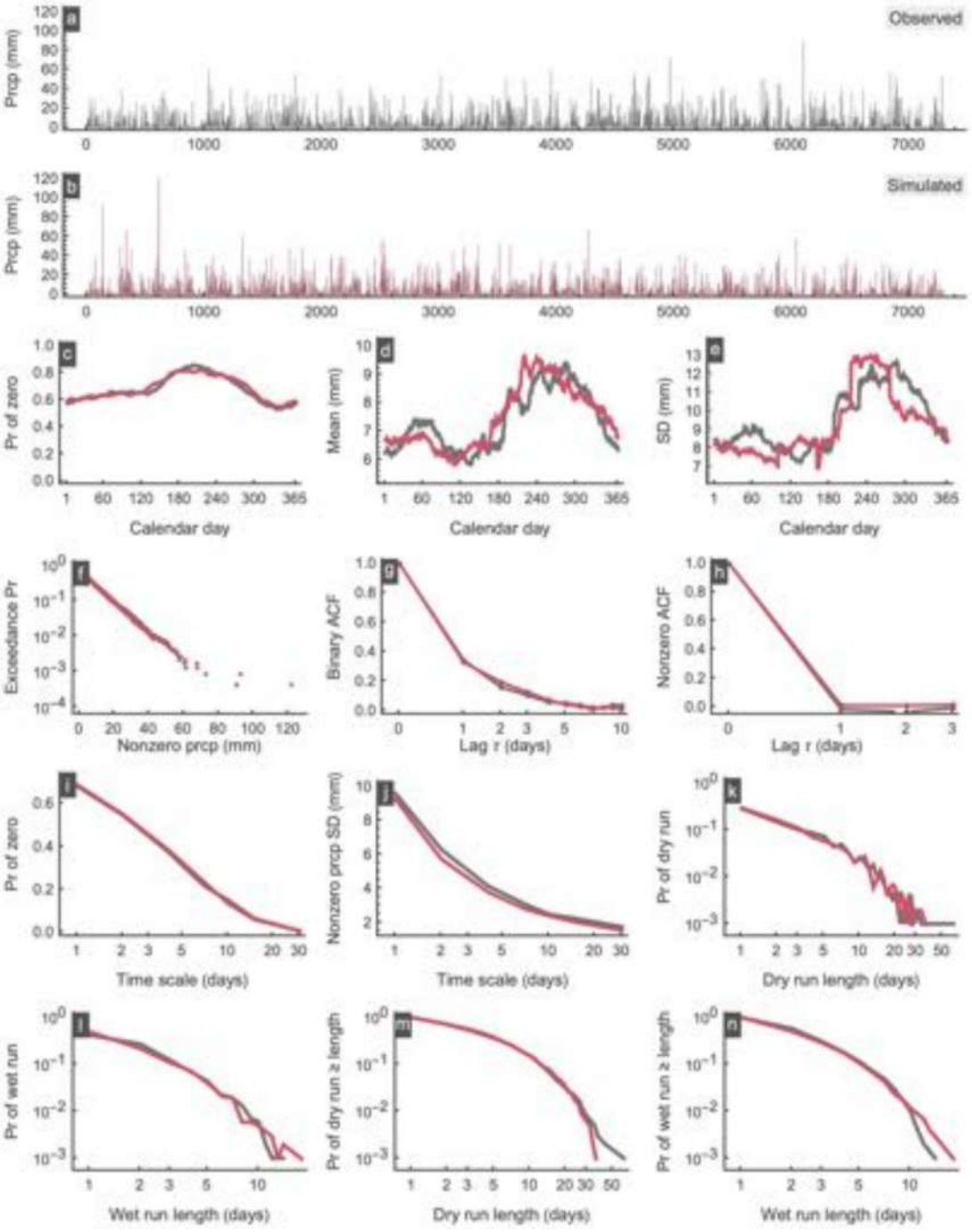

Figure A58. Simulation results for station PluvioMetro 66.

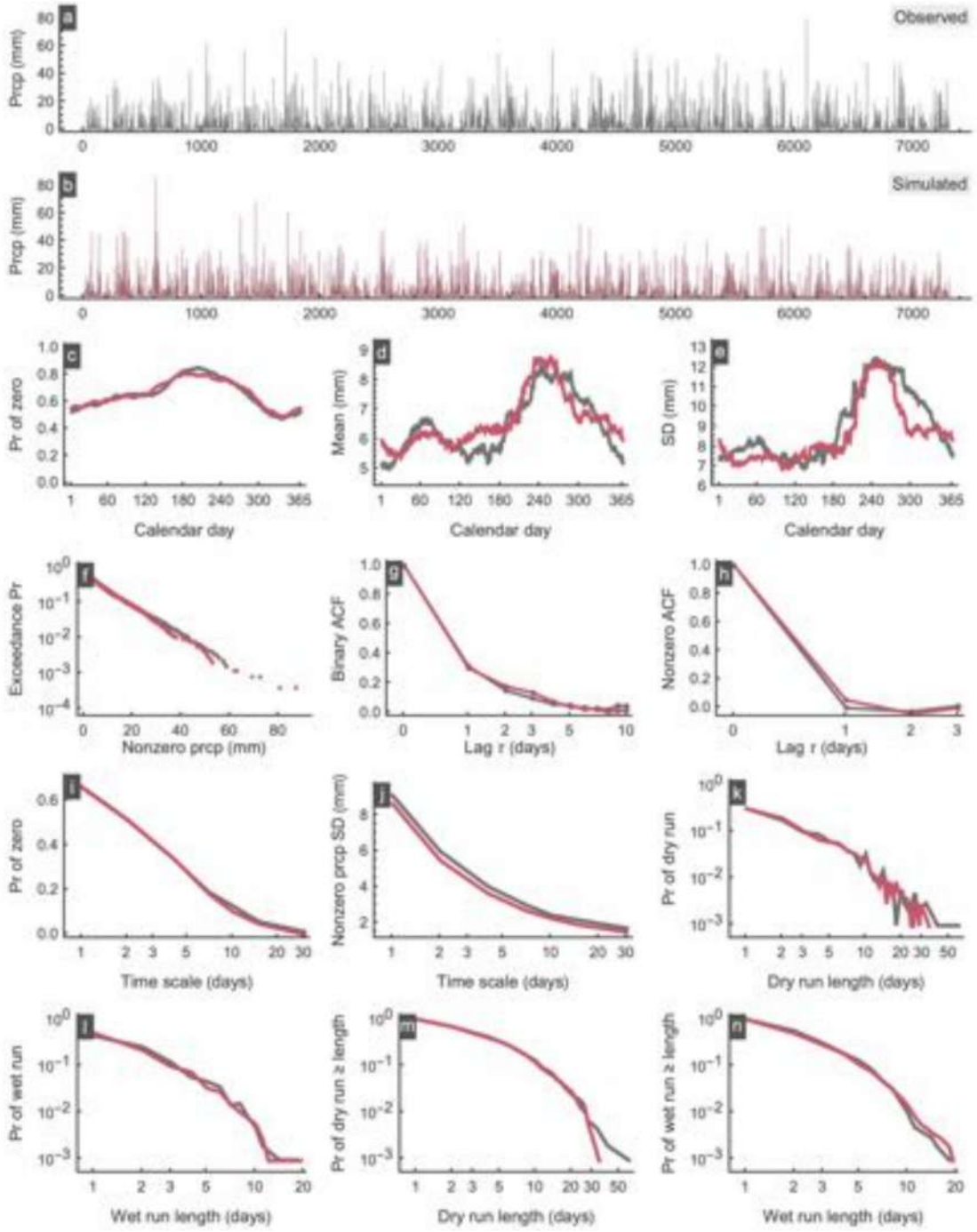

Figure A59. Simulation results for station PluvioMetro 67.

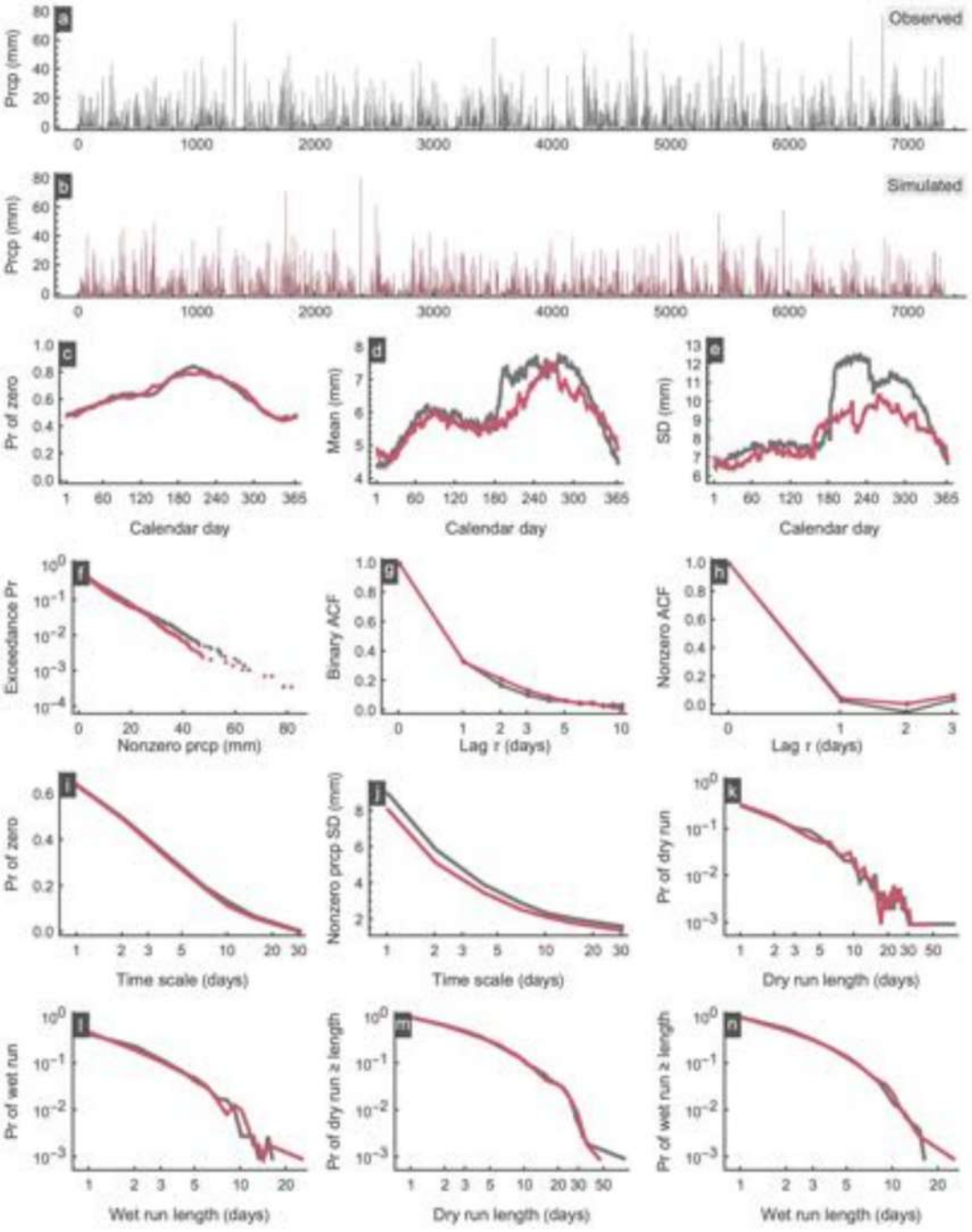

Figure A60. Simulation results for station PluvioMetro 68.

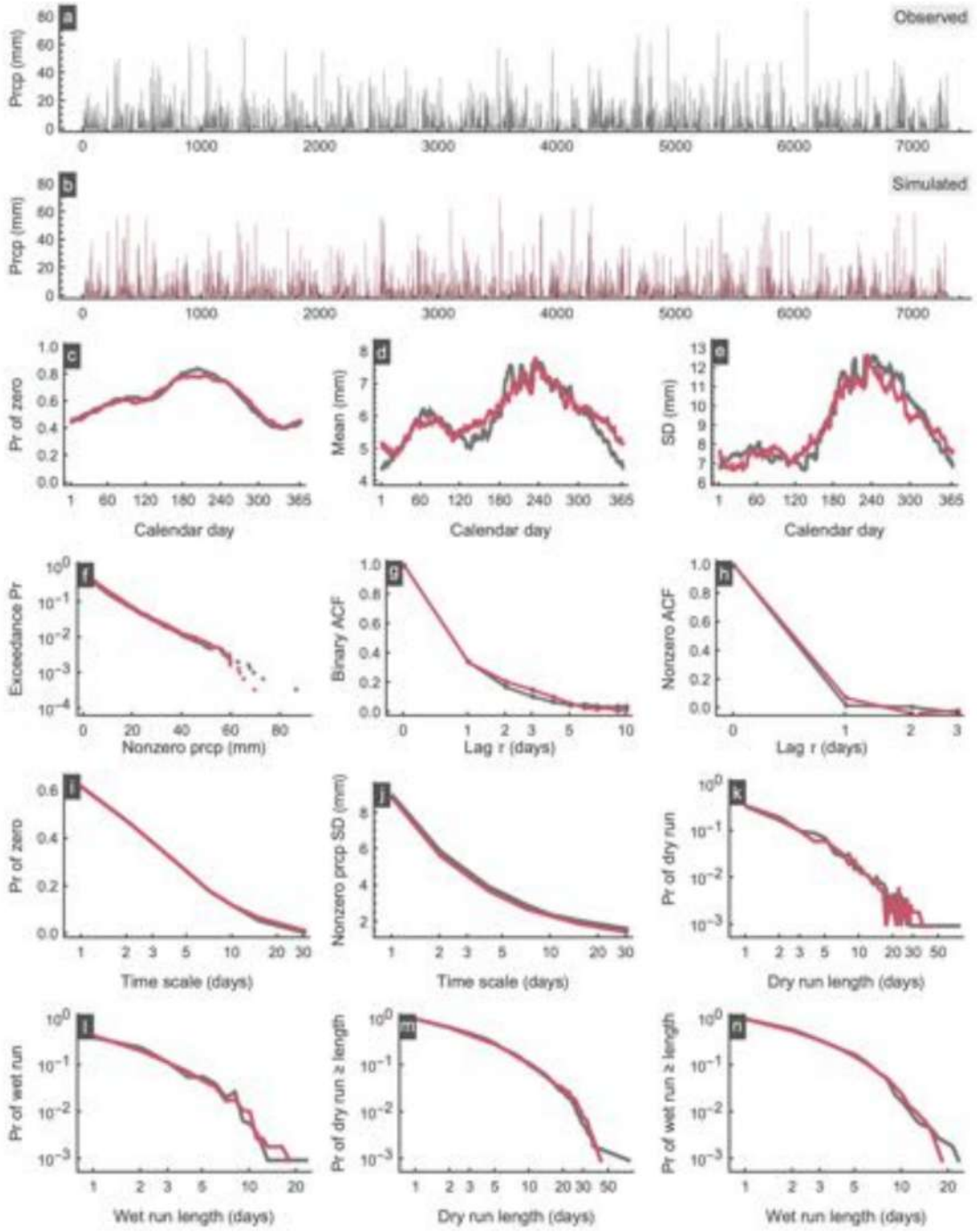

Figure A61. Simulation results for station PluvioMetro 69.

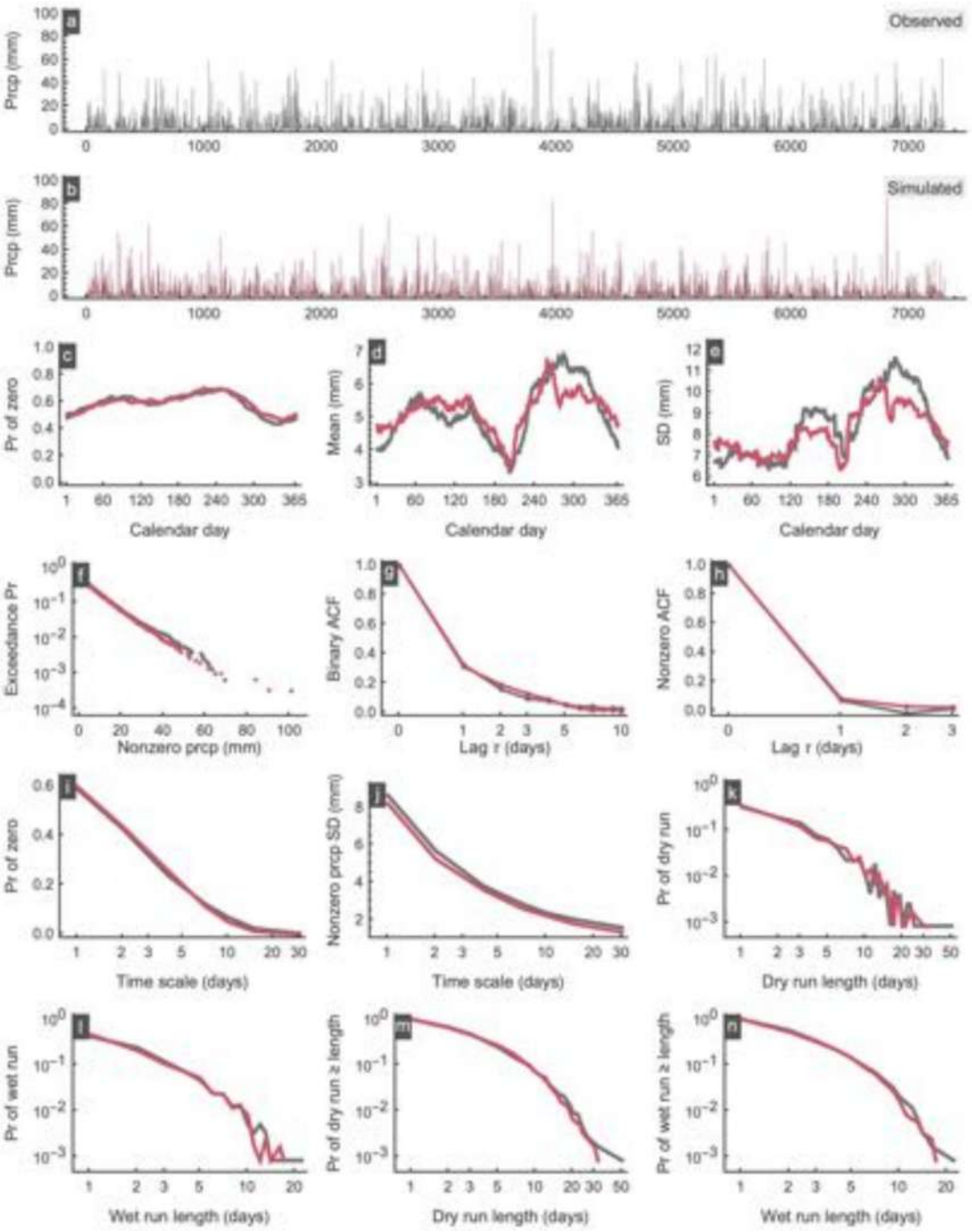

Figure A62. Simulation results for station PluvioMetro 70.

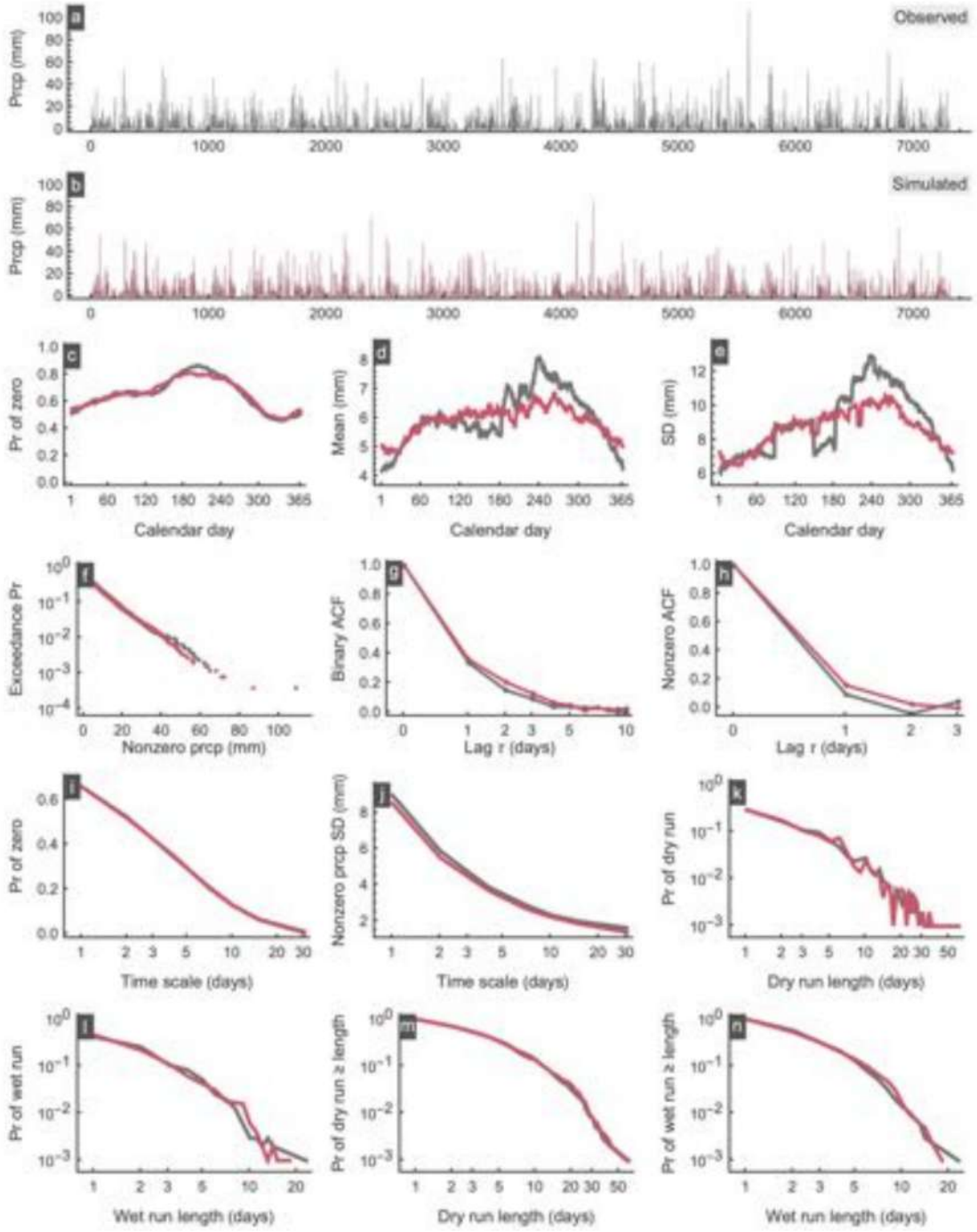

Figure A63. Simulation results for station PluvioMetro 71.

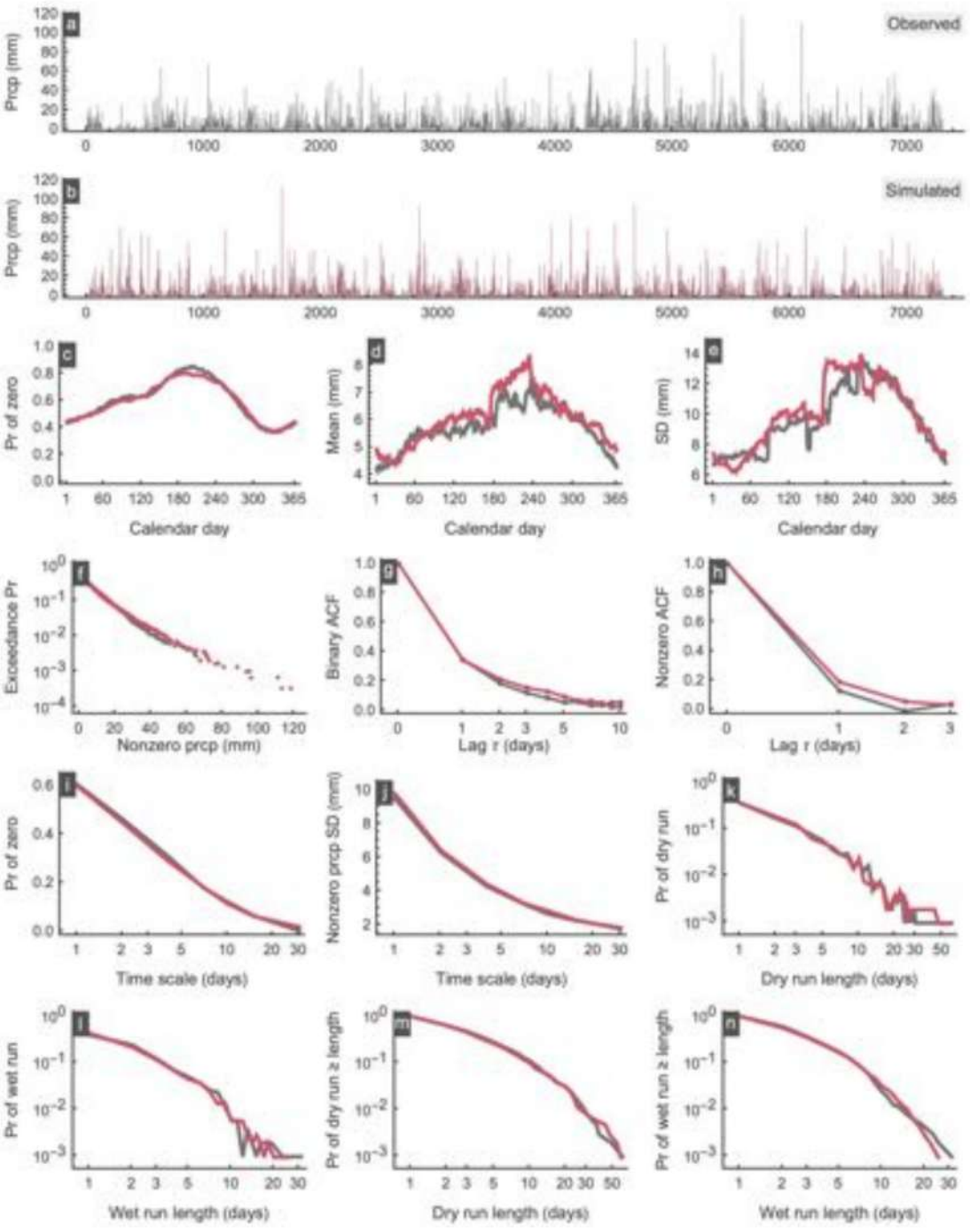

Figure A64. Simulation results for station PluvioMetro 72.

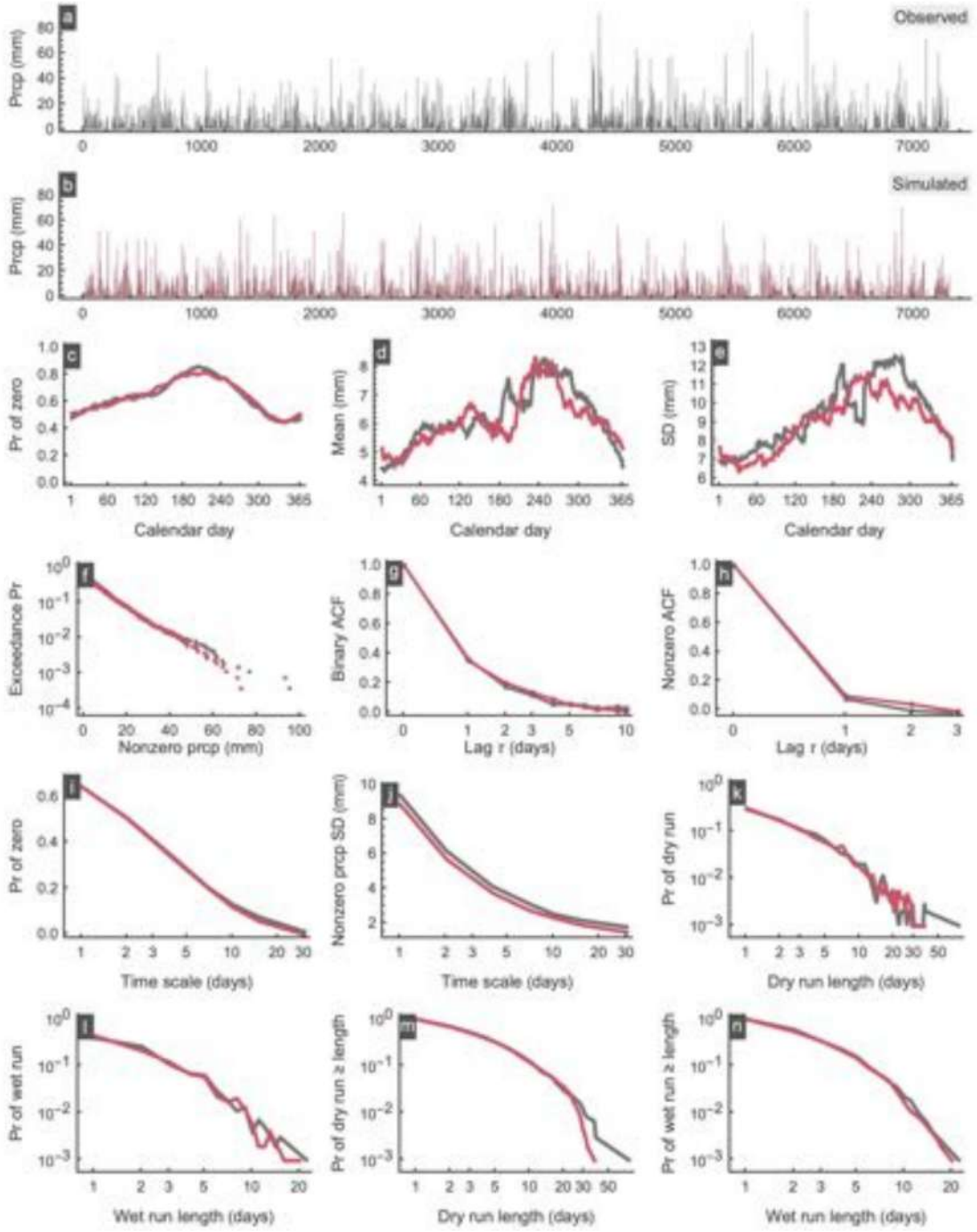

Figure A65. Simulation results for station PluvioMetro 73.

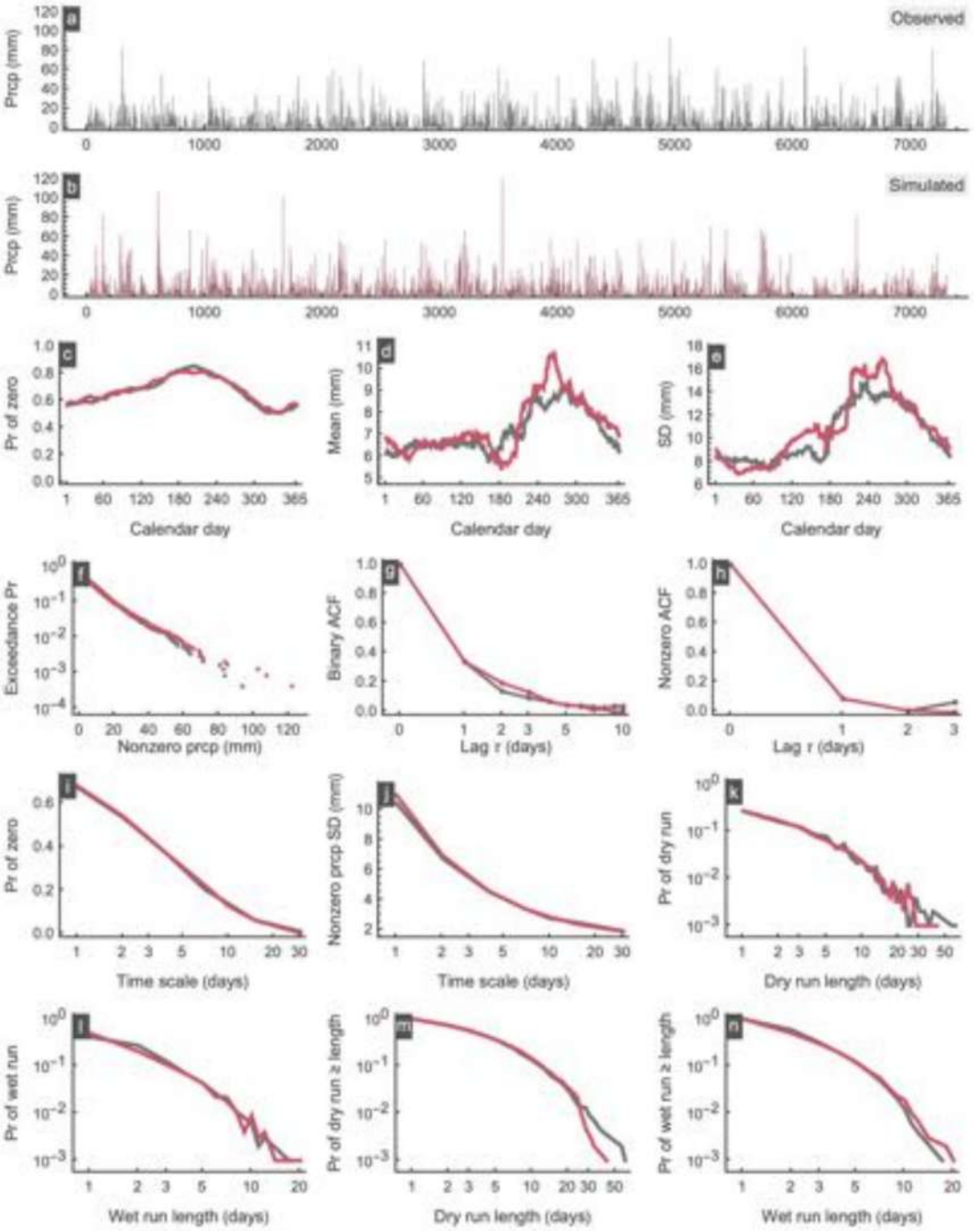

Figure A66. Simulation results for station PluvioMetro 75.

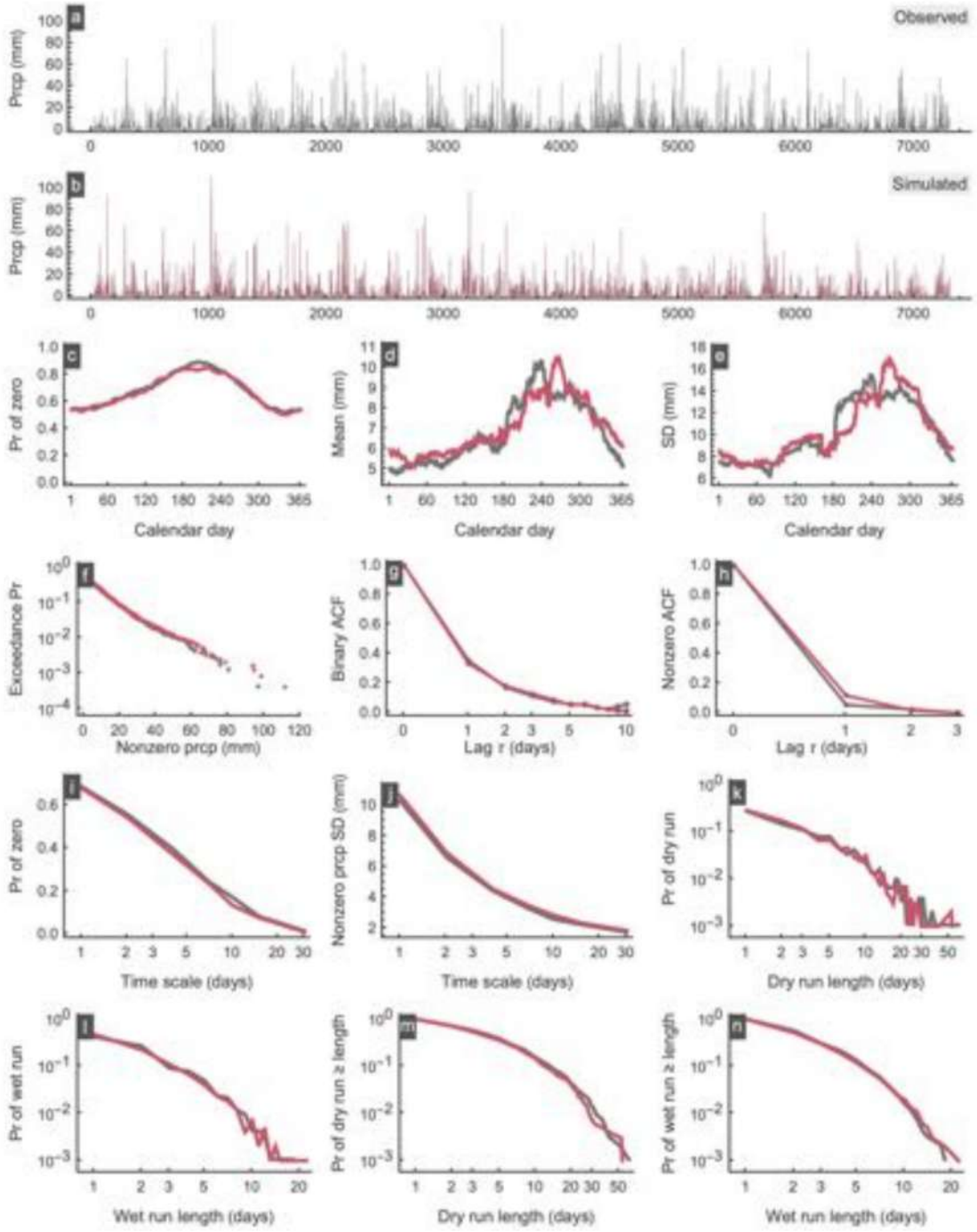

Figure A67. Simulation results for station PluvioMetro 76.

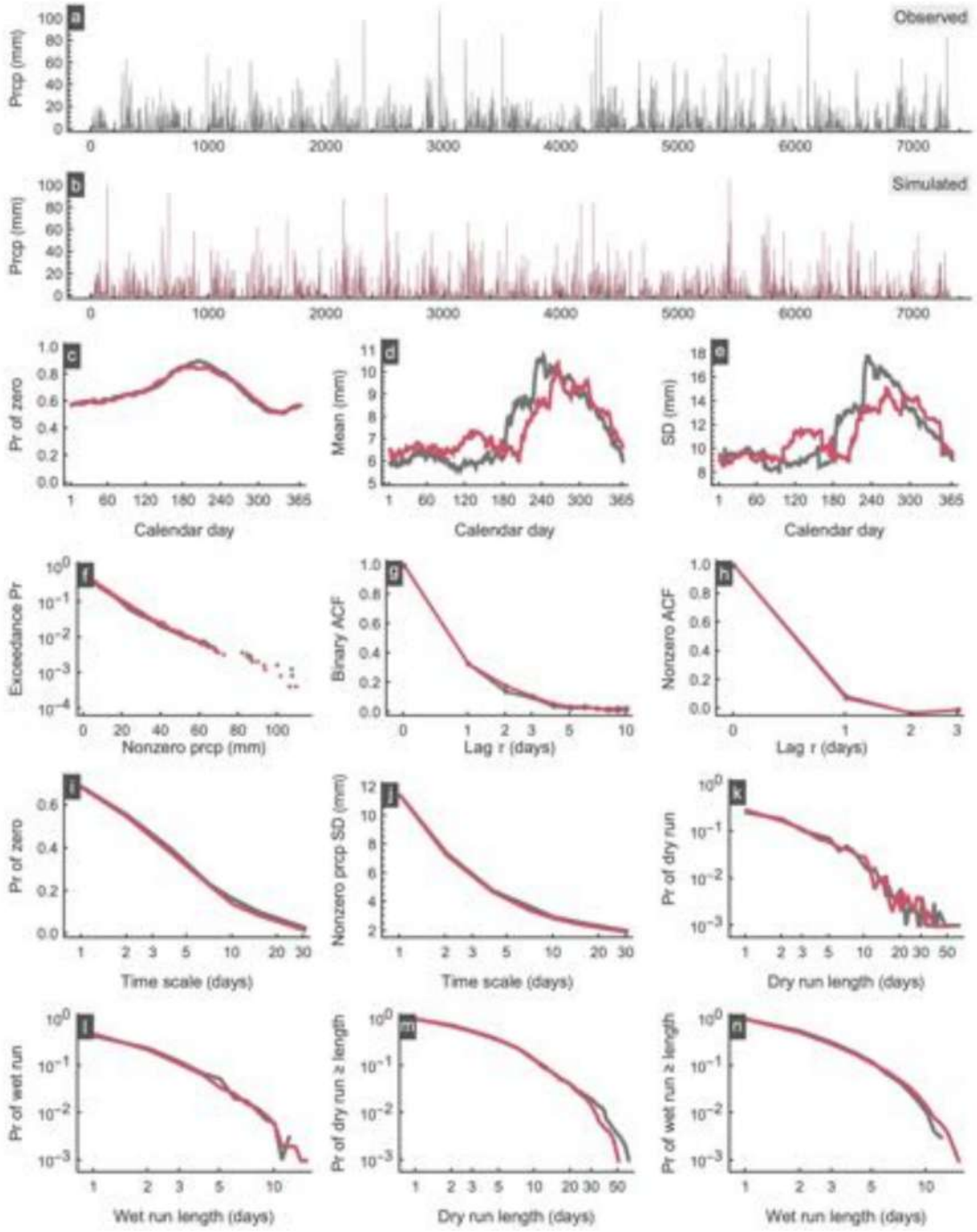

Figure A68. Simulation results for station PluvioMetro 78.

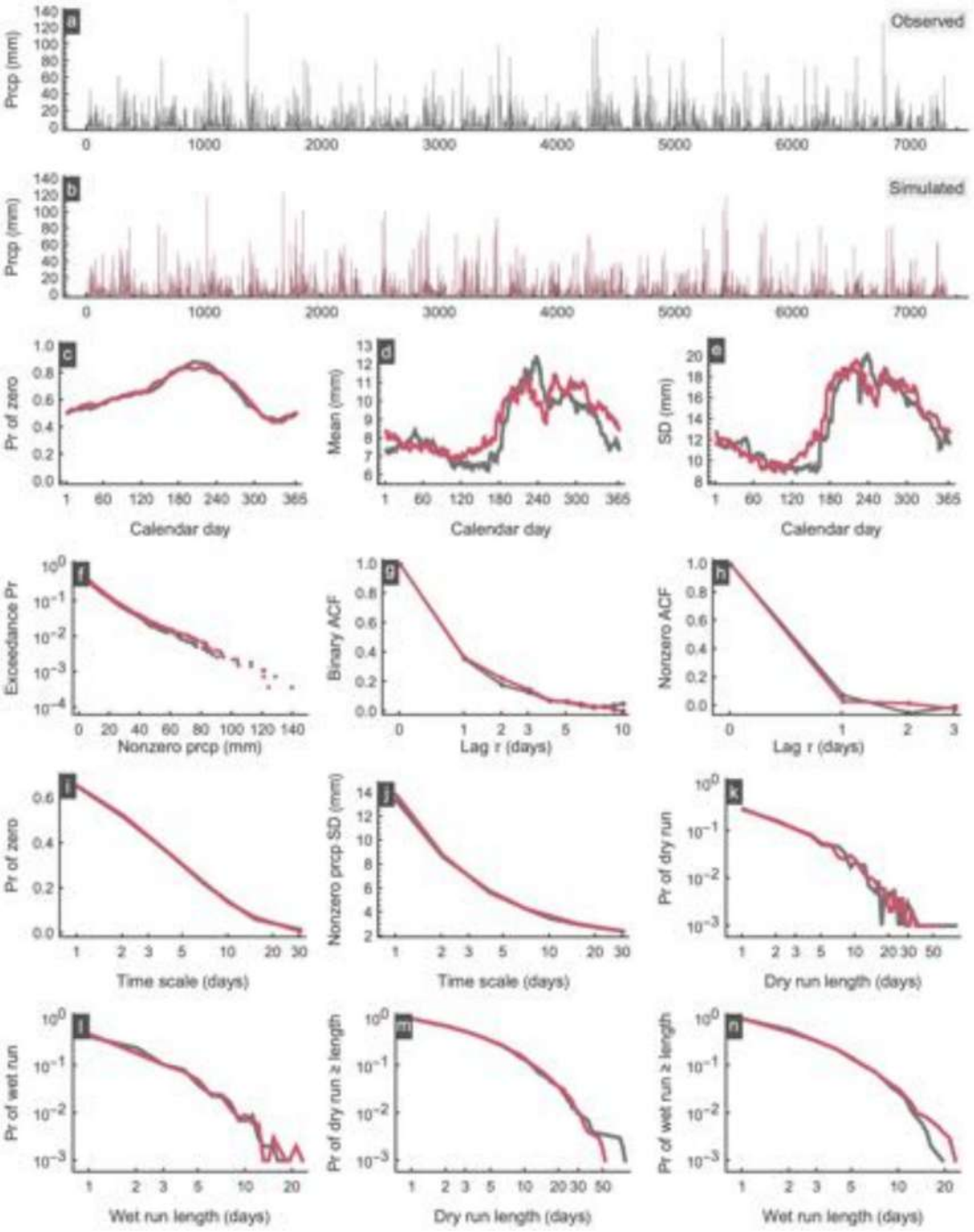

Figure A69. Simulation results for station PluvioMetro 79.

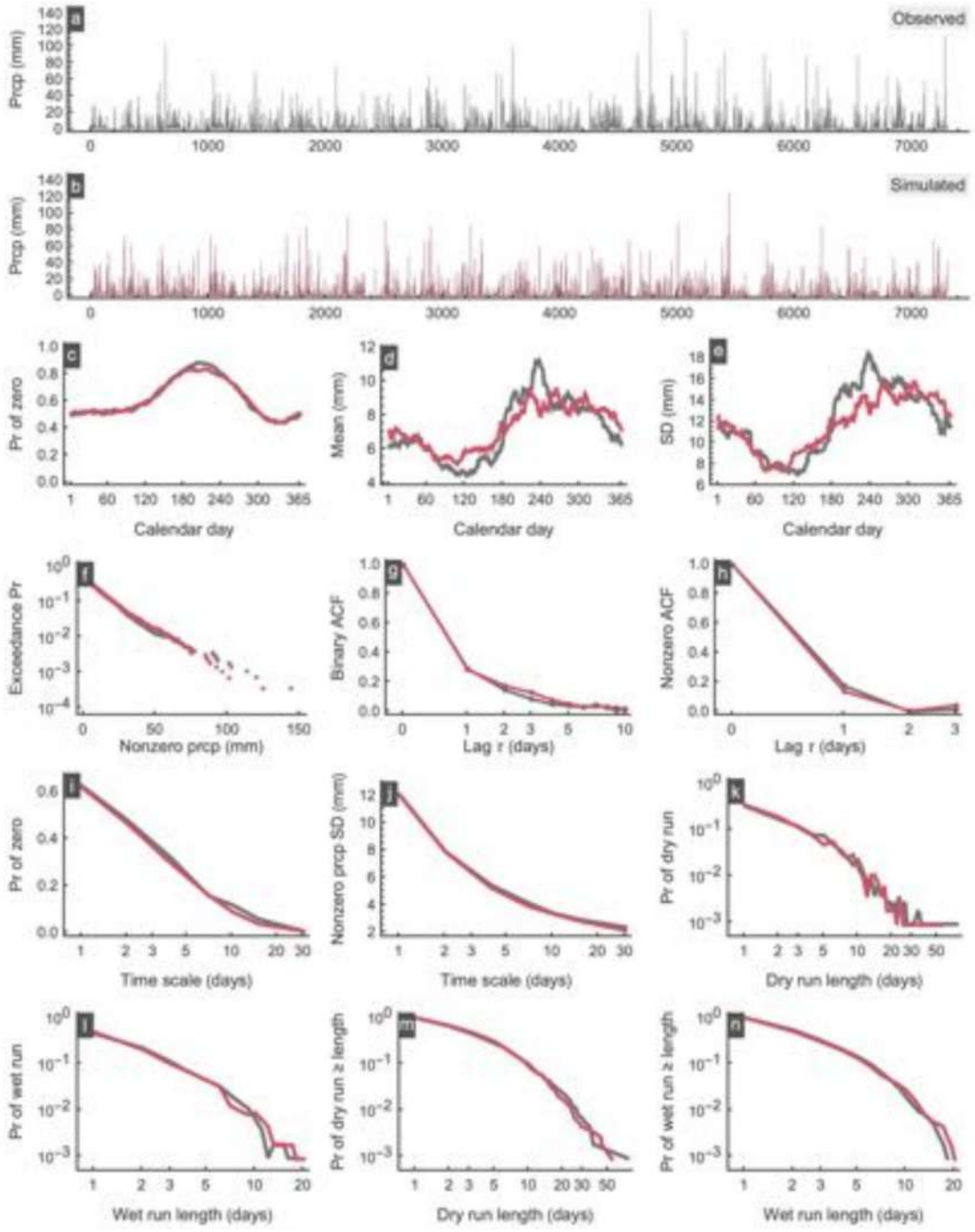

Figure A70. Simulation results for station PluvioMetro 80.

References

Papalexiou, Simon Michael, & Serinaldi, F. (2020). Random Fields Simplified: Preserving Marginal Distributions, Correlations, and Intermittency, With Applications From Rainfall

to Humidity. *Water Resources Research*, *56*(2), e2019WR026331. https://doi.org/10.1029/2019WR026331

Papalexiou, Simon Michael, Serinaldi, F., & Porcu, E. (2021). Advancing Space-Time Simulation of Random Fields: From Storms to Cyclones and Beyond. *Water Resources Research*, e2020WR029466. https://doi.org/10.1029/2020WR029466

Papalexiou, S.M. (2018). Unified theory for stochastic modelling of hydroclimatic processes: Preserving marginal distributions, correlation structures, and intermittency. *Ad*vances in Water Resources, 115, 234–252. https://doi.org/10.1016/j.advwatres.2018.02.013

Papalexiou, S. M. (2022). Rainfall Generation Revisited: Introducing CoSMoS-2s and Advancing Copula-Based Intermittent Time Series Modeling. Water Resources Research, 58(6), e2021WR031641. https://doi.org/10.1029/2021WR031641